DESIGN AND DEVELOPMENT OF

MULTILAYER VASCULAR GRAFT

by

KRISHNA MADHAVAN

B. E. Mechanical Engineering, University of Madras, 2002

M. S. Mechanical Engineering, University of Colorado at Boulder, 2005

A thesis submitted to the

Faculty of the Graduate School of the

University of Colorado in partial fulfillment

of the requirement for the degree of

Doctor of Philosophy

Department of Mechanical Engineering

2011

This thesis entitled:

Design and development of multilayer vascular graft

written by Krishna Madhavan
has been approved for the Department of Mechanical Engineering

WEI TAN

VIRGINIA FERGUSON

Date _____

The final copy of this thesis has been examined by the signatories, and we find that both the content and the form meet acceptable presentation standards of scholarly work in the above mentioned discipline.

ABSTRACT

Madhavan, Krishna (Ph.D., Mechanical Engineering)

Design and development of multilayer vascular graft

Thesis directed by Assistant Professor Wei Tan

Vascular graft is a widely-used medical device for the treatment of vascular diseases such as atherosclerosis and aneurysm as well as for the use of vascular access and pediatric shunt, which are major causes of mortality and morbidity in this world. Dysfunction of vascular grafts often occurs, particularly for grafts with diameter less than 6mm, and is associated with the design of graft materials. Mechanical strength, compliance, permeability, endothelialization and availability are issues of most concern for vascular graft materials. To address these issues, we have designed a biodegradable, compliant graft made of hybrid multilayer by combining an intimal equivalent, electrospun heparin-impregnated poly-ε-caprolactone nanofibers, with a medial equivalent, a crosslinked collagen-chitosan-based gel scaffold. The intimal equivalent is designed to build mechanical strength and stability suitable for *in vivo* grafting and to prevent thrombosis. The medial equivalent is designed to serve as a scaffold for the activity of the smooth muscle cells important for vascular healing and regeneration. Our results have shown that genipin is a biocompatible crosslinker to enhance the mechanical properties of collagen-chitosan based scaffolds, and the degradation time and the activity of smooth muscle cells in the scaffold can be modulated by the crosslinking degree. For vascular grafting and regeneration *in vivo*, an important design parameter of the hybrid multilayer is the interface adhesion between the intimal and medial equivalents. With diametrically opposite affinities to water, delamination of the two layers occurs. Physical or chemical modification techniques were thus used to enhance the adhesion. Microscopic examination and

graft-relevant functional characterizations have been performed to evaluate these techniques. Results from characterization of microstructure and functional properties, including burst strength, compliance, water permeability and suture strength, showed that the multilayer graft possessed properties mimicking those of native vessels. Achieving these FDA-required functional properties is essential because they play critical roles in graft performances *in vivo* such as thrombus formation, occlusion, healing, and bleeding. In addition, cell studies and animal studies have been performed on the multilayer graft. Our results show that the multilayer graft support mimetic vascular culture of cells and the acellular graft serves as an artery equivalent *in vivo* to sustain the physiological conditions and promote appropriate cellular activity. In conclusion, the newly-developed hybrid multilayer graft provides a proper balance of biomechanical and biochemical properties and demonstrates the potential for the use of vascular tissue engineering and regeneration.

DEDICATION

This dissertation is dedicated to

the world's finest doctor & medicine,

my mother & my father!

iduvum avanadu innaruḷe……sarvam śrīkṛṣṇārpaṇamastu

ACKNOWLEDGEMENTS

This study was partially funded by the Innovative Grant Program of the University of Colorado at Boulder, the Department of Mechanical Engineering of the University of Colorado at Boulder, the Graduate School of the University of Colorado at Boulder, NIH (NHLBI 097246-01 to W.T) and State of Colorado (Biodiscovery Program to W.T.).

I would like to thank my advisor Dr. Wei Tan, who has been a friend, guide and well-wisher throughout the five years of my Ph. D. dissertation. I would also like to express my gratitude to Dr. Wei Tan in accepting me into her research group and keeping immense faith in my research and analytical skills. I would like to thank all the members of Wei Tan Lab, John Twomey, Dr. Devon Scott, Walter Bonani, Kathryn Wingate, Jerry Vadakel and Richard Johnson, for their help extended throughout this Ph. D. dissertation. I would like to acknowledge the help provided by Dr. Dongjie Guo (Wei Tan Lab), Dr. Dongjoon Ahn (Rishi Raj Lab) and Dr. Neil Cramer (Chris Bowman Lab) for providing assistance in FTIR analysis. I would like to acknowledge Dmitry Belchenko (Wei Tan Lab) for assistance in cell studies and Sandra Walchak from CVP group for providing bovine pulmonary artery endothelial and smooth muscle cells. I would like to thank Walter Bonani (Wei Tan Lab/Claudio Migliaresi Lab) for the developing the protocol for the synthesis of the poly-ε-caprolactone tubes by electrospinning. I thank Winston Elliot and Jerry Vadakel for their assistance with electrospinning of the poly-ε-caprolactone tubes. I thank Dragan Mejic (Chemical Engineering Machine Shop) for manufacturing parts which were necessary for the synthesis of the multilayer graft. I also thank Aabhash Shrestha, Birendra Adhikari, Blair Dodson and Winston Elliot for their assistance with biomechanical testing. I also thank Dr. Eric Monnet and Dr. Mellissa Arbaugh (Colorado State University, Fort Collins, CO) for performing the implantations in the animal

models.

I thank Dr. Virginia Ferguson for taking time in helping the author by providing timely research suggestions, reading this entire document patiently and for serving on my Ph. D. dissertation committee. I also thank all the members of Virginia Ferguson Lab, Dr. Sara Campbell, Blair Dodson, Rachel Paietta and Brandi Briggs, for their help throughout this Ph. D. dissertation. I thank Dr. H. Jerry Qi, Dr. Timothy Scott, and Dr. Stephanie Bryant who served on my Ph. D. dissertation committee and provided valuable suggestions and encouragement at various points during this Ph. D. dissertation. I acknowledge the help provided by Dr. Peter Mariner (Kristi Anseth Lab), Navakanth Reddy Gandavarapu (Kristi Anseth Lab), Dr. Chris Kloxin (Chris Bowman Lab) and Dr. Neal Cramer (Chris Bowen Lab) for their assistance in vascular graft material synthesis, biomechanical and biochemical characterization. I also thank Dr. Antonella Motta (University of Trento, Trento, Italy) for helping with field emission scanning electron microscopy. I thank Daniel Fitzstephens for proof reading this document. I thank Sanjay Mohanty for helping me with the formatting of this dissertation. I would also like to thank all those who helped me during this dissertation and am unable to acknowledge them individually here.

CONTENTS

LIST OF FIGURES

LIST OF TABLES

CHAPTER 1

THE NECESSITY OF VASCULAR GRAFTS (LITERATURE REVIEW)

Abstract

Atherosclerosis is one of the major causes of human death. The failure of the kidney to function properly as a filtering system in the human body is also a major cause of death. Vascular grafts are currently used in the replacement of damaged blood vessels in bypass surgeries and as a vascular access in hemodialysis. There are a number of types of grafts available today including autologous grafts (saphenous vein, umbilical cord vein, right thoracic artery), synthetic grafts (extended Polytetrafluoroethylene, Dacron) and tissue engineered blood vessels (TEBV) produced by a wide variety of synthesis techniques. Current techniques of manufacturing TEBV include electrospinning, remodeling and assembly of extracellular matrix (ECM) by cells in bioreactors and common protein self-assembly methods with mechanical property improvement by reinforcements and crosslinking. There is a necessity to design a new material for replacement of small caliber blood vessels (diameter < 6mm) since current materials have some problems associated with them. The failure of small caliber vessels is generally caused by formation of intimal hyperplasia due to improper endothelialization, occlusion due to compliance mismatch and improper healing at the site of anastomosis. Proteins like collagen and elastin are the major components of the ECM which are commonly included in the design of materials for a vascular graft today. Chitosan closely resembles the other major components of the ECM, the glycosaminoglycans, and possesses superior

biomechanical and biochemical properties. The current study investigates the potential of the combination of these naturally occurring polymers as a substitute for small caliber blood vessels.

1.1 Introduction

The cardiovascular system is absolutely vital to the operation of the human body. This system consists of the heart and blood vessels which serve as pump and conduits respectively, which carry oxygen, carbon dioxide and nutrients to various parts of the body. A number of factors, including, age, genetics, stress, food habits, smoking and alcohol consumption are known to contribute to diseases and disorders associated with this system which are known as cardiovascular diseases (CVD). CVDs are among the most common reasons for death in this world today. One of the most common types of CVD is atherosclerosis (a.k.a. stenosis). Stenosis is the deposition of fat, cholesterol and other substances on blood vessels (or simply: formation of plaque). There were approximately 426,000 deaths in USA in 2006 due to stenosis, making it one of the main causes of death in USA alone [1]. The World Health Organization reports that there were at least 7,200,000 deaths due to stenosis around the world in 2004 [2]. A variety of methods have been used for treatment, namely, prophylactic medication, angioplasty, atherectomy, use of stents and bypass surgery. Bypass surgeries are used in the replacement of chronically blocked blood vessels by replacing them with vascular grafts.

In the kidney, the vascular system is involved in the removal of waste products such as creatine and urea from the blood. It is absolutely imperative for the elimination of such waste products to avoid adverse effects to the human body. At the same time, such elimination should be achieved in short periods of time. There are situations in which the kidney fails and the elimination of such waste

products becomes very difficult for the human body. Hemodialysis is, often, used for the removal of waste products in the case of such a renal failure. Hemodialysis is carried out using an arteriovenous fistula, an arteriovenous vascular access graft or a venous catheter[3]. The most common type of procedure involves the vascular access graft, in which, the vascular graft is used to connect the artery to the vein and is placed right under the skin[3]. Since the graft acts as a vein, it can be immediately used for needle placement and blood access during hemodialysis.

1.2 Anatomy of the human blood vessels [4]

The circulatory system in a human body can, generally, be divided into two major sections: the heart and the blood vessels. The fluid medium of transport for the exchangeable entities such as nutrients, gases, hormones, electrolytes, immune-system cells, etc., is called blood. The heart is the muscular organ which pumps the blood towards the tissues where exchange takes place. The conduits which carry blood are called blood vessels. These blood vessels can further be divided into three types: the arteries, the veins and the capillaries. The arteries generally carry blood from the heart towards the organs where exchange takes place. Most of the arteries carry oxygenated blood except for pulmonary and umbilical arteries. They are classified based on the size of the artery and the constituent layers present. The largest of the arteries are the Elastic Arteries. The pulmonary arteries, the aorta, and its branches generally constitute the elastic arteries. The next set of arteries is muscular arteries which are smaller in diameter than the elastic arteries. Apart from this there is not much difference in their anatomies. Some muscular arteries include the iliac artery, femoral artery, radial artery, renal artery, etc.

Elastic and muscular arteries, generally, consist of an inner layer called tunica interna (a.k.a intima), a middle layer of tunica media (a.k.a. media) and an external layer called tunica externa (a.k.a. adventitia). These layers not only act as barriers but also perform a vital function in maintaining homeostasis of the human body. The smallest type of artery is called the arterioles which basically consists of the intima and media. The major difference between arterioles and the other types of arteries is that there are only layers of cells present and no extracellular matrix. The veins are also classified similar to the arteries as venules, medium-sized veins and large veins. The major difference between the medium-sized and large veins and their counterparts in arteries is that the medial layer is thinner in veins. Capillaries are the smallest of the blood vessels situated the farthest away from the heart and this is where the (describe the exchange) exchange takes place. They are generally situated in major organs such as muscles, lungs, kidney and intestines. The blood vessels are further classified as systemic and coronary depending upon the delivery of blood. Systematic vessels transport blood to and from the organs in the body other than the heart. Coronary vessels transport blood to and from the various regions of the heart.

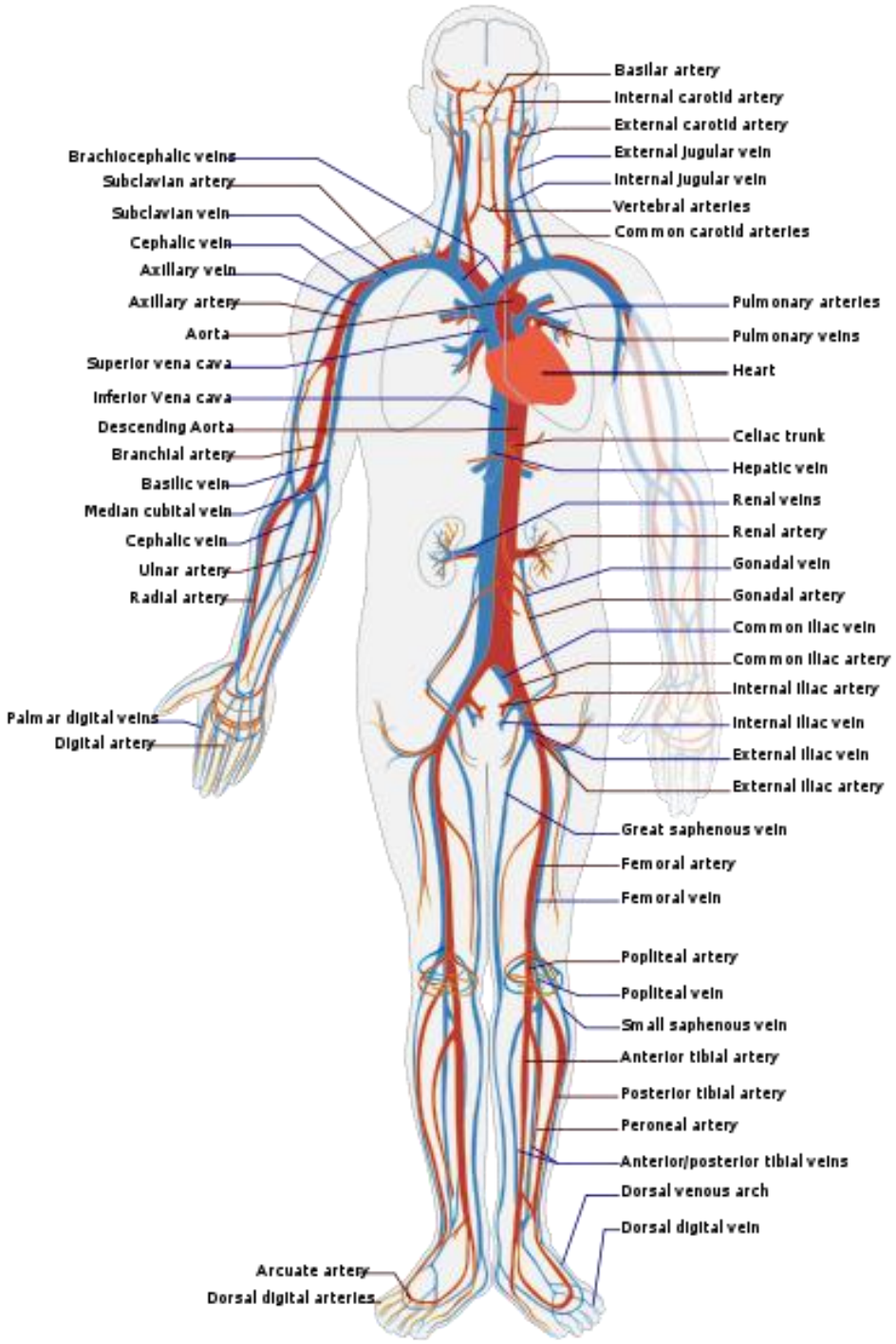

Figure 1.1: Human Circulatory System[4]

1.3 **Sections of an artery** [5]

1.3.1 Tunica interna (Intima)

Intima consists of the endothelium, the sub-endothelial layer and the fenestrated layer. The endothelium is a single layer of endothelial cells arranged longitudinally on a basal membrane parallel to the flow of blood. The function endothelium is to ensure hemocompatibility and to regulate blood pressure by vasoconstriction and vasodilation. It also produces nitric oxide (NO) which prevents occlusion and keeps the vessels patent (open). The sub-endothelial layer contains stellate cells (neurons and astrocytes with many dendrites) and connective tissue. This layer is a feature that is present only in large arteries. The third layer is a network of elastic fibers arranged principally in the longitudinal directions. Size of this layer is the largest in elastic arteries and decreases as the size of the arteries decreases. This layer also acts as a support to the underlying endothelium. Improper functioning of endothelium is a major factor causing occlusion leading to atherosclerosis.

1.3.2 Tunica media (Media)

Elastic and muscular arteries have a layer called the media which constitutes the bulk of the artery. The thickness of this layer is dependent on the size of the artery and the larger arteries have the thickest while the arterioles have pretty thin layers. This layer, generally, consists of smooth muscle cells (SMC) arranged concentrically (transversely) along with the ECM. The ECM consists of fibers such as collagen and elastin and proteoglycans (a.k.a glycosaminoglycans). The responsibility of this

layer is to aid in the transport of blood by the peristaltic movement by the contraction and the expansion of the SMCs based on various stimuli.

1.3.3 Tunica externa (Adventitia)

Adventitia is the outermost layer of the artery. It consists of longitudinal collagen fibers and fibroblasts (FB) embedded parallel to the fibers. The collagen fibers provide protection, support to the blood vessel by anchoring them to nearby organs and nutrient sustenance. The primary function of FB is to synthesize the ECM materials like collagen, elastin and glycosaminoglycans. In atherosclerosis, the thickening of the blood vessel is a common symptom and occurs due to the excessive production of ECM materials due to known factors (already listed in the previous section).

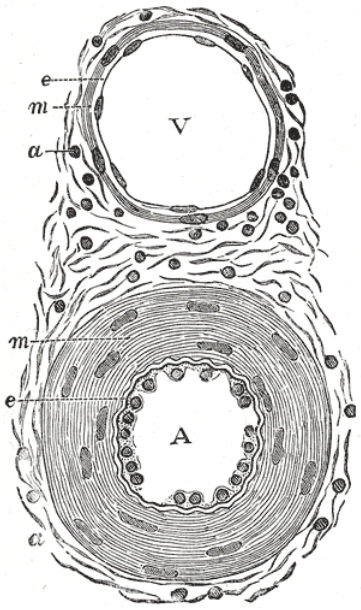

Figure 1.2: Section of an Artery (A) and Vein (V) from the mucus membrane of the epiglottis of a child: a-adventitia, m-media, e-intima. [6]

1.4 Components of the extracellular matrix

1.4.1 Collagen [7]

Collagen is a major structural protein of the human body found in abundant quantities in the connective tissue. It is synthesized by fibroblasts and secreted into the extracellular matrix (ECM). Collagen constitutes nearly 35% of the human protein content. There are at least 29 types of collagen identified in the human body till date out of which type 1 collagen is the most common. Some of the important types of collage and their locations in the human body are listed in Table 1.1. Collagen type I is present in scar tissue which is the end product of tissue healing by repair. Another important type of collagen is type III collagen which is present in granulation tissue. These fibers are also called reticular fibers and they are produced by young fibroblasts before the more rigid collagen type I. Some types of collagen are attached to the cell membranes through fibronectin and integrin.

The collagen molecule, the tropocollagen, is made up of three polypeptide chains arranged in a three-dimensional helical structure. Some of the major amino acids in the collagen molecule are glycine, proline, lysine, hydroxyproline and hydroxylysine. The content of these amino acids varies from one type of collagen to another. The precursor to tropocollagen, known as procollagen, is synthesized as a three-dimensional helical structure in the rough endoplasmic reticulum (RER) of fibroblasts through a series of steps. Then, the procollagen is transported to the golgi apparatus and secreted into the ECM by exocytosis. In the ECM, procollagen is converted into tropocollagen by procollagen peptidase and then assembled into cross-striated fibrils. This process is known as fibrillogenesis. Then, the self-assembled fibrils are further bundled to form collagen fibers.

Type	Location in the Human Body
I	Tendons, skin, blood vessel walls, endomysium of myofibrils, fibrocartilage, organic part of bones and teeth
II	Hyaline cartilage, Vitreous humor of eye
III	Granulation tissue, blood vessel walls, skin, intestines, uterus
IV	basal lamina, eye lens, part of the filtration system in capillaries, glomeruli of nephron in kidney
V	most interstitial tissue, placenta
VI	most interstitial tissue
VII	dermal epidermal junctions
VIII	some endothelial cells
IX	Cartilage
X	hypertrophic and mineralizing cartilage
XI	Cartilage
XIII	transmembrane collagen, basement membranes
XVII	transmembrane collagen
XVIII	source of endostatin

Table 1.1: Some types of Collagen and their location in the Human Body[7]

1.4.2 Glycosaminoglycans [8]

Glycosaminoglycans (GAGs) or mucopolysaccharides (MPS) are long chain sugars with disaccharide as the monomeric unit. Generally the disaccharide consists of hexose (a sugar with carbon atoms, a.k.a hexonic acid) and its corresponding amine, hexamine joined together by a C-O-C bond known as the glycosidic linkage. There are number of GAGs and they are found in ECM of various connective tissue. Table 1.2 lists some of the well-known GAGs and their location in the human body. GAG is a crucial structural component of the human body but also aids in brain development, health of eye and vision, blood coagulation, and lubrication. These GAGs combine with glycoproteins to form proteoglycans (PGs). These proteoglycans have the ability to attract and bind ions like sodium (Na^+), potassium (K^+) and calcium (Ca^+), and water (specifically, hydrogen (H^+) and hydroxide (OH^-)) moving through the ECM, thereby regulating the molecules moving through it. Due to this crucial property of bind water, glycoproteins give rise to the viscoelastic behavior of tissue under a load. Figure 1.3 illustrates some important cell-surface PGs and ECM PGs. Membrane proteoglycans either penetrate the plasma membrane or they are linked by a glycosylphosphatidylinositol anchor [9]. Some PGs are usually secreted into the ECM while some other PGs are cleaved and directly cast off from the cell surface into ECM [9]. Like collagen, GAGs and PGs are manufactured in the RER of fibroblasts, neurons, chondrocytes, osteocytes and lymphocytes.

Name	Monomer Unit	Location in the Human Body
Chondroitin sulphate	D-glucuronic acid and N-acetyl-D-galactosamine-4 (or 6)-sulphate	Cartilage, Bone, Heart valves
Dermatan sulphate	L-iduronic acid and N-acetyl-D-galactosamine-4-sulphate	Skin, Blood vessels, Heart valves, Tendons, Lungs
Keratan sulphate	galactose and N-acetyl-D-glucosamine-6-sulphate	Cornea, Cartilage, Bone, Central Nervous System
Heparin	L-iduronic acid-2sulphate and D-glucosamine-6-sulfate	Blood, Lungs, Liver, Skin, Sites of Tissue Injury
Heparan sulphate	L-iduronic acid-2sulphate and D-glucosamine-6-sulfate (have less sulphate groups than Heparin)	Blood, Lungs, Liver, Skin, Basement membranes, Sites of Tissue Injury and Vasculogenesis, Cell Surfaces
Hyaluronan	D-glucuronic acid and N-acetyl-D-glucosamine	Articular Cartilage, Skin, Epithelial Tissue, Neural Tissue Synovial Tissue, Vitreous Humor

Table 1.2: Major GAGs and their location in Human Body [8]

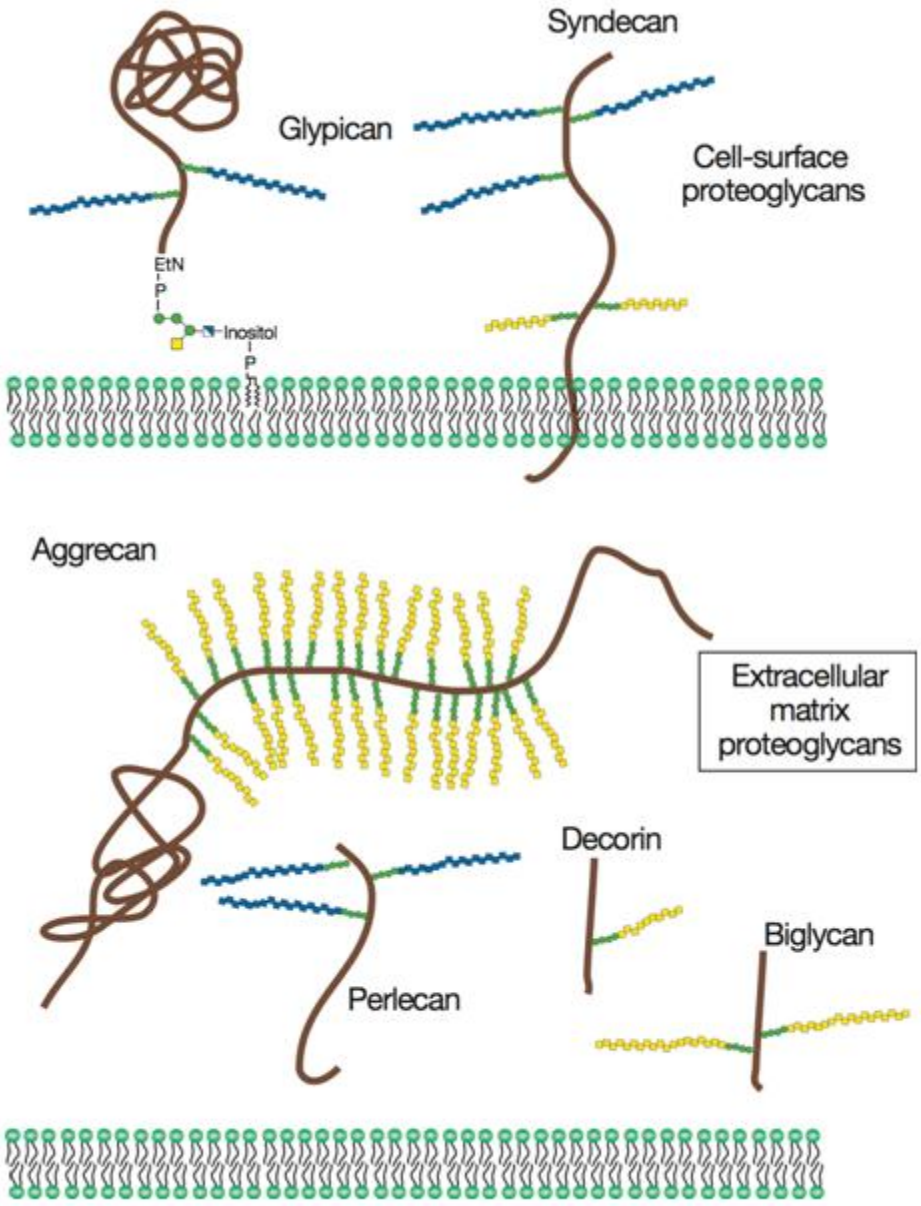

Figure 1.3: Proteoglycans consist of a protein core (brown) and one or more covalently attached GAG chains (blue: Hyaluronan Sulphate; yellow: Chondroitin Sulphate/Dermatan Sulphate) [9]

1.4.3 Elastin [10]

Elastin is the second major protein (after collagen) in the human body. It is the protein which imparts elasticity to connective tissue. It is found is various tissues of the human body such as blood vessels (mainly arteries), lungs, ligamentum nuchae, skin, urinary bladder, elastic cartilage, intervertebral disc over the sacroiliac joint. Of all the known locations of elastin in the human body, it is present in the largest amounts in the large elastic arteries. In these elastic arteries, there is a layer of elastin right below the intimal layer which is responsible for sustaining the pressure wave through the artery developed during the pumping of blood by the heart. The primary amino acids in the elastin monomer, tropoelastin, are glycine, valine, alanine and proline. Tropoelastin is synthesized in the RER of both fibroblasts and SMCs and secreted out of the cell into the ECM by exocytosis after packing at the golgi apparatus. Though tropoelastin is highly soluble in water, elastin is insoluble in water due to the crosslinking to form a strong network. There are two important crosslinkers in the case of elastin, desmosine and isodesmosine which are both modification of lysine and it is desmosine which imparts the yellow color to elastin fiber after crosslinking.

1.5 **Criteria for new materials or constructs for vascular grafts** [11-16]

1.5.1 Physiological requirements

1. Healing: Graft material should be capable of promoting healing or material should, at least, not hinder in healing.
2. Toxicity: Graft material should not be toxic to the host being.

3. Antigenicity: Graft material should not produce its own antigen which might affect the immune system of the host being.
4. Immunogenicity: Graft material should not produce any adverse immunogenic response inside the host cardiovascular system.
5. Oncogenicity: Graft material should not generate any cells which may be oncogenic or cancerous in nature.
6. Thrombogenicity: Graft material should not promote the formation of thrombus or blood clot.
7. Microbial Contamination: Graft material should be resistant to pathogenic infection.
8. Neointimal Hyperplasia: Graft material should not promote neointimal hyperplasia. Neointimal hyperplasia is an adverse condition in which the vascular smooth muscle cells from the adventitia of the vascular graft or native vessel migrate into the intima of the vascular graft thereby causing a thickening of the intima due to the detailed development of the extracellular matrix in the intima.
9. Other Physiological Requirements: The graft should be able to fulfill physiological requirements like vasoconstriction and vasodilatation. It should also be permeable to the movement of white blood cells.

1.5.2 Structural requirements

1. Fibrous: The basic structure of the graft material matrix is expected to be fibrous like the extracellular matrix.
2. Porosity: The graft material should be porous to promote the growth and movement of smooth muscle cells inside it.

3. Inclusion of Elastin: Researchers have shown that a missing path to a good vascular graft might actually be elastin and hence it should be included in the design.
4. Remodeling of Matrix: The graft material should promote alterations of the artificial extracellular matrix by the host cells.

1.5.3 Mechanical property requirements

1. Burst pressure: Vascular graft should have at least a burst pressure of 1700 mmHg. The burst pressure of the saphenous vein is approximately 1680 mmHg. It would be advisable to design grafts with strength over this limit as to avoid the use of the saphenous vein during the bypass surgeries.
2. Compliance: The graft must be compliant and elastic so that it is able to withstand the forces generated due to the blood flow to avoid formation of kinks. Compliance mismatch between the graft and the native vessel can cause adverse effects leading to occlusion as discussed in the earlier section.
3. Fatigue Resistance: The graft should be capable of withstanding 30 days of *in vitro* cycling of systemic flow without noticeable radial dilation.
4. Suturing: The graft material should be able to withstand the force exerted during and after suturing it to the native vessel. It should also promote easy suturing.

1.5.4 Manufacturing requirements

1. The graft should, preferably, be not synthesized in a complicated process so that it can be easily reproduced with the same accuracy.

2. The graft should have a short time for fabrication.
3. The graft should be producible in different sizes, i.e., diameter and lengths.
4. The graft, after production, should not require any extreme storing procedures.

1.5.5 Optional requirements

1. The graft should be capable of local drug release.
2. The graft should be of low cost.

1.6 State-of-the-art vascular graft technology

1.6.1 Types of vascular grafts

It appears that there are at least 35 patents for artificial blood vessels from the last 30 years [17]. Although these implants have had varying levels of accomplishments, none of them are close to satisfying all the requirements of the product [17]. Current materials for vascular grafts can be broadly classified into three categories based on graft size, construction and materials [18]. Further, the types of materials being used are either autologous, synthetic or bio-inspired [17]. Generally, grafts fall under three categories based on their size: large (7-30+ mm), small (6 or less mm) and coronary artery (1-4 mm) [18]. Table 1.3 lists all the types of vascular grafts being used today. In the following paragraphs we shall discuss the advantages and disadvantages of using the "State-of-the-Art" grafts and materials available today. Ideal properties of a vascular graft, generally, include a

wide variety of features encompassing strength, viscoelasticity, biocompatibility, hemocompatibility, and bio stability [19].

1.6.1.1 Autologous Grafts

The arteries or veins from the patient are the first choice for implantation. Though these are the best choice, in many cases, these vessels remain unavailable for implantation since they are diseased or were used in previous surgeries [20]. These grafts generally possess excellent biomechanical properties similar to the host vessels to be replaced. Patency or occlusion is defined as the state of quality of being open or unblocked. William Edwards [21] reported that the autologous saphenous veins generally have about 65% more patency than a glutaraldehyde tanned human umbilical cord vein first proposed by Dardik et al in 1979 [22]. There have been other instances, too, when these vessels failed to remain completely patent after implantation after a certain period [23]. These grafts readily replace small diameter blood vessels (<6mm) and coronary arteries (1-4 mm) [18].

1.6.1.2 Synthetic Grafts

In the absence of autologous grafts, synthetic grafts are the foremost choice for vascular implants [20]. Some of the commonly used synthetic grafts include extended-Polytetrafluoroethylene (e-PTFE) and Polyethylene terephthalate (Dacron). Synthetic grafts possess some very good properties making them the most used grafts during bypass surgeries [17]. They are as follows:

1. Simplicity of fabrication,
2. High control over properties of the bulk material,
3. Easy procurement,

4. Adaptability,
5. Excellent load bearing capacity of the bulk material,
6. Low probability of bacterial or viral contaminations,
7. Low possibility of antigenicity due to the relative inertness of the material in large diameter applications, and,
8. Rapid transmural-transanastomotic endothelialization in certain synthetic grafts [24, 25].

The following are some important drawbacks which arise due to the use of synthetic grafts:

1. Failure of graft material (particularly e-PTFE and Dacron) due to modulus mismatch and compliance mismatch resulting in intimal hyperplasia and thrombogenicity [16, 17, 23],
2. Higher occlusion rates in small caliber vascular grafts (particularly e-PTFE and Dacron and some polyurethane-based) due to failure of formation of endothelial layer either [16]
    a. from movement of cells from host native vessel to the graft at the site of suture, i.e., transmural-transanastomotic endothelialization, or,
    b. from fall-out cells from the blood stream, i.e., blood-borne endothelialization.
3. Improper healing due to the same reasons abovementioned.

Polyurethane-based grafts have reportedly been unstable due to one or more of the flowing reasons:

1. Hydrolysis in acidic or basic conditions [26],
2. Enzymatic attack [27],
3. Oxidative environment [27],
4. Stress [27],
5. Lack of porosity [17],
6. Poor attachment at the anastomotic site [28], and,

7. Thrombogenicity due to poor-run off or distal blockage [29].

In spite of these reasons, what baffles many researchers is that e-PTFE still remains to be one of the most sought-after vascular grafts today [16, 17].

1.6.1.3 Bio-inspired vascular grafts

With the increase in the number of subjects with failed synthetic implants, researchers have turned to an idea of mimicking the physiological systems, a process simply known as biomimicking. This has improved not only the design of the vascular graft but has also added a number of qualities to it, which makes the bio-inspired vascular graft superior to the synthetic vascular graft. Bio-inspired vascular grafts are better than synthetic grafts for the following reasons:

1. Lower occlusion rates and neo-intimal layer formation [30],
2. Good endothelialization of the inner surfaces [30],
3. Degrades and promotes tissue growth inside and around it [31-34], and,
4. Use of natural materials like collagen, elastin, chitosan, fibrin, etc., in as constructs leads to lesser rejection of implants.

In spite of the superior qualities of these bio-inspired materials, researchers have pointed out certain important aspects due to which these materials fail as vascular graft prostheses. Some of them are as follows:

1. Some biodegradable materials are either too fast ("premature") or too slow in degradation leading to undesired results. [17]
2. Some materials have shown very slow cell in-growth rate. [33]

3. Since there have been no human trials with biodegradable vascular grafts, there is no *in vivo* data available which may help us improve the designs.

Generally bio-inspired grafts can be broadly classified under three groups:

1. Tissue Engineered Grafts
2. Bio-hybrid Grafts
3. Biodegradable Grafts

S.No.	Type	Subtype	Example
1	Autologous	Artery	Internal Mammary, Iliac, Right Thoracic
		Vein	Saphenous
2	Synthetic	Woven and Knitted	Dacron
		Extruded	E-PTFE
		Polyurethane (PU)-Based	Polyester Based PU, Polyether based EU, Polycarbonate based PU
		Electrospun	PLG-PLA, PEO-PLA
3	Bio-Inspired	Tissue Engineered	Cellular and Acellular
		Bio-Hybrid (Combination of Synthetic and Natural)	Composites, Collagen-based
		Biodegradable (Synthetic or Natural)	PLG-PLA, PDO-Elastin, PEO-PLA

Table 1.3: State-of-the-Art Blood Vessel Replacements [17, 18]

1.6.2 Tissue engineered vascular grafts

One of the most essential features of tissue engineering is the ability to imitate the ECM constructs that physically support and direct cell behavior. The ECM contains specific biomolecules which are used to provide information to the cells present in the ECM through biochemical and biomechanical stimulations. With sufficient knowledge about the effects of these biomolecules present in the ECM on the fundamental cell processes and how they contribute to the biomechanical and structural deformations of the ECM, new and improved constructs can be designed for tissue repair and replacement. Researchers in the past have not only used natural materials but also synthetic materials in designing vascular grafts. Tissue engineering not only allows us to mimic natural ECM but also fine tune biomechanical, biochemical and micro-structural properties of constructs. This section discusses the design, the synthesis and the properties of tissue engineered materials which have been proposed for development into vascular grafts and some of the well-known tissue engineered grafts.

1.6.2.1 History

In this section, we shall discuss the design, synthesis and properties some of the famous vascular grafts from the last few decades when tissue engineering for vascular grafts evolved. Table 1.4 enlists some the finest examples of tissue engineered vascular grafts and materials synthesized for their design in detail.

Weinberg and Bell [35] were the first set of researchers to demonstrate that porcine skin collagen can be reconstituted *in vitro* and cast in the form of a tube inside an incubator at 37°C for 1 week. The vascular graft design involved the formation of two layers, an inner layer of collagen mixed with

bovine aortic SMCs and an outer layer of collagen mixed with bovine aortic fibroblasts. There was a layer of Dacron sheet in between the inner and the outer layer suspended to offer mechanical support to the tube. The tubes were also coated with bovine aortic endothelial cells (EC) by injecting a suspension of the ECs into the lumen and the tube was rotated about the flow axis at 1 rev/min for a week. Some tubes without the ECs were mechanically tested yielding a burst strength of 100 mmHg. Though the model did not include elastin during synthesis, this model was able to demonstrate some important results, namely;

1. collagen can be casted into tubes along with SMCs and ECs harvested earlier;
2. the secretion of elastin by the SMCs over longer periods of culture; and
3. the orientation of collagen and the SMCs toward the longitudinal axis of the tube.

After Weinberg and Bell, there have been some significant advances made in the field of tissue engineering vascular grafts. L'Heureux et al [36] successfully demonstrated the first bioreactor method of tissue engineering a vascular graft. In this method, they used cellular sheets of human umbilical SMCs and human skin FBs as the medial and the adventitial layers. They used a non-pulsatile semi-perfusion flow in the bioreactor which produced shear stresses and radial distention for 3 months. They also seeded ECs in the vessel lumen. This process produced a small-caliber vascular graft with three distinct layers, a high burst strength of 2300 mmHg and ECM proteins like elastin. The authors report that implantation in dogs also produced desired results. Later in 2006 [52], they improved the model with a similar bioreactor process. The burst strength increased to 3500 mmHg after maturation for 4 months. The main difference with the graft from 1998 was that the graft in 2005 had a decellularized medial layer. They extended their implantation studies to nude rats and primates. The one point of concern for this model is that the compliance was about 1.5%, one-third of the native artery [37-39].

Tranquillo et al [40] were the first ones to demonstrate that the orientation of the collagen I fibers can be controlled and aligned using a strong magnetic field during fibrillogenesis. Murine aortic SMCs were isolated and added to the collagen Pre-gel mixture. This SMC-collagen Pre-gel mixture was then gelled inside a special polycarbonate mold which rotated once every 5-10 minutes under the presence of a strong magnetic field. The total incubation time varied from about 1.5 hours to 5.5 hours depending on the magnetic field alignment and the initial SMC concentration. They were able to ascertain the orientation of the fibers and cells by double refraction. They found the mechanical properties of the medial equivalent material varied drastically with the variation of the aforementioned parameters. With the increase in the orientation, the stiffness of the material increased while creep decreased in the circumferential direction of the vascular graft. They also found that due to the magnet alignment of the collagen fibers and SMCs, the vascular graft material was able to compact faster and resist swelling due to internal pressure.

Niklason et al [41] developed a graft from a biodegradable polyglycolic acid (PGA) scaffold which was cultured for two months in a bioreactor, under pulsatile radial stress, after been seeded with bovine aortic SMCs and ECs. This work established the effects of dynamical stresses on the remodeling of vascular grafts. The burst strength was in excess of 2000 mmHg and the suture retention force of over 90g. The SMCs were able to produce collagen and replace it in place of the degraded PGA fibers. The vascular graft was also able to respond to chemoattractants by contraction and remained patent up to 90% after a month of implantation in a porcine model.

Berglund et al [42] demonstrated the use of crosslinking methods on improving the mechanical properties of a tissue engineered vascular graft. They strengthened collagen I gels with a glutaraldehyde or ultraviolet or dehydrothermal crosslinked biological supports. A two-layer

approach was adopted by the authors, in which the inner layer was the cross-linked layer of collagen I while the second layer was collagen I seed with neonatal human dermal FBs. Later they seeded the lumen with human coronary ECs. They reported substantial changes in the biomechanical properties of the uncross-linked grafts and the cross-linked grafts, particularly the burst strength improved from 100 mmHg to 650 mmHg.

Roeder et al [43] performed uniaxial tensile tests on COL gels with varying concentrations and pH. They incubated the COL gels in dog bone-shaped molds procuring gels suitable for uniaxial tensile testing. They found that all COL gels had a characteristic tensile test stress-strain curve. They identified three distinct regions in the curve and named them toe, linear and failure region. They found that on an average these gels had a linear modulus of about 30 kPa, a failure stress of 10 kPa and a failure strain of 90%. They reported that acidic pH would produce fibrils of greater diameter than basic pH while basic pH would produce fibrils of greater length than basic pH. They did the fibril diameter measurement by confocal microscopy. They have also reported that the increase in concentration and pH showed an increase in the mechanical properties.

Table 1.4: Tissue Engineered Vascular Grafts-Synthesis Techniques (Arranged Chronologically)

	Reference	Cells	Scaffold	Burst Strength	Maturation Period	Major Observations
1	[35]	Bovine aortic SMC, EC and adventitial FC	Collagen gel supported by Dacron mesh	100 mmHg	3 weeks	Feasibility of generating triple layered structure with collagen
2	[44]	Canine jugular vein SMC and EC	Collagen gel supported by Dacron mesh	NA	NA	Implanted in canine models; Higher SMC seeding and lower initial collagen concentration induced more rapid and prominent shrinkage
3	[36]	Human umbilical vein SMC and EC and human skin FC	None	2300 mmHg	3 months	Non-pulsatile semi-perfusion producing shear stresses and radial distention; No Scaffold to start with, use a cell seeded membrane

4	[45]	Polyester Graft cross-linked with gelatin	NA	NA	NA	Canine Bilateral carotid–femoral implantation; Biochemical analysis done by FTIR to study the effect of length of implantation
5	[41]	Bovine aortic SMC and EC	Polyglycolic Acid	2000 mmHg	2 months	Pulsatile producing radial stress; Effects of dynamical mechanical stresses
6	[46]	None	Collagen-Silicone Composite tubes	NA	NA	Grafts were treated with Triton X-100, Neutralized Ovine Skin Collagen I, Heat-Denatured Ovine Skin Collagen I, Bovine Gelatin, Sheep Serum, Bovine Serum Albumin, Dexamethazone and heparin to study the various biological responses imparted after implantation.

7	[47]	Adult Rat Aortic SMC	Collagen I gels	NA	8 days	Pulsatile dynamic conditioning at 10% strain from 4-8 days; Cells were by attaching the collagen gel with cell seeded Silicon tubes dipped with Collagen I and Chitosan
8	[48]	Ovine carotid artery myofibroblasts and EC	Polyglycolic Acid coated with P4HB (Human Gene)	300 mmHg	1 month	Pulsatile profusion in the lumen producing shear stresses and pressure indicated by the flow; Effect of pulsatile flow studied
9	[49]	Aortic rat SMC	Fibrin	NA	NA	Fibrin stimulates collagen production by SMC
10	[50]	Adult Human Aortic SMC	Collagen Gels	NA	2 months	Effect of Ascorbic and Retinoic Acid were studied. Biochemical analysis helps understand biomechanical properties and changes.

11	[42]	Neonatal human dermal FC and human coronary EC	Collagen gel supported by cross-linked collagen film	650 mmHg	NA	Feasibility of cross-linked collagen to support gels
12	[51]	Rat Aortic SMC	Collagen-Fibrin Gel	NA	NA	TGF-β strongly inhibited cell proliferation and increase SMA expression especially in the presence of mechanical strain
13	[52]	Ovine Umbilical SMC from near-term fetal lambs	Fibrin Tubes	NA	2 Weeks	Effect of aprotonin concentration variation, thromboxane and endotheline was studied; Similarity to collagen-elastin scaffold in vascular remodeling and fibrogenesis have been reported.

14	[53]	Rabbit SMC	Poly(lactide-co-caprolactone)	NA	NA	Pulsatile profusion in the lumen producing shear stresses and pressure indicated by the flow; Rubber-like scaffold beneficial in delivering mechanical signals to cells
15	[54]	Human umbilical vein SMC	Bovine Achilles Tendon Collagen I and Equine Ligamentum Nuchae Elastin gels crosslinked with EDAC/NHS	NA	2 weeks	Dynamic conditioning stimulates SMC to orient collagen fibers in the direction of force

16	[55]	Human umbilical vein SMC and EC and human skin FC	None	3500 mmHg	4 months	Non-pulsatile semi-perfusion producing shear stresses and radial distention; Implanted in Canine, Nude Rat and Primate Models; No Scaffold to start with, use a cell seeded membrane. Decellularized medial layer. Abundant elastin production has been reported.

17	[56]	NA	Pullalan-Dextran Hydrogels with acellularized Wistar rat aorta tubes attached to the ends	NA	NA	Implanted in Wistar Rats Models as a replacements for abdominal aorta; Polysaccharide gels capable of withstanding pressures and remain patent under physiological conditions; *in vivo* cell colonization and vascular reconstruction observed
18	[57]	New Born Wistar Rat Cardiac EC, Vena Cava SMC and Bladder SMC	Porcine Collagen Membrane cross-linked with Glutaraldehyde	NA	7 days	Rat inferior vena cava completely regenerated from cell-seeded collagen absorbable guide in 12 weeks and smooth surface due to cell seeding caused less thrombosis

19	[58]	None	Salmon Collagen gels ethanol shrunk and cross-linked with EDAC	1500 mmHg	1 day	Implanted in Wistar Rats Models Collagen gels were dehydrated in ethanol and then cross-linked with EDAC. No Cells have been used. No adverse biological effects were seen during and after implantation in rats.

1.6.2.2 Improvement of Biomechanical Properties by Cross-linking

Since the first demonstration of a COL construct for a vascular graft various researchers have used cross-linkers like glutaraldehyde [59], formaldehyde [59], carbodiimides [60], succinimides [60] & physical treatments methods including ultraviolet radiation [59], freeze-drying [59], heating during the process of COL gel formation [59]. This has allowed them get COL constructs with better mechanical properties and better cell-adhering capabilities. Other researchers [61-63] have all studied the effect of cross-linkers on the COL gel and their mechanical properties. Orban et al [61] demonstrated vascular graft material crosslinked with transglutaminase which had 30 mmHg higher burst pressures than pure COL graft. Gildner et al [62] reported a 5-fold and a 13-fold increase in the ultimate strength and the toughness of the COL gels when they were cross-linked by polymerizing fibronectin along with the gels. They reported that the GAGs increased the strength

and toughness while the fibroblasts decreased it. Osborne et al [63] studied the effect of cross-linking agents like the water-soluble 1-ethyl-3-(3-diaminopropyl) carbodiimide (EDAC), and 1,1-carbonyldiimidazole (CDI), on COL gels with and without chondroitin sulphate and GAGs. They reported that the addition of chondroitin sulphate and GAGs to the COL gel and cross-linking the COL gel with EDAC and CDI increased the ultimate strength and modulus. They however suggested that the CDI would inhibit the infiltration and proliferation of FBs.

1.6.2.3 Chitosan [64]

Chitosan is a linear long chain sugar composed of D-glucosamine (deacetylated unit) and N-acetyl-D-glucosamine (acetylated unit) distributed arbitrarily. It is commercially manufactured by deacetylation of chitin, which can be obtained from the exoskeleton of crustaceans like crabs, shrimps, etc. Since chitosan has an acid dissociation constant of about 6.5, it is positive charged and dissolves in acidic to neutral solutions. The amount of dissolutions depends up on the pH of the solvent and the degree of chitin deacetylation. Chitosan closely resembles mammalian GAGs and hence has been a preferred substitute for GAGs due to the ease of availability, ease of production and better biomechanical properties. Due to the cationic nature of chitosan, it can attract anions and water thereby contributing to the mechanical properties of the scaffold.

Over years of research, chitosan has developed into one of the favorite materials in tissue engineering of vascular grafts because it promotes bioactivity due its high biocompatibility with mammalian cells. Zhu et al [65] used a chitosan/heparin complex bound to the inner lumen of an e-PTFE graft which promoted reduced platelet adhesion and longer duration of good patency in a canine model. Chupa et al [66] demonstrated that a GAG-Chitosan scaffold controlled SMC and EC

migration and proliferation. They also reported that these scaffold promoted their attachment to the scaffold which in turn reduces the risk of and SMC hyperplasia and incomplete endothelialization leading to intimal hyperplasia. Okamoto et al [67] and Mori et al [68] have demonstrated the promotion of migration of fibroblasts by chitosan and hence improved healing.

Tan et al [69] studied the potential nature of the collagen-chitosan as a bioengineered vascular scaffold. They found that the scaffold was stable under pulsatile flow and the matrix integrity improved with the concentration of chitosan in the scaffold. They also reported the influence of chitosan on the crosslinking and the pore size of the collagen matrix. They demonstrated that the decrease in the proliferation and increase in the cytokine activity of K562 cells was influenced by the increase of chitosan in the scaffold. Hence, the superior properties of chitosan, as shown by other researchers [65-69], have given it a boost as a potential component of the vascular graft scaffolds.

1.7 Necessity for a new vascular graft

We have already discussed the various issues associated with present day vascular grafts in section 6 of this chapter. Here, we summarize, not going into details, some of the key problems associated with the graft which is of importance to this study. These reasons justify the selection of materials and the methodology for the development and characterization of a new vascular graft material.

1.7.1 Small caliber grafts

Small caliber grafts are vascular grafts with an inner lumen diameter less than 6mm. Most tissue engineering today is concentrated around designing a suitable vascular graft for replacement of small

arteries like the coronary arteries in bypass surgeries. Large arteries can easily be replaced by the saphenous vein and synthetic grafts like e-PTFE and Dacron. Since there are not many commercially available grafts for small caliber vessel replacement, there is a necessity to design a graft for less than 6mm inner diameter.

1.7.2 Occlusion

Occlusion is the failure of a vascular graft to remain open. For good functioning of the graft as the replacement to a blood vessel, it is necessary for the graft to remain patent, i.e. open, after implantation. It is reported [16] that higher occlusion rate is due to two important reasons.

1.7.3 Compliance mismatch

This is due to the difference in the mechanical properties of the graft and the target vessel at the site of suturing.

1.7.4 Improper healing

Another factor which influences occlusion is the healing of the graft at the site of suturing. This is contributed by the construct-cell interaction at the site of anastomosis. The abovementioned compliance mismatch also contributes to improper healing by inhibiting cell migration at the site of anastomosis.

1.7.4.1 Long time of manufacture

The average time of synthesis of a tissue engineered graft has been around 6-8 weeks, since most Sresearchers prefer a long time of maturation in a bioreactor. This increases the risk for patients who may urgently require a vascular graft for bypass surgery or hemodialysis.

1.8 Conclusions

Currently, there are no good designs for small caliber grafts (diameter < 6mm). Higher occlusion rates are reported due to compliance mismatch and improper healing. The time of synthesis of present day grafts is to be reduced to improve the accessibility and availability of these grafts to heart and kidney patients. Hence, it is necessary to design, develop and characterize a new material with suitable biomechanical properties and cellular compatibility.

CHAPTER 2

EVALUATION OF COMPOSITION AND CROSSLINKING EFFECTS ON COLLAGEN-BASED COMPOSITE CONSTRUCTS

Abstract

Vascular grafts are widely used for a number of medical treatments. Strength, compliance, endothelialization and availability are issues of most concern for vascular graft materials. With current approaches, these requirements are difficult to satisfy simultaneously. To explore an alternative approach, the present study has engineered the collagen gel construct by incorporating mimetic components and crosslinking the construct with different crosslinkers. The effects of component additives, such as chitosan and elastin, have been evaluated in terms of their mechanical and biological properties. Results demonstrate that the incorporation of chitosan and/or elastin alter stress-strain curves in the low stress loading region, and significantly improve the stretching ratio and ultimate stress of gel constructs compared to collagen constructs. Electron microscopy results suggest that the mechanical improvements might be due to microstructural modifications by chitosan sheets and elastin fibers. The effects of crosslinkers, such as formaldehyde, genipin and ethyl-(dimethyl aminopropyl) carbodiimide hydrochloride (EDAC) have also been evaluated. Results demonstrate that formaldehyde, EDAC and genipin employ different mechanisms to crosslink collagen-based constructs, and use of genipin as a construct crosslinker exhibits improved elongation and endothelial coverage as compared to formaldehyde and EDAC. In addition, extending gelation time increased the elastic modulus but not the ultimate strength. Therefore, this

study suggests that the mimicry of natural vessel tissues with properly crosslinked biopolymer composites could be a potential material design strategy for vascular graft materials.

2.1 Introduction

Vascular grafts are widely used for a number of medical treatments including bypass surgery for atherosclerosis and vascular access for hemodialysis. Often these vascular grafts are made up of synthetic polymers such as expanded polytetrafluoroethylene (e-PTFE) and Dacron (polyethylene terephthalate) [70]. Though these inert, stiff polymeric grafts successfully replace large arteries, problems arise with small-diameter (< 6mm) vessels resulting in high occlusion rates [23, 71]. Major pathogenic factors leading to occlusion include compliance mismatch [16, 23] and lack of endothelialization [16, 72]. Alternatively, native blood vessels such as saphenous veins have been used. For many patients such as those with diabetes complications, these veins are not suitable for implantation. In the past two decades, many new approaches including tissue-engineered blood vessels and compliant synthetic materials such as polyurethane have emerged. In particular, tissue engineering approaches, which induce cells to produce collagen, elastin or other matrix components, have evolved into a highly promising strategy to address complications associated with current grafts [55]. Several obstacles still must be overcome before this enormous engineering feat can be realized. Most concerned are clinical-related issues including time and efforts involved, possibility of contamination and quality control over the long course of *in vitro* production [55]. Thus, an alternative approach to achieving proper strength, compliance and endothelialization for vascular structure could involve engineering biopolymer materials to mimic structural, mechanical and biological properties of natural vessels. The present study explored this approach by employing multiple equivalent

components of the vascular extracellular matrix (ECM) to construct vessel substitutes and different types of crosslinkers to strengthen the constructs.

Collagen type I is the most abundant protein in the human body where it constitutes the majority of the ECM and is the essential structural and mechanical building block of various physiological systems. Collagen has many advantages including its high density of the RGD sequence and other functional sequences for cell adhesion and cell differentiation [51, 69, 73]. The ability of collagen to polymerize into a three-dimensional fibrous matrix makes it an appealing material for extensive therapeutic applications including medical implants [53, 74-76]. However, collagen matrix constructs lack desired mechanical properties for vascular grafts [77]. Hydrated reconstituted collagen matrices are mechanically weak and stiff [43, 63, 77, 78]. They thus need to be modified for high compliance and elongation as vessel substitutes and be strengthened to be ready for *in vivo* use. The ECM of natural vessels is a collagen-based composite consisting of fibrous proteins such as collagen and elastin, and proteoglycans containing long chain polysaccharides, glycosaminoglycans (GAGs). GAGs such as chondroitin-6-sulphate play an important role in tissue elasticity and interacting with functional proteins [63, 78, 79]. Chitosan or "poly D-glucosamine", a natural polysaccharide, is characterized by excellent biocompatibility and structural similarity to gags. Our prior study used chitosan in conjugation with collagen to make constructs that can control cell growth [69]. Additionally, elastin is another indispensable component contributing to high elasticity in natural vessels and engineered vessels [13]. Solubilized elastin is able to markedly promote elastin synthesis and tissue regeneration [80, 81]. Thus, if properly bound, addition of elastin and/or GAG-equivalent components into the collagen matrix is expected to increase compliance and elongation as well as biological properties.

To increase collagen strength, two strategies are generally implemented - crosslinking [78, 82, 83] and reinforcement [51, 69, 73]. Crosslinking involves the use of physical or chemical crosslinkers such as glutaraldehyde [84, 85], formaldehyde [85-87], N-ethyl-*N'*-(3-dimethyl-aminopropyl) carbodiimide hydrochloride (EDAC) [63, 82], and genipin [78, 88]. These crosslinkers form covalent bonds between characteristic chemical groups on biopolymers. Reinforcement involves the addition of mechanically stronger components to the collagen matrix [73]. This process, if precisely controlled, might increase the ultimate strength of the matrix. The main advantage of using crosslinking or reinforcement to gain mechanical strength is reducing the manufacture time required for a strong vascular graft. Previous studies often used one crosslinker or one reinforcement component, and thus the relative potentials of these matrix-strengthening approaches are not known. Comparative studies to evaluate the efficiency of different approaches in terms of their capability of strengthening collagen-based constructs and inducing cytotoxicity are critical to future studies and use of collagen materials in various biomedical applications. To this end, the present study has investigated mechanical, structural and biological properties of the materials that are constructed from mixtures of collagen, chitosan and/or elastin, and are crosslinked with EDAC, formaldehyde or genipin, in order to evaluate their potentials in vascular graft applications.

2.2 Materials and methods

2.2.1 Synthesis of collagen-based gel constructs

All types of experimental collagen-based constructs were prepared in dog-bone shaped molds which were designed by modifying the ASTM D638-03 standard. The whole design was scaled down by

half. Two strips of polyurethane mesh were placed at both ends of the mold to improve gripping. All collagen-based gel constructs were prepared at 3.0 mg/ml collagen concentration. Denatured rat tail collagen (type I) in 0.02N acetic acid (pH 4.0) at 9 mg/ml (BD Biosciences Inc., San Jose, CA) was transferred to a tube. Then, 10X Hank's balanced salt solution (HBSS) containing phenol red and 0.1 M sodium hydroxide were added to the collagen solution. The pH of the pre-gel mixture was adjusted to 7.3. Finally, the mixture was finally topped off with 1X HBSS to achieve the desired volume. The final mixture was poured into molds with care to avoid bubble formation. To further remove bubbles which influence mechanical properties by introducing void defects and high variations in gel constructs, the pre-gel solution was placed at room temperature for five minutes before it was transferred into the incubator. Finally, the molds were transferred into a cell culture incubator at 37°C to initiate gel formation.

Chitosan (Molecular Weight = 100,000-300,000 g/mol, 90% deacetylation, Milan Panic Biomedicals Inc., Solon, OH) was dissolved in 1% acetic acid resulting in a chitosan suspension of 10 mg/ml concentration with a viscosity of 2000-3000 mPa.s. The elastin suspension was prepared by suspending elastin (Elastin Products Co., Owensville, MI) in 0.2 M Tris solution (pH 8.8) with Triton X100 surfactant, which was followed by filtering and washing the elastin suspension with 0.2 M Tris solution (pH 8.8) without surfactant. The elastin solution was finally resuspended in 0.2 M Tris solution at a concentration of 20 mg/ml. Preparation of all the pre-gel mixtures of various collagen-based constructs, including collagen (COL), collagen-chitosan (COL-CHI) and collagen-chitosan-elastin (COL-CHI-ELN), followed a similar procedure as explained above. The samples for mechanical, chemical, structural and biological characterization underwent gelation for 3 hours. The final concentrations of the collagen, chitosan and elastin in the collagen-based constructs were 3 mg/ml, 3.5 mg/ml and 7 mg/ml, respectively.

2.2.2 Crosslinking of collagen-based gel constructs

After gelation, the constructs were removed from the molds and placed in a crosslinker bath for 5 hours to promote crosslinking by diffusion. The COL, COL-CHI and COL-CHI-ELN constructs were crosslinked with 10 mg/ml EDAC (Sigma Aldrich Inc., St. Louis, MO), 4% formaldehyde (Mallinckrodt Baker Inc., Phillipsburg, NJ) or 10 mm genipin (Wako Chemicals USA Inc., Richmond, VA). These concentrations of the crosslinkers chosen for this study have been commonly used in literature [89-91]. After crosslinking, all the constructs were retrieved and stored in 1X Dulbecco's Phosphate Buffered Saline (DPBS). Constructs crosslinked with genipin exhibited greenish-blue color while other crosslinkers did not cause any color changes.

2.2.3 Fourier transform infrared spectroscopy for biochemical characterization

Uncrosslinked and crosslinked COL, COL-CHI and COL-CHI-ELN constructs were frozen in liquid nitrogen (~195°C), following which they were dried in a critical-point drying chamber (Labconco, Kansas City, MO) for approximately 48 hours. The biochemical compositions and the crosslinking mechanisms were studied using an attenuated total reflectance Fourier transform infrared (FTIR-ATR) spectrometer, Nicolet 4700 (Thermo Fisher Scientific Inc., Waltham, MA). Comparisons were made between samples and pure collagen constructs to study the effect of various matrix components and the effect of crosslinkers. OPUS software (Bruker Optik gmbh, Ettlingen, Germany) was used to find the peaks and to calculate the areas under the peak.

2.2.4 Uniaxial tensile testing for mechanical characterization

All of the experimental gel constructs were subjected to uniaxial tensile tests employing the same testing protocol. An MTS Insight electromechanical testing system (MTS Systems Corp., Eden Prairie, MN) was used. Testing was performed in a 1X DPBS bath at room temperature. A special set of grips in delrin was used to avoid corrosion. One of the grips was loaded on the lower end of the instrument while the other grip was mounted under a 5 N load cell (MTS Systems Corp., Eden Prairie, MN) attached to the other end of the instrument. Samples were loaded and the dimensions of thickness, gauge length and width were measured using a vernier caliper. Only crosslinked constructs were tested at a strain rate of 1% per second. All the samples were tested until failure. The stress-strain curves were plotted for each of the samples to determine peak stress, strain at break and linear elastic modulus. These curves were fit with a 5th order polynomial using Matlab (MathWorks Inc., Natick, MA). With this fit data, the curvature of the stress-strain (σ-ε) curve was plotted against the strain. The curvature was calculated using the general curvature formula,

$$k = \frac{\left|\frac{d^2y}{dx^2}\right|}{\left(1 + \left(\frac{dy}{dx}\right)^2\right)^{\frac{3}{2}}}$$

where *k* is the curvature, *y* is the abscissa (stress - σ) and *x* is the ordinate (strain - ε). On the curvature-strain curve, the strain value at the largest local maximum was taken to be the transition point. Using the transition point and peak stress, the toe, the linear and the failure regions were determined. The toe region was characterized as the region on the stress-strain curve up to the

transition point. The linear elastic modulus was slope of the straight line fit in the region between transition point and peak stress. Data collected were statistically analyzed using the one-way ANOVA test. Student's *t* test was then used to compare the means of each individual group. The level of significance was set at $\alpha = 0.05$ for 95% statistical significance. Error bars on all the histogram charts represent the standard error of the mean (SEM) based on the total number of the samples.

2.2.5 Biocompatibility testing for biological characterization

Biocompatibility testing was performed on the experimental constructs using the Live/Dead Viability Kit (Molecular Probes-Invitrogen Detection Technologies, Carlsbad, CA) to determine the construct cytotoxicity. COL, COL-CHI and COL-CHI-ELN constructs were gelled and crosslinked directly in 24-well culture plates. In order to remove crosslinker residues, samples were washed thoroughly in 1X DPBS 4 times in addition to being stored overnight in 1X DPBS. Then, bovine pulmonary arterial endothelial cells (BPAECs) were seeded onto each of the gel samples and the empty wells of the cell culture plate were used as controls. After one-day culture, samples were washed thoroughly in 1X DPBS. Then, the stain from the cytotoxicity test kit, consisting of a mixture of calcein-AM (live cell stain) and ethidium bromide homodimer-1 (dead cell stain) in 1X DPBS was applied to each of the gel samples by following the protocol provided by the manufacturer. Finally, samples were imaged under a Zeiss Axiovert S-100 fluorescence microscope (100X magnification) and the images were captured with a Zeiss Axiocam camera (Carl Zeiss Inc., Thornwood, NY). Images were then analyzed using NIH ImageJ software to determine cell numbers.

2.2.6 Field emission scanning electron microscopy for structural characterization

Crosslinked COL, COL-CHI and COL-CHI-ELN constructs, gelled in polystyrene clone cylinders (11mm height x 1mm thickness x 2 mm in diameter), were frozen in liquid nitrogen (~195 °C) following which they were dried in a critical chamber for approximately 48 hours. These samples were sectioned parallel to the circular cross section. Then, they were examined using a field emission scanning electron microscope (FESEM, JSM-7401F, Jeol Ltd., Tokyo, Japan).

2.3 Results

2.3.1 FTIR-ATR characterization results showing the incorporation of component additives in collagen gel matrix and the effects of different crosslinkers

The characteristic peaks derived from the stretching vibrations of N-H_x (x=1, 2), O-H, C-H_y (y=1-3), C-O-C, C=O, and the bending vibrations of N-H, C-O-C, C-H, are exhibited in the FTIR spectra of various biopolymer matrices, as shown in Figure 2.1 and Figure 2.2. Areas under the peaks calculated by integration are presented in Table 2.1. Figure 2.1 demonstrates the spectrum of each matrix component and the spectra of the different types of collagen-based matrices, showing the incorporation of component additives. For the spectra of collagen (Curve 2.1A) and elastin (Curve 2.1C), two main typical peaks derived from amide I (C=O stretching at 1630 cm^{-1}) and amide II (N-H bending at 1550 cm^{-1}) are clearly present. For the spectrum of chitosan (Curve 2.1B), a strong broad peak attributed to the mixed stretching and bending vibrations of the C-O-C bond (1150 cm^{-1}-970 cm^{-1}) appears. The spectra of uncrosslinked COL-CHI (Curve 2.1D) and COL-CHI-

ELN (Curve 2.1E) can both be interpreted as linear combinations of the individual collagen, chitosan, and elastin spectra. With the additions of chitosan and/or elastin, both the absorbance frequencies and intensities of amide I and amide II shift slightly. Additionally, compared to Curve 2.1B, the C-O-C peak areas in Curves 2.1D and 2.1E have considerably decreased from 42.85 to 9.71 and 2.08, respectively, due to the addition of collagen and/or elastin. The addition of chitosan does not appreciably change the ratio of A_{N-H} (area of N-H bending) to $A_{C=O}$ (area of C=O stretching), while the addition of chitosan and elastin to the COL scaffold cause this ratio to change from 51.40 % in COL to 39.56 % in COL-CHI-ELN.

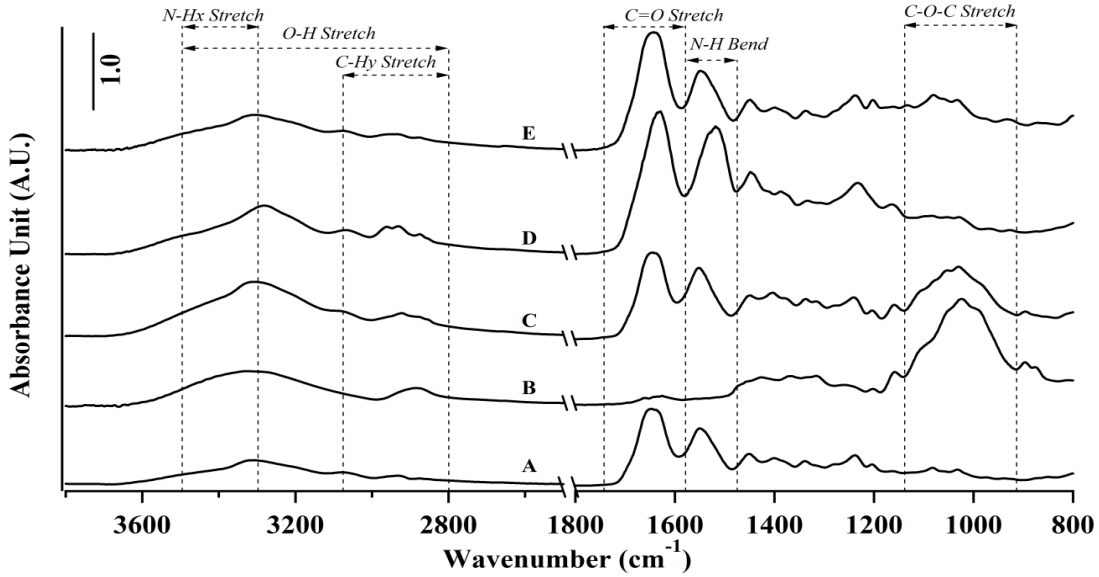

Figure 2.1: ATR-FTIR spectra for material comparison. (A) Uncrosslinked COL; (B) CHI; (C) Uncrosslinked COL-CHI; (D): ELN; (E): Uncrosslinked COL-CHI-ELN

Figure 2.2 demonstrates the effects of the three crosslinkers, EDAC, formaldehyde and genipin, on the gel matrices. Curve 2.2B shows that the intensity of the N-H bending peak appreciably increases after the matrix is crosslinked with EDAC; thus the ratio of A_{N-H} to $A_{C=O}$ increases from 51.40% to

57.77%. There is no significant change in this ratio when the matrix is crosslinked with formaldehyde (Curve 2.2C). But this spectrum shows a double peak of C-O-C bond with an area is 8.51. The spectrum of the genipin-crosslinked matrices (Curve 2.2D) shows a weak peak at 1740 cm^{-1}, which is attributed to an ester group of C-O-O from genipin, and an increase in C=O group, which reduces the ratio of A_{N-H} to $A_{C=O}$ from 51.40% to 46.46%. Because the FTIR spectra of crosslinked COL-CHI and COL-CHI-ELN matrices are complicated and show mixed effects of component and crosslinking, the data are not shown here. However, these results are in good agreement with the data shown in Figures 2.1 and 2.2.

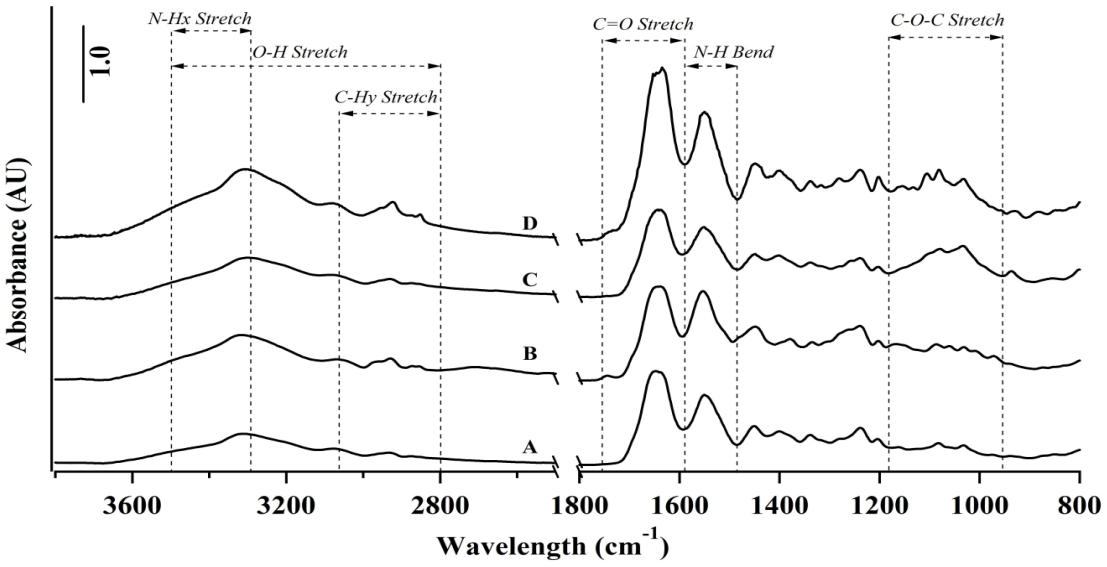

Figure 2.2: ATR-FTIR spectra for crosslinker comparison. (A) Uncrosslinked COL; (B) COL with EDAC; (C) COL with formaldehyde; (D): COL with genipin

2.3.2 Typical stress - strain curves for crosslinked collagen-based constructs

The characteristic stress-strain curves of crosslinked collagen-based constructs are shown in Figure 2.3. The curves exhibit the three regions, namely the toe, the linear and the failure regions. These regions are typical for vascular tissues and collagen-based reconstituted tissue. The shape of the curves, characterized by the extension of each of the three regions, varies according to the composition in the construct matrix. In general, COL constructs have a short toe region, typically within the low strain range (< 15%). In comparison, COL-CHI and COL-CHI-ELN constructs displayed much longer toe regions which extend to high strains up to 30% and 40% respectively. Additionally, COL constructs fail instantaneously, while COL-CHI and COL-CHI-ELN constructs yield after attaining the peak stress. The slope of the linear region in the curve is used to determine the linear elastic modulus. Experiments have been performed on samples crosslinked by different crosslinkers, and it is found that the shape of the stress-strain curves is not dependent on the crosslinker used, although the extension of the linear region and the linear modulus vary with the crosslinker.

Area	**$A_{C=O}$**	**A_{N-H}**	**$A_{N-H}/A_{C=O}$**	**A_{C-O-C}**
Wave # Range (cm^{-1})	**1790-1580**	**1580-1470**	**(%)**	**1150-940**
COL	7.49	3.85	51.40	-
CHI	-	-	-	42.85
ELN	17.52	12.00	68.49	-
COL-EDAC	4.12	2.38	57.77	-
COL-FLN	5.76	2.94	51.04	8.51
COL-GPN	15.77	7.32	46.46	-
COL-CHI	9.18	4.88	53.15	9.71
COL-CHI-ELN	6.85	2.71	39.56	2.08

Table 2.1: Evaluations of C=O, N-H, C-O-C peak areas due to addition of different components and crosslinking

Figure 2.4 demonstrates the quantitative results from uniaxial tensile testing performed on the collagen-based constructs crosslinked with EDAC. Figure 2.4 shows that COL-CHI and COL-CHI-ELN constructs are characterized by significantly higher peak stress and strain at the break as compared to COL constructs. With the addition of chitosan to the collagen matrix, the strain at the break (or the elongation percent) significantly increases from 29% to 47%. Further, the addition of elastin to the COL-CHI matrix significantly improves the strain at the break by an additional 6%. The peak stresses of COL-CHI-ELN and COL-CHI constructs are about two-fold of that of COL constructs. Additionally, the COL-CHI-ELN construct has significantly higher elastic modulus than

the other constructs. No significant differences in the linear elastic modulus are observed between crosslinked COL and COL-CHI constructs.

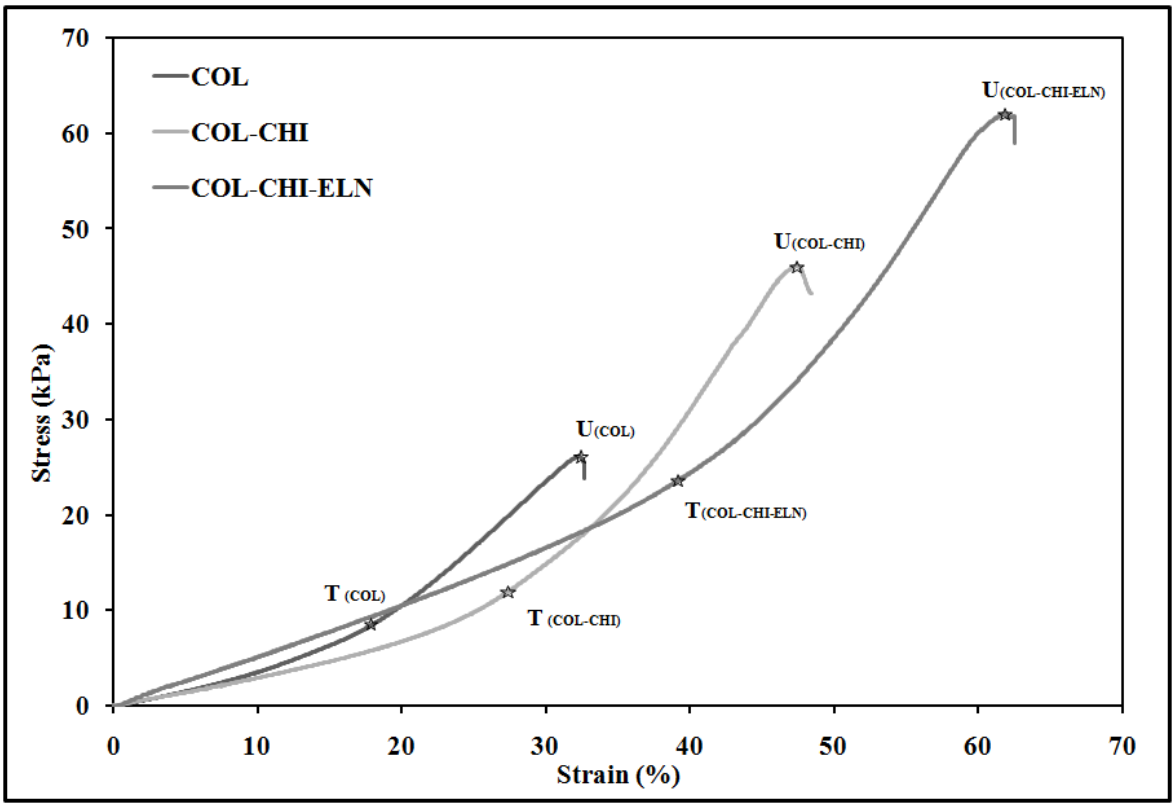

Figure 2.3: Typical stress - strain curves of crosslinked COL based constructs. Point T on each of the graphs shows the end of the toe region and Point U shows end of the linear region. Beyond the linear region lies the failure region. The determination of Effect of matrix composition on mechanical properties of collagen-based constructs

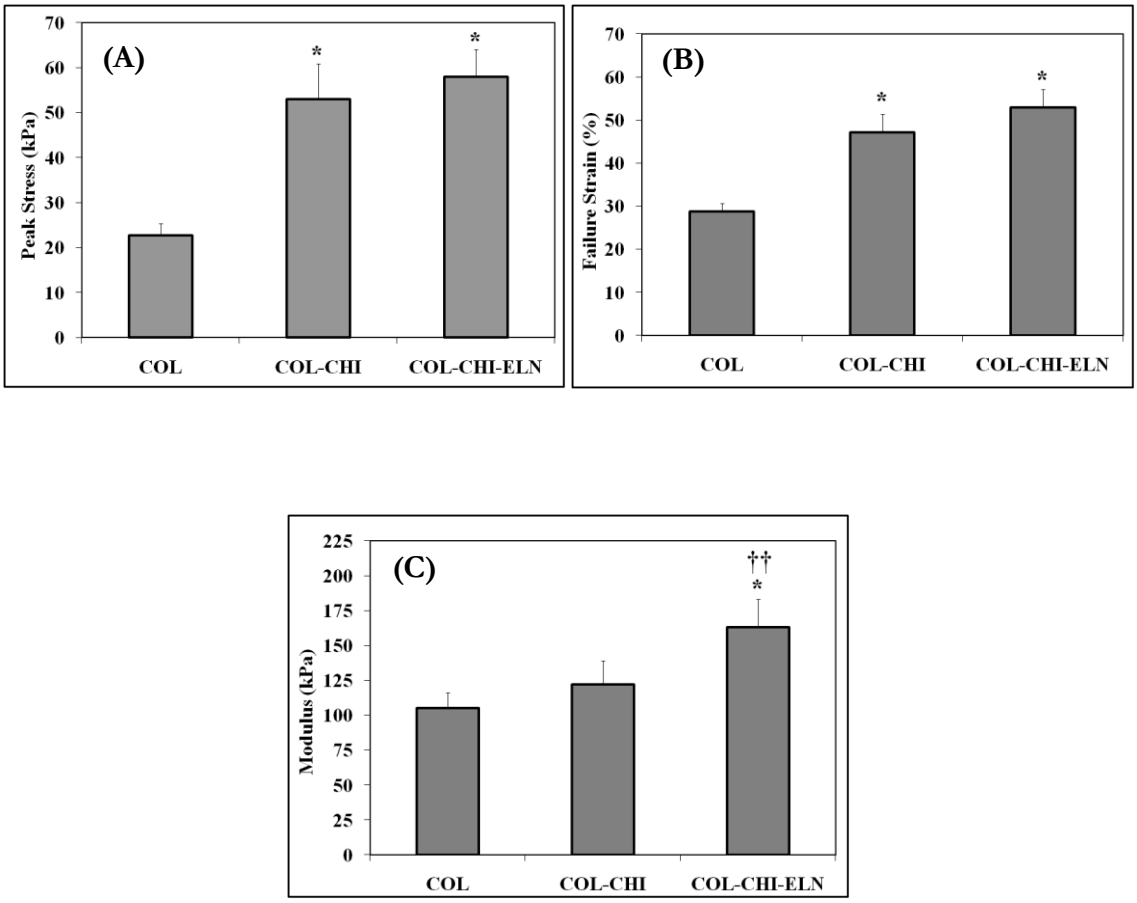

Figure 2.4: Effect of material composition (CHI, ELN) of COL-based constructs on their mechanical properties with (A) Peak stress, (B) Failure Strain and (C) Modulus. Note: * - statistically significant difference in comparison to COL gel, † - statistically significant difference in comparison to COL-CHI gel for a statistical significance of $p < 0.05$ in Student's t test. †† - Indicates statistical difference between the COL-CHI and COL-CHI-ELN for $p < 0.1$. The error bars indicate the standard error mean.

2.3.3 Effect of chemical crosslinkers on mechanical properties of collagen-based constructs

Three different crosslinkers, EDAC, formaldehyde and genipin, were used to strengthen the collagen-based constructs. Results of mechanical testing are shown in Figure 2.5. Genipin-crosslinked constructs have significantly higher strain at break than EDAC-crosslinked and formaldehyde-crosslinked constructs. Genipin-crosslinked constructs also have significantly higher peak stress ($p<0.05$) and modulus ($p<0.1$) than formaldehyde-crosslinked constructs. Although EDAC-crosslinked constructs and formaldehyde-crosslinked constructs do not show significant differences in peak stress and failure strain, their moduli are significantly different. Similar results have also been found in the other collagen-based constructs including COL-CHI and COL-CHI-ELN constructs crosslinked by these crosslinkers.

2.3.4 Effect of gelation time on mechanical properties of collagen constructs

The effect of gelation time has been studied by using 3, 5, 10, 15, 20 and 25 hours of gelation time with subsequent crosslinking in EDAC for 5 hours. As shown in Figure 2.6, improvement in the modulus is significant as it changes from 261 kPa after 3 hour gelation to about 417 kPa after 25 hour gelation, while the strain at break decreases slightly. The ultimate tensile strength does not significantly change over the gelation time.

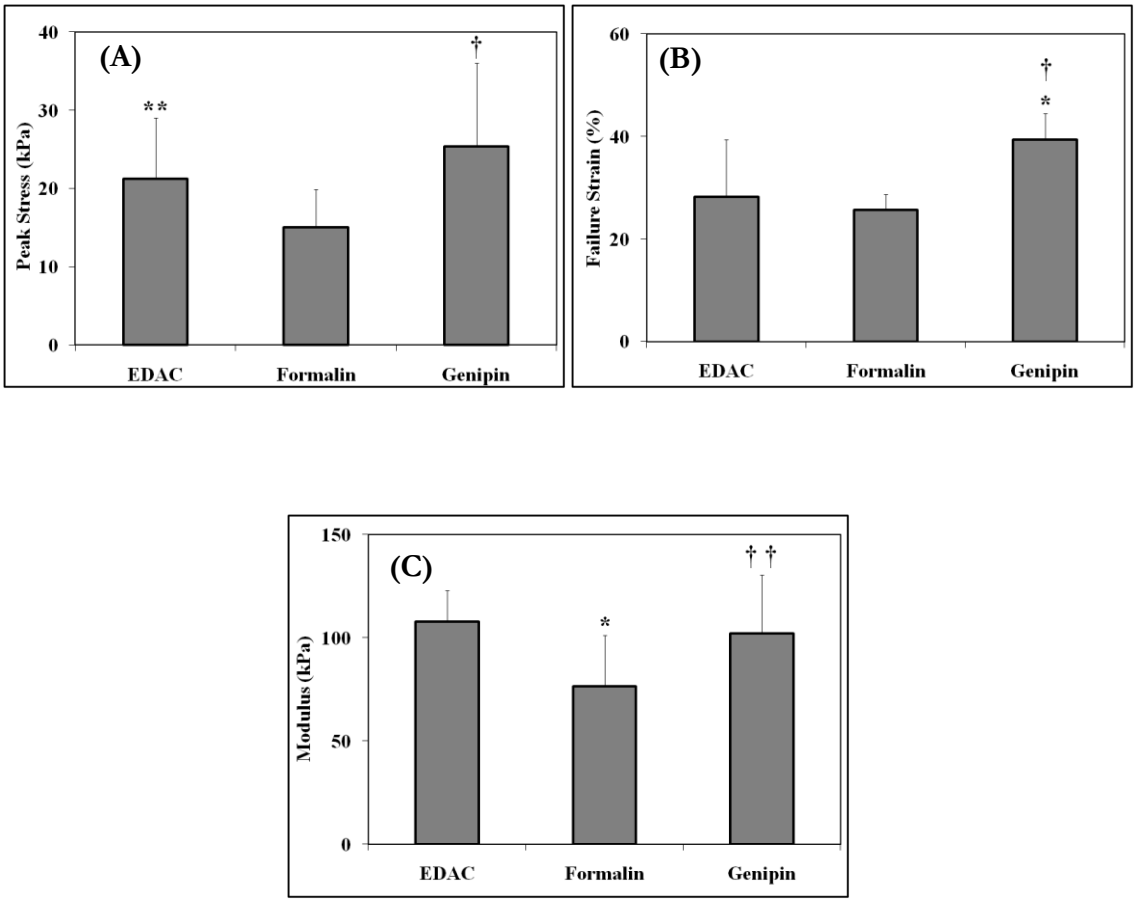

Figure 2.5: Effect of chemical crosslinkers on mechanical properties of COL constructs with (A) Peak stress, (B) Failure Strain and (C) Modulus. Note: * - statistically significant difference in comparison to EDAC crosslinked COL gel and † - statistically significant difference in comparison to formalin crosslinked COL gel for statistical significance of $p < 0.05$ in Student's t test.

†† - Indicates statistical difference between the formalin crosslinked COL gel and genipin crosslinked COL gel for $p < 0.1$. The error bars indicate the standard error mean.

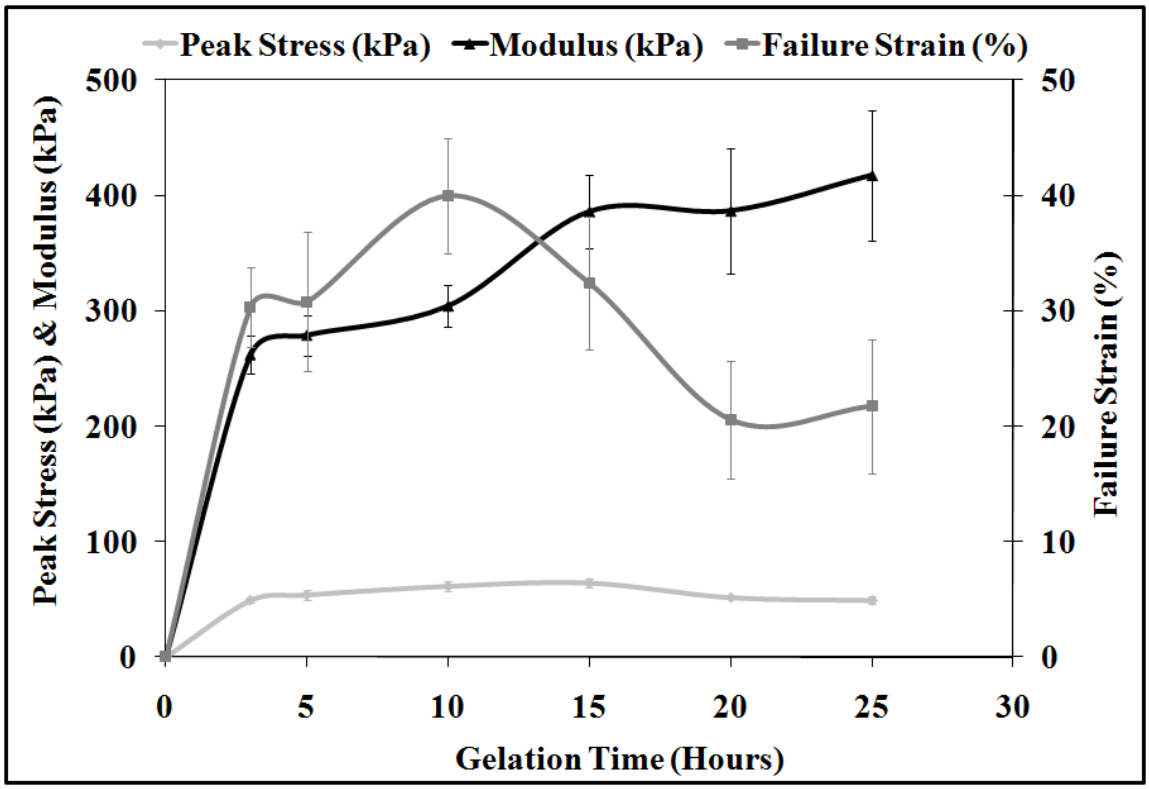

Figure 2.6: Effect of gelation time on collagen constructs

2.3.5 Biocompatibility testing results on collagen-based constructs

Figure 2.7 shows the images of cells stained using the Live/Dead Assay. The images combine green fluorescence (for living cells) and red fluorescence (for dead cells). The cytotoxicity test reveals that EDAC-crosslinked or genipin-crosslinked constructs are more favorable for endothelial adhesion than formaldehyde-crosslinked constructs which might contain toxic residues that lead to significant cell death even after thorough washing steps as described in the method section. Additionally, genipin-crosslinked constructs show higher endothelial coverage percent than EDAC-crosslinked constructs, suggesting better biocompatibility. Our results also show that the crosslinkers have more significant effects on cell compatibility of constructs than the construct compositions. Regardless of

the composition, formaldehyde-crosslinked constructs are always characterized by significant cell death while genipin-crosslinked constructs are always the most compatible ones.

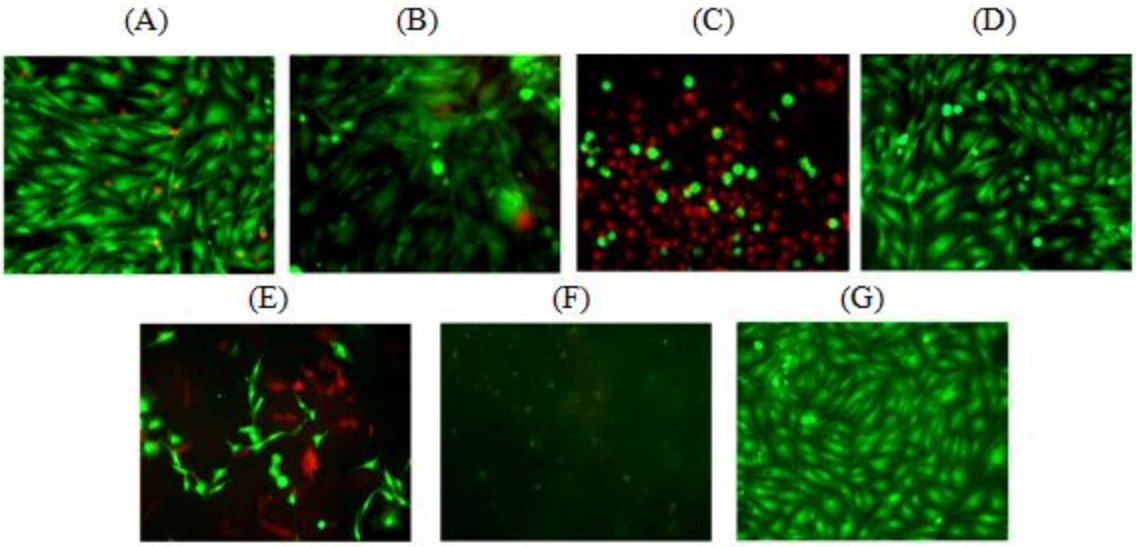

Figure 2.7: Cytotoxicity test results using live-dead assay on following constructs:

(A) control - culture petri dish; (B) EDAC-crosslinked COL; (C) formalin-crosslinked COL;

(D) genipin-crosslinked COL; (E) EDAC-crosslinked COL-CHI-ELN;

(F) formalin-crosslinked COL-CHI-ELN; and (G) genipin-crosslinked COL-CHI-ELN.

Note: Green fluorescence shows living cells and red fluorescence shows dead cells.

2.3.6 Field emission scanning electron microscopy results on collagen based constructs

Figure 2.8 shows the microstructure of collagen-based constructs as viewed under FESEM. Collagen is characterized as a fibrous protein in Figure 2.8A. With addition of chitosan or elastin in collagen constructs, the formation of collagen fibers is not affected. Chitosan is generally known to

polymerize into thin sheets in the space between the collagen fibrils forming a highly porous interpenetrating structure [92-94] . The FESEM images Figures 2.8B-C for COL-CHI and COL-CHI-ELN constructs also suggest the same. COL-CHI and COL-CHI-ELN basically have similar structural features that are characterized by thin sheets along with interfibrils. The COL-CHI-ELN constructs clearly showed an increase in the fiber density which also could possibly due to the addition of elastin. Though it is difficult to distinguish between collagen and elastin fibers, larger fiber bundles are seen in COL-CHI-ELN. As suggested by a previous study [78], it is possible that elastin forms thicker fiber bundles than collagen.

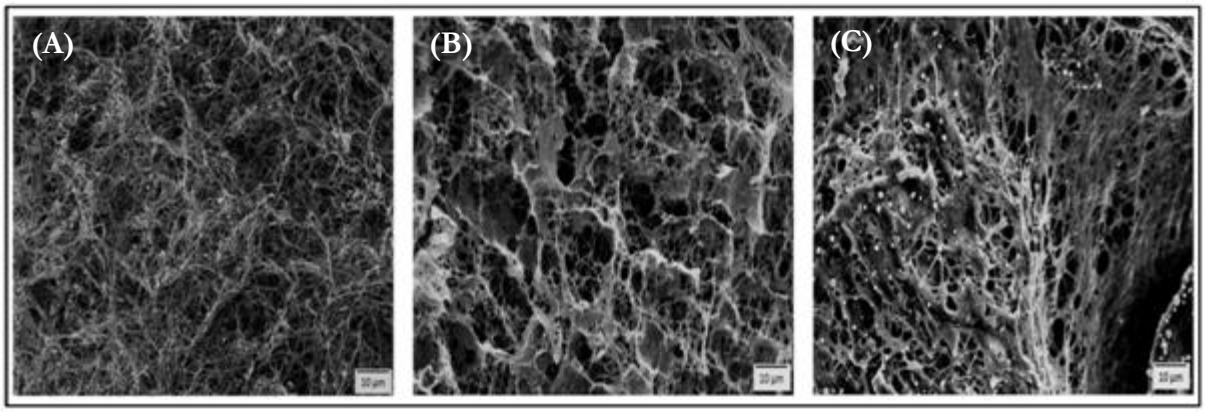

Figure 2.8: FESEM images of (A) COL, (B) COL-CHI, and (C) COL-CHI-ELN constructs

2.4 Discussion

This study has explored approaches to improve mechanical and biological properties of collagen-based materials for vascular constructs. It is demonstrated that the incorporation of chitosan and/or elastin altered stress-strain curves in the low stress loading region, and significantly improved the stretching ratio and peak stress of gel constructs compared to pure collagen constructs. It also

demonstrated that formaldehyde, EDAC and genipin employ different mechanisms to crosslink collagen-based constructs and the use of genipin as a construct crosslinker exhibits improved elongation and endothelial coverage as compared to formaldehyde and EDAC.

Mechanisms of mechanical improvements through the construct composition should consider the interplay among microstructural components. The incorporation of chitosan and/or elastin in the collagen network is confirmed by the presence of C-O-C bonds and changes in the ratio of A_{N-H} to $A_{C=O}$ in the FTIR curves (Figures 2.1C and 2.1E) while the FESEM images in Figure 2.8 also suggest the same. It is known that collagen fibrils are characterized with low elongation (about 3% elongation for individual fibril [95]) and high stiffness with elastic modulus of 10mpa [96], but collagen gel constructs are often weak and show non-linear stress-strain relationship because they are biphasic materials with the solid phase, the fibril, bearing the majority of the force under tensile loading [97]. Similar to the structure and mechanics of pure collagen gel matrices [43], COL-CHI and COL-CHI-ELN show biphasic structure and three regions (toe, linear and failure) in the stress-strain curves. The toe region can be attributed to the rotation of wavy collagen fibers in the reconstituted tissues, which store some energy and release upon initial tension, towards the direction of force [98]. The microstructure of the collagen matrix changes with the addition of chitosan by the formation of chitosan sheets amongst the collagen fibers as suggested by Figure 2.8B. The viscous nature of chitosan possibly increased the water retention in the matrix making COL-CHI more stretchable than the COL as well as reinforcing it to improve the ultimate strength and the linear modulus. This is probably why the toe region in the COL-CHI scaffold is longer than that in COL. Our results of COL-CHI mechanics are consistent with previous study [99]. The further extension of the toe region with the addition of elastin might be attributed to the potential formation of an interpenetrating network of elastin with collagen fibers as suggested by FESEM Figure 2.8C.

Although elastin is similar in fiber structure to collagen, these fibers have much lower strength and higher elongation. Our results on COL-CHI-ELN mechanics, to some extent, are comparable with the mechanics results of natural vessels demonstrated in prior studies. These studies showed that elastin in a natural vessel affected the toe region and contributed to the modulus in the low stress region [100-102]. Furthermore, our results show that the addition of elastin in COL-CHI constructs affects the linear region besides the toe region while the addition of chitosan in the collagen do not significantly change the linear region. The exact mechanisms of this reinforcement of elastin need further explorations. Therefore, this study has shown that compositional and structural modification of collagen-based constructs using ECM-equivalent components is an effective way to simulate mechanical performances of native blood vessels whose high stretching ratio, non-linear stress-strain curve and viscoelasticity are largely dependent on viscous polysaccharides, elastin fibers and highly tortuous, wavy collagen fibers.

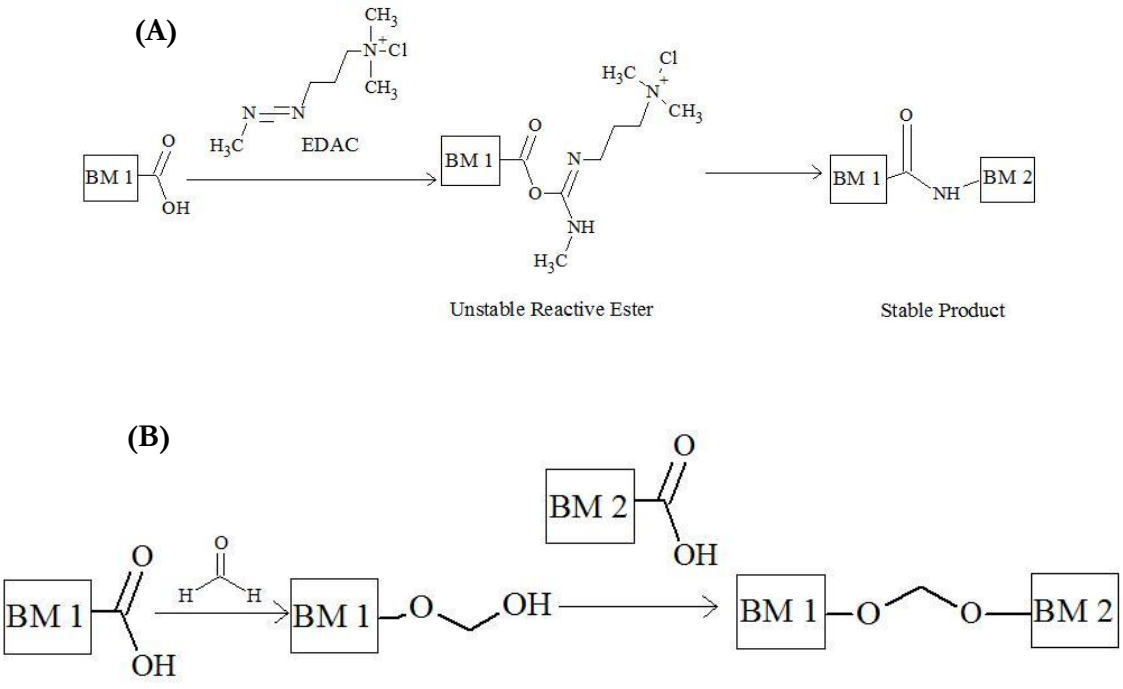

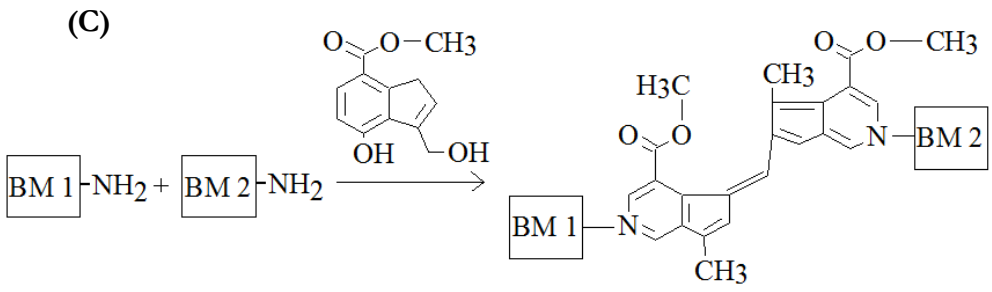

Figure 2.9: Biopolymer crosslinking mechanisms (A) EDAC, (B) Formaldehyde & (C) Genipin

(Note: BM = Biomolecule)

Hydrated collagen-based constructs are often very weak *in vitro*. Crosslinkers such as glutaraldehyde have been used to increase the strength of these constructs. However, the drawbacks are the potential of glutaraldehyde to high levels of toxicity and immunogenicity, as well as high stiffness which was associated with adverse cell responses [84]. More recently, EDAC, formaldehyde and genipin have been used as glutaraldehyde substitutes due to their lower toxicity [103, 104]. This study has evaluated the effects of these crosslinkers on mechanical behaviors and endothelial coverage of hydrated collagen-based constructs because these properties are major considerations in vascular grafts. Genipin-crosslinked constructs seem to be promising for these applications because genipin-crosslinked constructs show a higher elongation percent and are more biocompatible than formaldehyde- and EDAC- crosslinked ones. Formaldehyde-crosslinked constructs showed significant cytotoxicity after thorough washing. This was possibly due to the presence of the residues from crosslinkers which might be difficult to remove and were slowly released from the constructs over time [84]. Though EDAC is more cytocompatible than formaldehyde, endothelial coverage on EDAC-crosslinked gels are lower than that on genipin-crosslinked ones. This might be because EDAC more effectively reduces RGD sequences by crosslinking them in the biopolymer matrices. EDAC toxicity has also been demonstrated by Kataropoulou et al [105]. The differences among

these crosslinkers might be explained by their crosslinking mechanisms. In agreement with previous reports [104, 106, 107] the crosslinking mechanisms suggested by our FTIR results are demonstrated in Figure 2.9. EDAC, a zero-length carbodiimide crosslinker, crosslinks the carboxyl and amine groups presented in the biopolymer matrix, forming stable amide bonds (Figure 2.9A). The consumption of the amine group is confirmed by an increase in the intensity of amide II peak (1550 cm^{-1}) and the ratio of A_{N-H} to $A_{C=O}$ (Figure 2.2B). Formaldehyde, on the other hand, in neutral solutions reacts with the hydroxyl group presented in the biopolymer matrix, forming -C-O-C- bonds (Figure 2.9b). This is confirmed by an increase in the intensity of the -C-O-C- stretch (1150 cm^{-1}-970 cm^{-1}) in Figure 2C. There is no change in the intensity of the amide II peak and in the ratio of A_{N-H} to $A_{C=O}$, indicating that formaldehyde does not attack carboxyl or amine groups. Genipin forms a dimer or a longer oligomer [106, 107] with itself and forms two hemiaminal bonds with collagen during crosslinking [108] (Figure 2.9C). The insertion of genipin in the collagen network after crosslinking is confirmed by Figure 2.2C in that the decrease in the ratio of A_{N-H} to $A_{C=O}$ is due to the carboxyl group from genipin and a weak peak at 1740 cm^{-1} is due to the ester group from genipin. The formation of the genipin dimer or oligomer possibly explains why genipin-crosslinked constructs yield a higher elongation percent than EDAC- or formaldehyde- crosslinked ones. It should be noted that this study has been focusing on investigating how the different chemical crosslinkers involve different crosslinking mechanisms and attack different functional sites on the biopolymer matrices, rather than comparing how the crosslinking density or efficiency influences the constructs. Thus, one limitation in this study must be acknowledged: crosslinking density was not taken into account. Nevertheless, in spite of having different concentrations (or crosslinking density) the crosslinker, both EDAC and formaldehyde imparted very similar peak stress and failure strain to COL while EDAC and genipin imparted similar linear elastic modulus.

2.5 Conclusions

Results from this study have demonstrated that the properties of collagen constructs are tunable with the addition of mimetic components and the selection of crosslinkers. Chitosan and elastin improve the strength, elongation and stretchability of collagen-based gel constructs. Crosslinkers impart critical effects on the strength and modulus of the constructs as well as cell compatibility. Constructs crosslinked with genipin demonstrate higher elongation and endothelial coverage without reducing strength compared to EDAC and formaldehyde. In addition, extending gelation time increased the modulus but not the ultimate strength or the elongation at the break. Therefore, the constructs composed of a combination of collagen, chitosan and/or elastin and crosslinked with genipin, hold potential for superior performance in both mechanical properties and biological properties. This study has given important implications to engineering collagen-based gel matrix materials for vascular graft applications.

CHAPTER 3

COMBINATION OF GENIPIN CROSSLINKING AND BIOACTIVE MOLECULES IN COLLAGEN-CHITOSAN-ELASTIN MATRIX FOR VASCULAR MEDIA EQUIVALENT

Abstract

The vascular media layer, containing smooth muscle cell (SMC), is often a target functional tissue in the construction of artificial blood vessels, because it has major contribution to mechanical properties and other important vascular functions such as contraction of the vessel and regulation of endothelial functions. The present study aimed to construct mechanically strong and stable, biologically functional scaffold for vascular media equivalents. To this end, a biocompatible crosslinker genipin was used to crosslink collagen-chitosan-elastin (CCE) constructs, and the effects of genipin concentration on the mechanical properties, SMC activity and degradation of collagen-chitosan-elastin (CCE) constructs were examined. Results revealed that mechanical strength, stiffness and stability of CCE gel constructs increased with the addition of genipin and with its concentration increasing from 1mM to 25mM, but genipin significantly inhibited SMC contraction of and invasion in the CCE gels. No SMC contraction or invasion was observed in the gels crosslinked with genipin at a concentration of 5mM or above. These results were shown to be correlated with the chemical characterization results from ATR-FTIR. Since cell activities become increasingly important for regenerative medicine, the incorporation of soluble factors in insoluble structural matrices is crucial for regenerating biological activities of cells. We thus incorporated

several growth factor conditions in the genipin-treated CCE constructs and evaluated their effects on SMC activities. These conditions include heparin, platelet-derived transforming growth factor (PDGF), high-concentrated fetal bovine serum (h-FBS) and their combinations. Results showed that the addition of h-FBS in genipin-crosslinked gels significantly increased SMC contraction and invasion, PDGF increased SMC invasion while heparin reduced this PDGF effect, and the synergetic effects of h-FBS and PDGF stimulated SMC invasion more significantly than a single factor. Thus, the use of combination of h-FBS and PDGF with 1mM genipin-crosslinked CCE constructs might potentially achieve a vascular media equivalent with superior performances. Our study suggests that designing a suitable engineering equivalent to blood vessels which allow immediate implantation and encourage tissue regeneration *in vivo* should employ an appropriate combination of crosslinking condition and soluble biomolecule factors, striking a balance between mechanical and biological properties.

3.1 Introduction

Synthetic vascular grafts or artificial blood vessels are widely used for a number of medical treatments including bypass surgery for atherosclerosis and vascular access for hemodialysis. Often these vascular grafts are made from synthetic polymers such as expanded polytetrafluoroethylene (e-PTFE) and Dacron (polyethylene terephthalate)[70]. Though these inert, stiff polymeric grafts successfully replace large arteries, problems arise with replacement of small-diameter (< 6mm) vessels, which results in high occlusion rate[23, 71]. To overcome these problems, more recent efforts have been focusing on tissue engineering approaches. In the general paradigm of tissue engineering, vascular cells are often seeded *in vitro* on a synthetic or biological porous scaffold, and

are allowed to proliferate and produce matrices before final implantation. Recent successes in this area have demonstrated the use of bioreactor, imposing appropriate biochemical and/or mechanical stimuli on cell-scaffold, to reproduce architecture and function of a blood vessel, simulating part or all of its multiple layers, namely intima, media and adventitia L'Heureux, 1998 [41] L'Heureux, 2006. These approaches often start with mechanically weak extracellular matrix (ECM) materials or biodegradable polymers and, through a few weeks of culture in a bioreactor, result in a mimetic vascular structure with high tensile modulus and strength L'Heureux, 2006 [53]. However, due to the weak initial tensile properties of the engineered constructs, the main problem encountered with these approaches is the time, cost and effort necessary to prepare the biological grafts [17]. A long culture time is not suitable for many grafting procedures requiring an immediate replacement. Also, due to lack of elastic lamina in these constructs, long-term implants showed dilation of vessel[13]. Furthermore, harvesting vascular cells from patients and then culturing them could be problematic[17, 20]. An alternative approach omits *in vitro* cell culture by chemically crosslinking decellularized or acellular extracellular matrix scaffolds using glutaraldehyde to enhance mechanical properties for immediate implantation and allow cells to migrate and form tissues *in vivo* [22, 93]. But cytotoxicity and host response are major concerns when a chemical crosslinker such as glutaraldehyde is in use [84]. To that end, our previous study evaluated the biological, mechanical and structural properties of collagen-based constructs which were crosslinked with more biocompatible crosslinkers such as formaldehyde, ethyl-(dimethyl aminopropyl) carbodiimide and genipin [109]. Results demonstrated that genipin-crosslinked materials had comparatively favorable mechanical properties and cell compatibility.

The vascular media layer, containing smooth muscle cell (SMC), is often a target functional tissue in the construction of artificial blood vessels, because it has major contribution to mechanical

properties and other vascular functions such as contraction of vessel and regulation of endothelial functions [98]. The extracellular matrix (ECM) of vascular media is a composite consisting of fibrous proteins such as collagen and elastin, proteoglycans formed by glycosaminoglycan polysaccharides, and biomolecules such as growth factors. Both collagen and elastin fibers are indispensable components in native and engineered vessels, due to their critical roles in maintaining strength and elasticity meanwhile promoting matrix synthesis and tissue regeneration[81, 102]. Chitosan or "poly D-glycosamin" is a natural polysaccharide derived from chitin and is characterized by structural similarity to glycosaminoglycan and excellent biocompatibility. We have thus chosen collagen, chitosan and elastin as structural components of the scaffold material for a vascular media equivalent. In addition to structural components, various growth factors are also present in vascular media to support the cellular processes necessary for optimal functions of the tissue. Thus, the present study is to construct mechanically strong and biologically functional vascular media equivalents composed of a combination of structural components and growth factors and properly crosslinked with genipin. We first examined the effects of genipin concentration on the mechanical properties, SMC activities and matrix degradation of collagen-chitosan-elastin (CCE) constructs. Then, we incorporated several growth factor conditions in the genipin-treated CCE constructs and evaluated their effects on SMC activities. Heparin and platelet-derived transforming growth factor (PDGF) are substances known to influence vascular cells and are often incorporated or analyzed in the vascular graft device. Also, standard fetal bovine serum (FBS) provide nutrients to cells and has a rich content of growth factors like transforming growth factor-β (TGF-β) and PDGF. Therefore, heparin, PDGF, high-concentrated FBS (h-FBS), and their combinations are used for biomolecule conditioning in the study. This study is important to our ultimate goal of producing an engineering equivalent to blood vessels, which may allow immediate implantation and encourage tissue regeneration *in vivo*.

3.2 Materials and methods

3.2.1 Preparation of CCE gel constructs

Collagen-chitosan-elastin (CCE) gel constructs were prepared according to the following procedure: First, the Pre-gel mixture was prepared on an ice bath under sterile conditions. After agitation, 3ml of elastin solution (in 0.2M Tris, at a concentration of 20mg/ml) was placed in a 50ml centrifuge tube. Then, 1ml of 10x Hank's Balanced Salt Solution (HBSS) containing phenol red was added. This was followed by addition of 3.6ml of collagen (at a concentration of 8.4mg/ml), 1.5ml of chitosan (at a concentration of 10m/ml), 100µl of 7% $NaHCO_3$, and then 30µl of 1M NaOH. At this point, the solution was agitated to ensure a homogeneous mixture. Then, a pH paper was used to confirm the pH of the solution (~ 7.4). Finally, 850µl of nanopure water was added to bring the solution to a final volume of 10ml. The final concentration of collagen, chitosan, and elastin were respectively: 3mg/ml, 3.5mg/ml, and 7mg/ml. Pre-gel solutions were cast into 12-well or 24-well plates and allowed to polymerize 1 hour in a cell culture incubator at 37°C. They were then crosslinked with 0mM (no crosslinking), 1mM, 5mM, 10mM and 25mM genipin. After five hours, the genipin solutions were aspirated, replaced with 1ml of PBS per well. The culture plate was then maintained overnight at room temperature. The next day, the gels were washed 6 times with 30 minutes each wash using sterile PBS.

3.2.2 Treatment of CCE constructs with growth factors

The heparin growth factor solution was prepared by dissolving 100 units of heparin per mL of 1X PBS. The platelet-derived growth factor (PDGF) solution was obtained by mixing 400ng of PGDF per mL of 1X PBD. A solution with a combination of heparin and PDGF was prepared by dissolving 100 units of heparin and 400ng of PDGF per mL of 1X PBS. Highly concentrated fetal bovine serum (h-FBS) solution was prepared by dissolving 75% FBS, 24% DMEM, and 1% Penicillin/Streptomycin/Amphotericin per mL of 1X PBS. A solution with a mixture of h-FBS and PDGF was prepared by dissolving 75 % FBS and 400ng PDGF per mL of 1X PBS. The CCE constructs were soaked in each of the solution for 1 hour to allow the growth factors to get embed in the matrix by diffusion.

3.2.3 Fourier transform infrared spectroscopy for biochemical characterization

The CCE gel constructs were frozen in liquid nitrogen (~195˚C), following which they were dried in a critical-point drying chamber (Labconco, Kansas City, MO) for approximately 48 hours. The biochemical compositions and the crosslinking mechanisms were studied using an attenuated total reflectance Fourier transform infrared (ATR-FTIR) spectrometer, Nicolet 4700 (Thermo Fisher Scientific Inc., Waltham, MA). Comparisons were made between samples and pure collagen constructs to study the effect of various matrix components and the effect of crosslinkers. OPUS software (Bruker Optik GmbH, Ettlingen, Germany) was used to find the peaks and to calculate the areas under the peak.

3.2.4 Uniaxial tensile testing for mechanical characterization

All of the experimental gel constructs were subjected to uniaxial tensile tests employing the same testing protocol. An MTS Insight electromechanical testing system (MTS Systems Corp., Eden Prairie, MN) was used. Testing was performed in a 1X DPBS bath at room temperature. A special set of grips in delrin was used to avoid corrosion. One of the grips was loaded on the lower end of the instrument while the other grip was mounted under a 5 N load cell (MTS Systems Corp., Eden Prairie, MN) attached to the other end of the instrument. Samples were loaded and the dimensions of thickness, gauge length and width were measured using a vernier caliper. All the samples were tested at a strain rate of 1% per second until failure. The stress-strain curves were plotted for each of the samples to determine peak stress, strain at break and linear elastic modulus. These curves were fit with a 5^{th} order polynomial using Matlab (MathWorks Inc., Natick, MA). Data collected were statistically analyzed using the one-way ANOVA test. Student's *t* test was then used to compare the means of each individual group. The level of significance was set at $\alpha = 0.05$ for 95% statistical significance. Error bars on all the histogram charts represent the standard error of the mean (SEM) based on the total number of the samples.

3.2.5 Cell culture, adhesion, viability and proliferation assay

The SMCs freshly separated from bovine pulmonary arteries were cultured and cells between passages three and six were used in all biological assays. Cells were cultured in Dulbecco's Modified Eagle's Medium (DMEM) supplemented with 10% FBS, 2% L-Glutamine, and 1% penicillin-streptomycin at 37°C and 5% CO_2, unless otherwise stated. SMCs were cultured until approximately

90% confluence before cell seeding. All the cell assays were carried out after the removal of genipin and thorough washing steps.

For cell viability and proliferation assay, the SMCs were seeded in 12-well plates (cell concentration = 235,700 cells per mL per well, which is approximately 50% confluence), covered with 1ml of cell culture medium and incubated for one day before the gel were plated. After the gels were polymerized and crosslinked, the gels were thoroughly washed in PBS and transferred into the 12-well plates seeded with SMCs; this was referred to as day 0. For cell adhesion assay, the SMCs were directly seeded onto the gel constructs. On the next day (day 1), cell viability assay (LIVE/DEAD kit obtained from Invitrogen Corporation, Carlsbad, CA) was performed. After aspirating the medium and five washes with D-PBS, 500µl of LIVE/DEAD staining solution (obtained by mixing 20µl of 2mM ethidium homodimer-1 stock solution followed by 5µl of 4mM calcein AM stock solution in 10 mL of D-PBS) was added to each well. Plates were then incubated at room temperature for 40 minutes. The staining solution was then aspirated and the gels were washed five times with D-PBS and covered with cell culture medium. The cells were then viewed under a Zeiss Axiovert S100 inverted fluorescent microscope, six photographs per well were taken. The applied stain presented by live cells was green (calcein) while the nuclei of dead cells were stained red (ethidium). The obtained images were then analyzed using ImageJ software (NIH, Bethesda, MD) to determine cell counts. The percentage of viable cells was determined by the number of live cells and the total number of cells including live and dead cells. Similar viability assay was again carried out on the same plates on day 4 to determine cell number and thus the cell proliferation was determined by the increase percentage of the live cell number from day 1 to day 4.

3.2.6 Cell contraction assay

Pre-gel solutions were cast into 24-well plate wells and allowed to polymerize 1 hour in a cell culture incubator at 37˚C. They were then crosslinked with 0mM (no crosslinking), 1mM, 5mM, 10mM and 25mM genipin. After five hours, the genipin solutions were aspirated, replaced with 1ml of PBS per well and then the culture plate was maintained overnight at room temperature. The next day, the gels were washed 6 times with 30 minutes each wash using sterile PBS. The gels were then covered with fresh PBS and were left in the cell culture hood under UV light for 1 hour. Following sterilization with UV light, the gels were covered with culture media (DMEM containing 10% FBS, 2% L-Glutamine, and 1% penicillin/streptomycin/amphotericin) and incubated at 37˚C and 5% CO_2 for 1 hour. Gels were then seeded with 200µl of SMCs, incubated at 37˚C and 5% CO_2 for one hour to allow cell adhesion. After seeding, the gels were covered with 1ml of cell culture medium, allowed the cells to attach to the gels for 1 hour, and then detached from the culture plate wells by running a pipette tip around the circumference of the gel. SMC seeded gels were then cultured at 37˚C and 5% CO_2 for 72 hours, with medium being changed every 24 hours. The seeded gels were subsequently photographed at 24-, 48-, and 72-hour time points. The gels were placed on a light box and were photographed using a Nikon Coolpix 995 camera at full optical zoom at a height of approximately 40cm above the light box. The images were then processed using ImageJ software to determine gel area. Gel areas were calculated for each of these time points and compared to the original gel area. Gel contraction was determined by the comparison ratio.

3.2.7 Cell invasion assay

After performing gel contraction experiments, the gels that were used to determine contraction were used to evaluate cell invasion. After the 72-hour time point, they were washed once with PBS. Gels were then immersed with formalin for 10 minutes. The formalin solution was then replaced with PBS. The gels were then embedded in paraffin, sectioned and then stained with hematoxylin and eosin to examine histology. Nine total sections per gel were made, with three on one edge, three in the center of the gel, and three on the opposite edge of the gel. The sections were then viewed using a Zeiss Axiovert S100 microscope at 100x magnification and photos were taken of the gel sections. Using Zeiss Axiovision software, photos of gel sections that exhibiting SMC invasion were analyzed for invasion depth. This was done by measuring the distance, in micrometers, from the gels top surface (seeding surface) to the location of the cells inside the gel.

3.2.8 Gel degradation assay

CCE gel constructs were prepared and polymerized as described above. The gels were then crosslinked using 0mM (no crosslinking), 1mM, 5mM, 10mM and 25mM genipin solutions. Gels were then washed three times in PBS for 30 minutes each, three times in culture medium for 30 minutes each, and again three times in PBS for 30 minutes each. Gels were then detached and removed from the 24-well plates and placed on glass slides which were placed in a vacuum oven (room temperature, -18 inHg) for 48 hours to dry. Air was allowed to leak in to prevent water vapor buildup and to facilitate drying. After gels were dried, they were carefully scraped off the slides ensuring that they stayed intact using a razor blade. The gels were then weighed, and their masses

recorded. The gels were then placed in 1.5ml microfuge tubes, to which 1ml of collagenase type I (100μg/ml) solution was added. The gels were then incubated at 37°C for 4, 8, 12, and 24 hours. At each time point, gels from each crosslinking condition were removed from the incubator and placed on ice for 5 minutes to arrest digestion. The supernatant from each microfuge tube was aspirated and the gels were again dried in a vacuum oven, and then weighed. The percentage of degradation was then determined based on the mass loss of the gel.

3.3 Results

3.3.1 Effect of genipin concentration on the mechanical properties of CCE constructs

First, the influence of the concentration of genipin applied on the mechanical properties of CCE constructs was studied. Figure 3.1 demonstrates quantitative results from uniaxial tensile testing performed on the CCE constructs crosslinked with genipin at various concentrations. The figures shows that compared to uncrosslinked constructs, the peak stress and linear modulus of any genipin-treated construct significantly increase. Uncrosslinked samples have peak stress (or failure strength) of 18.01 ± 6.48 kPa and modulus of 84.75 ± 26.45 kPa. Crosslinking the construct with 1mM genipin increases the peak stress to 47.1 ± 15.38 kPa, and the linear modulus to 294.68 ± 75.12 kPa. Thus, the 1mM genipin-crosslinked CCE samples demonstrate mechanical improvement around 2-3 times over the uncrosslinked samples, but they show no significant difference in strain at break from the uncrosslinked ones. As the concentrations of genipin crosslinker increase to 5mM, 10mM, and 25mM, the peak stresses increase to 49.17 ± 16.01 kPa, 54.3 ±11.59 kPa, and 61.34 ± 18.81 kPa, respectively, and the moduli increase to 365.41 ± 148.57 kPa, 393.07 ±94.82 kPa, and

400.22 ± 78.5 kPa, respectively. Compared to 1mM genipin-treated samples, 25mM genipin-treated samples show significant mechanical improvements in peak stress and linear modulus, increasing by about 30% and 36%, respectively. Compared to 1mM genipin-treated samples, 5mM and 10mM genipin-treated samples did not show any significant improvement (4% and 13%) in mechanical strength but they increased the linear modulus by 24% and 33%, respectively. Uncrosslinked samples fail at 31.35 ± 10.49% strain, while samples crosslinked with genipin concentrations of 1mM, 5mM, 10mM and 25mM reduce the strain at break by 5%, 6%, 8% and 7%, respectively.

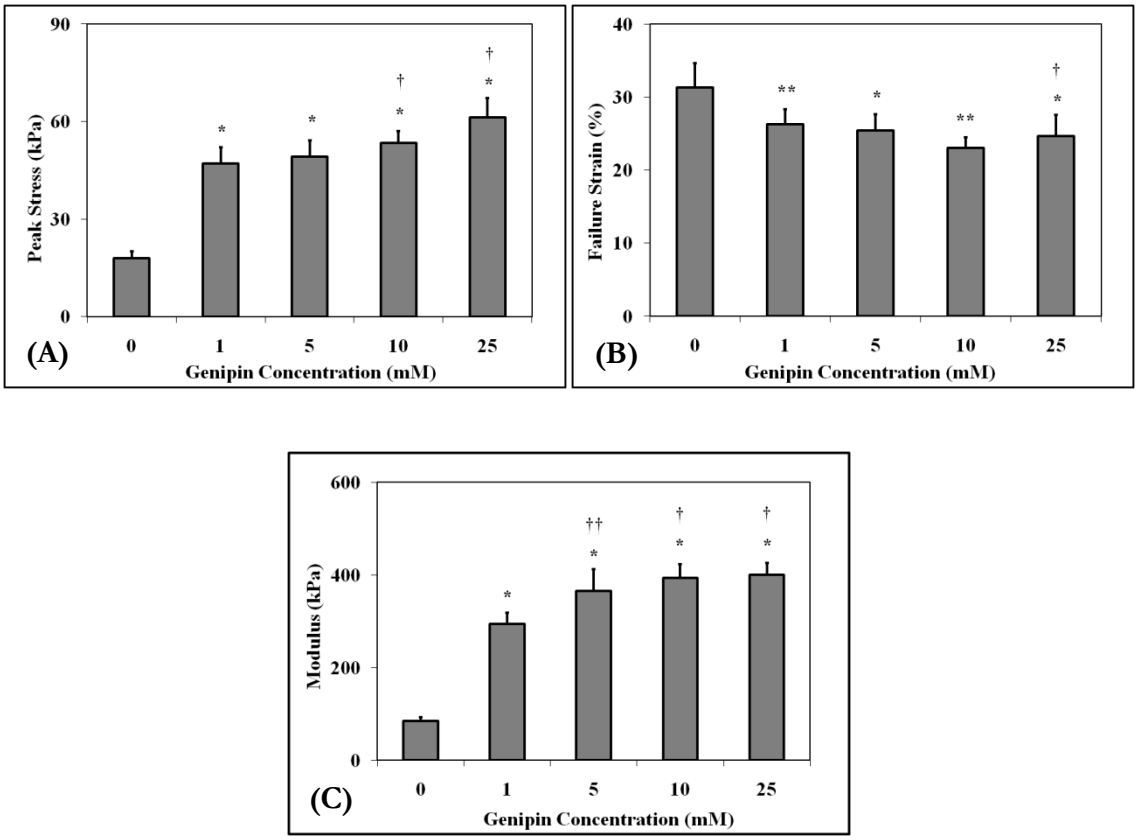

Figure 3.1: Results from uniaxial tensile test showing the effects of the genipin concentration on mechanical properties of CCE constructs. (A) Peak Stress (B) Strain at break and (C) Linear modulus. For statistical significance, $p < 0.05$ in Student's *t*-test, "*"and "†"respectively represent significantly different ($p < 0.05$) from uncrosslinked constructs (0mM) and 1mM genipin crosslinked constructs; "**" and "††"respectively represent possibly different ($0.05 < p < 0.1$) from 0mM and 1mM. The error bars indicate the standard error mean

3.3.2 ATR-FTIR characterization results showing the incorporation of genipin and the effect of genipin concentration

Since crosslinking CCE constructs with genipin change the construct mechanical properties, we asked whether changes in the mechanical properties are due to the chemical structure changes with the crosslinking conditions. ATR-FTIR was used to characterize the chemical changes in the construct. Figure 3.2 demonstrates the spectra of genipin (Curve 3.2A), uncrosslinked CCE samples (Curve 3.2B) and genipin-crosslinked samples (Curves 3.2C-3.2E) showing the incorporation of genipin and the effect of genipin concentration. The spectrum of uncrosslinked samples demonstrate the incorporation of all component additives, as it can be interpreted as linear combinations of the individual collagen, chitosan, and elastin spectra [109]. Compared to the spectrum of uncrosslinked samples, the changes in the ATR-FTIR spectra of the genipin-crosslinked CCE samples are described as followings: (1) The spectra of all the genipin-crosslinked samples show a decrease in the characteristic peak derived from amine ($-NH_2$) stretch between 3500 cm^{-1}-3200 cm^{-1}. With the increase in the concentration of genipin from 1mM to 5, 10 or 25mM, this peak further decreases slightly. This can be attributed to the usage of the amine ($-NH_2$) group during the formation of the hemiaminal group. (2) The amide II peak (N-H bend at around 1550 cm^{-1}) shifts to the right by about 15 cm^{-1}-20 cm^{-1}. This may be due to the consumption of N-H and the covalent addition of carbon-carbon structures such as C–C in–ring stretch and -C=C- stretch, whose peaks are stronger than the amide (-NH-) peak. This can be attributed to the aromatic and alkene structures in the genipin molecule. (3) There is also a substantial change in the range of -C-O-C- stretch (1170 cm^{-1}-950 cm^{-1}). A new peak at around 1105 cm^{-1} shows up in the crosslinked samples. This change may be due to the incorporation of genipin oligomer in the crosslinked structure and thus some genipin molecules retain -C-O-C- group. Therefore, the ATR-FTIR characterization

results demonstrate the incorporation of genipin in the CCE constructs and demonstrate the slight increase in the crosslinking density with the increase in the genipin concentration.

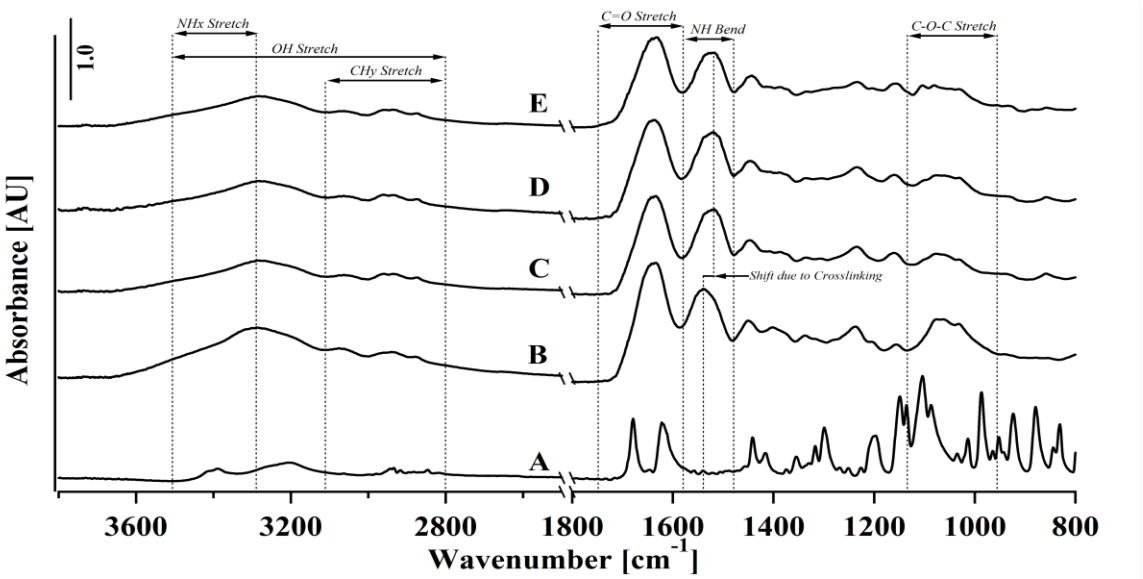

Figure 3.2: ATR-FTIR spectra demonstrate the incorporation of genipin in the CCE constructs. Genipin; (B) Uncrosslinked constructs; (C) 1mM genipin-treated constructs; (D) 5mM genipin-treated constructs; (E) 25mM genipin-treated constructs. The spectrum of 10mM genipin-treated constructs is the same as that of 5mM.

3.3.3 Effect of the genipin concentration on SMC activities

The materials for vascular media equivalent should not only be mechanically strong but also provide amiable environment to SMCs. The most concern with chemical crosslinkers is the cell toxicity and other unfavorable influence on cell activities. We thus used SMCs to examine cell viability, proliferation and invasion in the genipin-treated CCE constructs. Cell viability assay has shown that

there are no significant differences among uncrosslinked samples and all the genipin-crosslinked samples (Figures 3.3A and 3.3B). It also shows that the number of cells attached onto the surface of CCE constructs is not significantly affected by the concentration of genipin solution. Additionally, cell proliferation study shows that there are no significant differences between the uncrosslinked samples and the genipin-crosslinked samples except 25mM genipin-crosslinked samples which significantly reduce cell proliferation by entirely preventing the cells from growing (Figure 3.3C).

Cell contraction assay is an assay to evaluate the cell-matrix interaction, particularly the contractile function of SMCs on the gel matrix. Here, it was determined by comparing the gel area after 24-, 48- or 72- hour cell seeding to the original gel area. Contraction assay results (Figure 3.4) show that only the uncrosslinked samples and the 1mM genipin-crosslinked samples exhibited contraction by SMCs, while the samples that were crosslinked with higher concentrations of genipin did not. The average contraction percentages of 0mM (uncrosslinked samples) and 1mM genipin-crosslinked samples after 24 hours were 61.75% and 13.34%, respectively. The gel contractions after 48 hours and 72 hours did not show significant differences as compared to those after 24 hours. In addition, cell invasion assay showed that cells did not migrate into all the genipin-crosslinked samples including 1mM, 5mM, 10mM and 25mM genipin treated samples (data not shown).

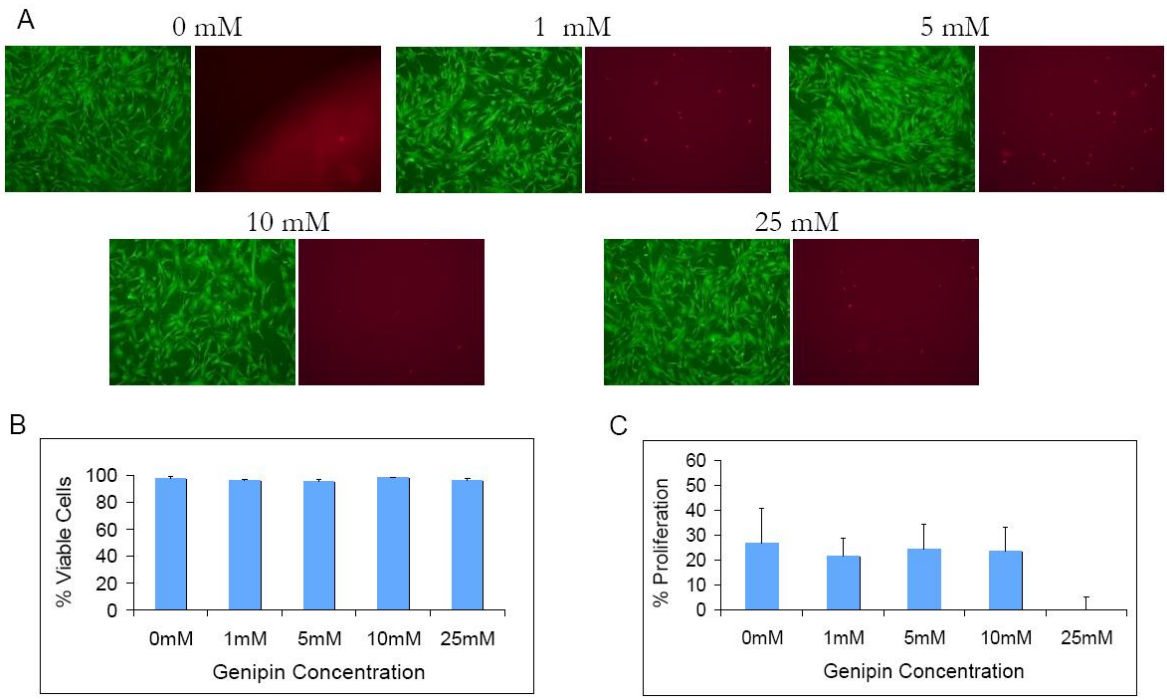

Figure 3.3: (A) Representative images from SMC viability assays on the CCE constructs crosslinked with genipin at different concentration (0mM, 1mM, 5mM, 10mM and 25mM). Live cells showed green stain and dead cells showed red stain. (B) Quantitative results of SMC viability assay; (C) Results from SMC proliferation assay.

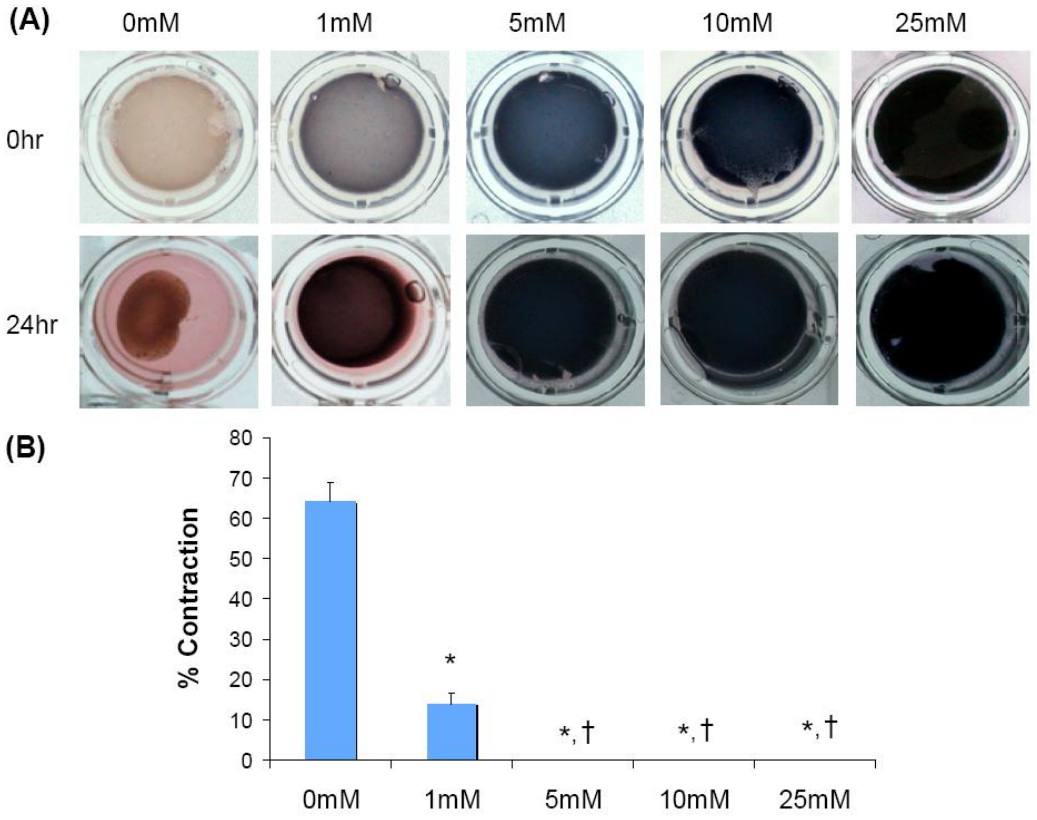

Figure 3.4: (A) Representative images from contraction assay showing SMC contraction of uncrosslinked (0mM) and crosslinked gel constructs (1mM, 5mM, 10mM and 25mM) after 24hr as compared to those just detached from the bottom (0hr). (B) Quantitative measurements of the gel contraction which changes with the genipin concentrations. "*" and "†" represent significantly different from 0mM and1mM, respectively.

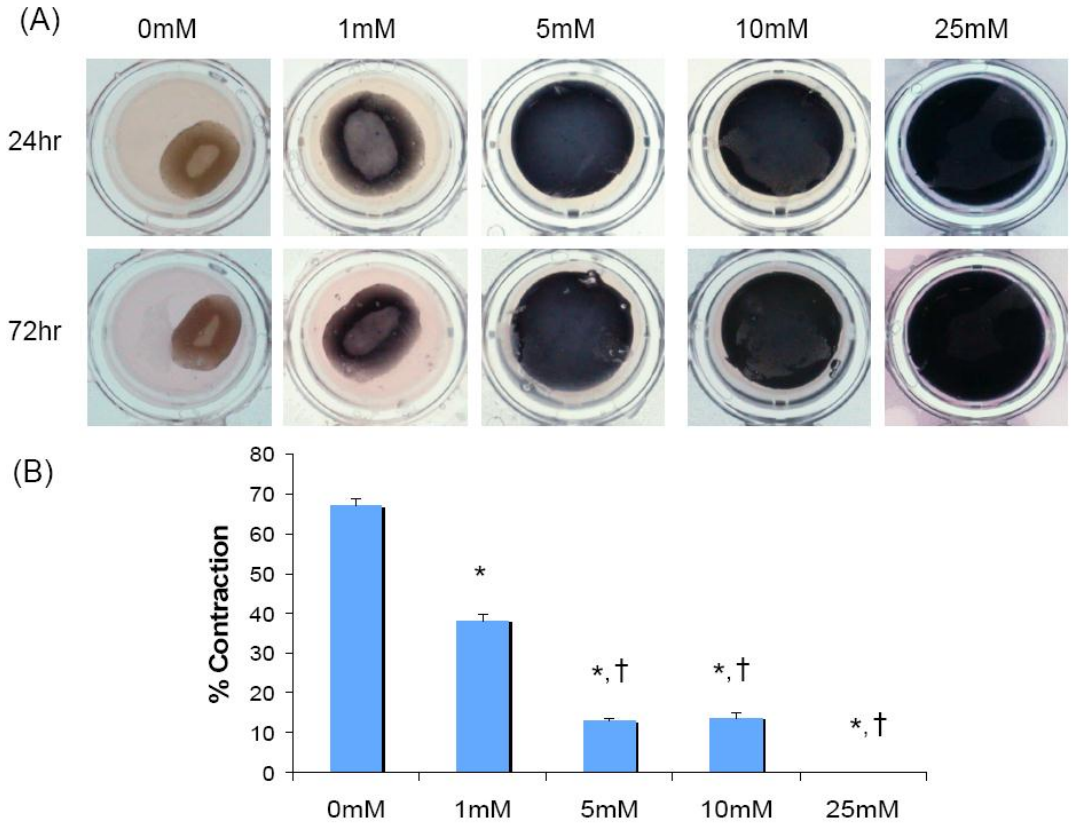

Figure 3.5: (A) Representative images from contraction assay showing the effect of h-FBS on SMC contraction of uncrosslinked and crosslinked gel constructs after 24hr and after 72 hr.; (B) Quantitative measurements of the changes in gel contraction with genipin concentrations after 24hr. "*" and "†" represent significantly different from 0mM and 1mM, respectively.

3.3.4 Effect of growth factor conditions on SMC activities

As demonstrated in 3.3.3, the genipin crosslinking significantly inhibits SMC-matrix interactions and SMC activities, such as contraction and migration, but it does not significantly affect cell adhesion, viability and proliferation except for the concentration of 25mM. To overcome this inhibition effect, several growth factor conditions, including h-FBS, PDGF, heparin, mixture of h-FBS and PDGF

and mixture of heparin and PDGF, were designed in the present study. Heparin, PDGF, and h-FBS are known to have the ability to stimulate vascular cell proliferation and/or chemotaxis. Solutions containing growth factors were used to condition crosslinked gel constructs. Figure 3.5 illustrates the effect of h-FBS on SMC contraction of the gels. Compared to Figure 3.4, this result shows that the increased concentration of FBS, a mixture of nutrients and low-concentrated growth factors, increased SMC contraction of all the genipin-crosslinked CCE gel constructs except 25mM, while the h-FBS condition did not significantly influence SMC contraction of uncrosslinked gels. However, the gel contractions of crosslinked samples were still significantly lower than the gel contraction of the uncrosslinked samples. Also, the gel contraction of 1mM genipin-crosslinked samples was significantly higher than that of 5mM or 10mM genipin-crosslinked samples.

These studies indicated that higher genipin crosslinking conditions, 5mM and above, significantly inhibit SMCs in spite of growth factor conditioning. Therefore, we further examined the effects of growth factors on SMC traction and invasion using only two types of COL-CHI-ELN constructs, uncrosslinked and 1mM genipin-crosslinked ones. Figure 3.6 shows the results of cell contraction assays performed on the 0mM and 1mM genipin-crosslinked samples with different biomolecule conditions including heparin, PDGF, h-FBS, a combination of heparin and PDGF and a combination of h-FBS and PDGF. The results are shown in comparison to the "null" condition which use only standard 10% FBS with no additional growth factors. For 1mM genipin-crosslinked samples, the addition of h-FBS or a combination of h-FBS and PDGF significantly increased the gel contraction when compared to the null condition. For uncrosslinked samples, only the addition of a combination of h-FBS and PDGF significantly increased the gel contraction when compared to the null condition.

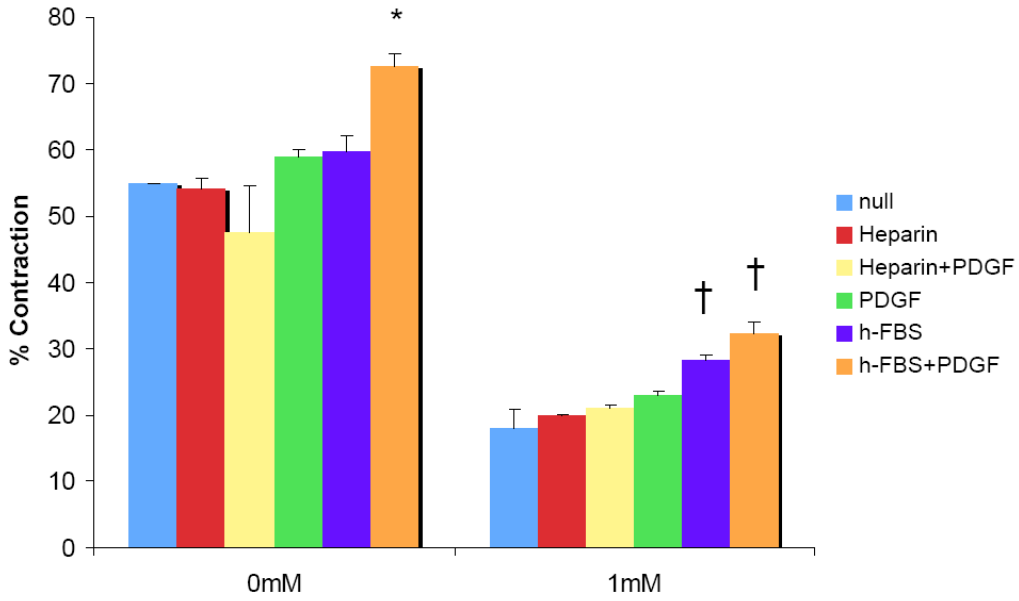

Figure 3.6: Effects of soluble factors on SMC contraction of uncrosslinked and crosslinked gel constructs. "*" and "†"respectively represent significantly different from null condition at 0mM and null condition at 1mM.

The SMC invasion assay results are demonstrated in Figure 3.7. SMCs invaded deep into the uncrosslinked gel constructs, and the use of h-FBS did not significantly influence SMC invasion. Without the use of h-FBS or the addition of biomolecules, the cellularity in the gel constructs was limited to the periphery of the 1mM genipin-crosslinked CCE construct, with almost no cells found in the center of the construct. The use of h-FBS significantly increased the SMC invasion depth, and a combination of h-FBS and PDGF further increased SMC invasion in the crosslinked construct. The addition of PDGF also increased SMC invasion, but the addition of heparin together with PDGF into the crosslinked construct showed reduced SMC invasion in comparison to PDGF alone. This indicated that heparin has inhibitory effects on PDGF-induced SMC invasion into the crosslinked constructs.

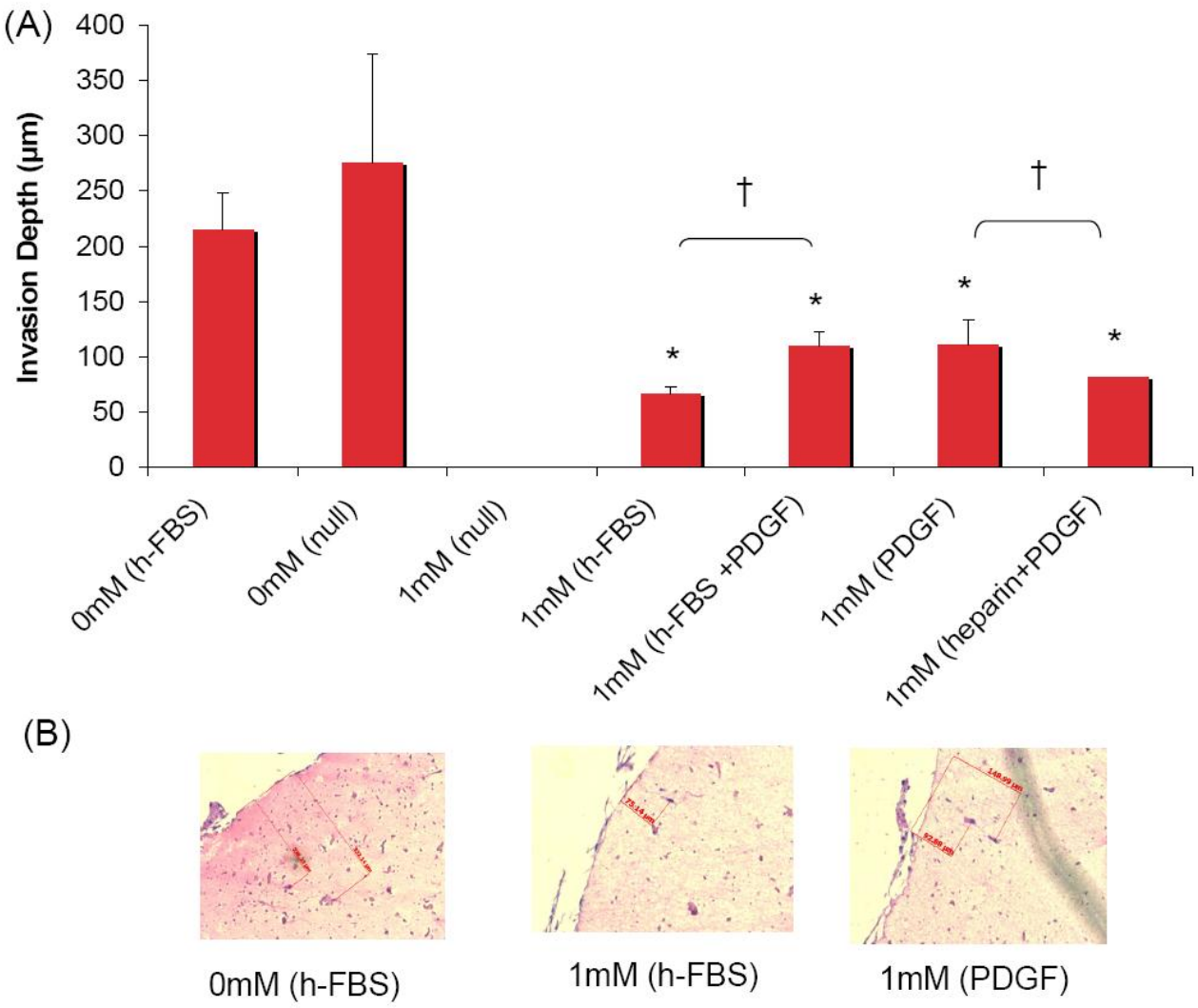

Figure 3.7: Effects of soluble factors on SMC invasion in uncrosslinked and crosslinked gel constructs. (A) The relationship between cell invasion depth and the conditioning of soluble factors and crosslinker concentration. "*"represent significantly different from the null condition (1mM). (B) Representative images from the histology study.

3.3.5 Effect of genipin crosslinking on the degradation of CCE matrices

Crosslinking of the gel matrix is also expected to increase its stability after implantation. We thus examined the degradation of genipin-crosslinked CCE matrices in response to collagenase (Figure 3.8). Uncrosslinked constructs showed gradual degradation, with an average degradation of 4.5% at 4hr to an average of 20% at 24hr. Genipin-crosslinked CCE matrices showed much slower degradation. With the increase of genipin concentration, the degradation rate of the matrix constructs decreased. The 10mM-crosslinked CCE matrices did not demonstrate significant degradation within the first 24 hours. No differences in construct degradation were found among samples crosslinked with 5, 10 and 25mM genipin.

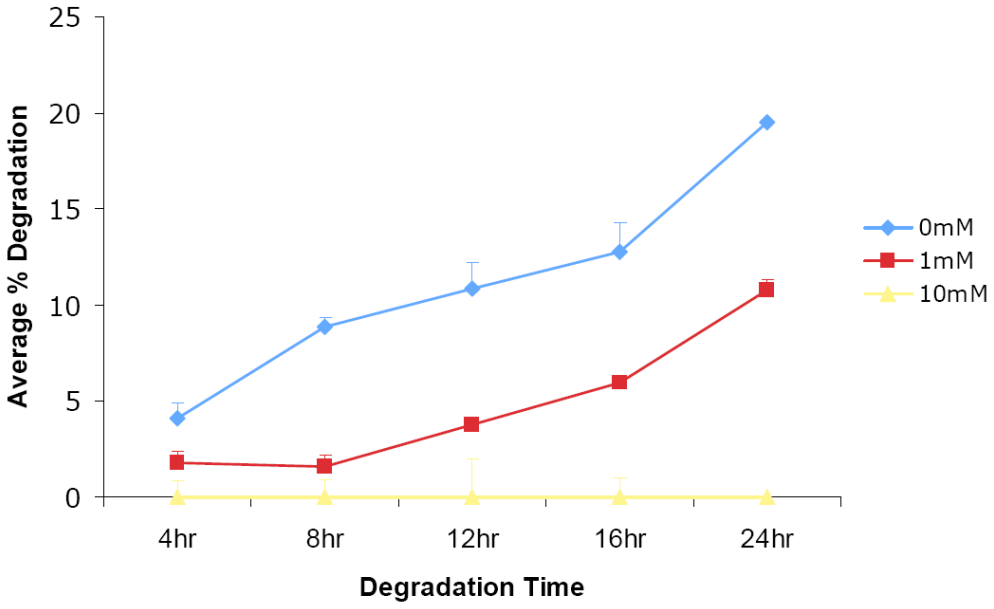

Figure 3.8: Degradation of different CCE gel constructs over time. The degradation curves of 5mM and 25mM genipin-treated constructs are similar as that of 10mM.

3.4 Discussion

Vascular media equivalents require sufficient mechanical strength, stability and amiable environments for SMC function. In general, cell environment is composed of several factors which fall into one of two categories: insoluble cues such as the composition and stiffness of the ECM and soluble cues such as growth factors [110]. Thus, the present study has demonstrated the effect of the concentration of genipin, a natural-derived crosslinker, on the mechanical strength, stiffness and stability (resistance to biodegradation) of CCE gel constructs, and further explored the use of soluble growth factors in the genipin-crosslinked CCE matrices to enhance SMC activities. We found that mechanical strength, stiffness and stability of the gels increased with the addition of genipin and with its concentration increasing from 1mM to 25mM, but genipin significantly inhibited SMC contraction of and invasion in the CCE gels. No SMC contraction or invasion was observed in the gels crosslinked with genipin at a concentration of 5mM or above. We thus incorporated soluble growth factor conditions, including h-FBS, PDGF, heparin and their mixtures in the genipin-crosslinked gels. The addition of h-FBS in the 1mM genipin-crosslinked gels increased SMC contraction and invasion, PDGF increased SMC invasion, heparin reduced this PDGF effect, and the synergetic effects of h-FBS and PDGF stimulated SMC invasion more significantly than a single factor. This study suggests that the use of combination of h-FBS and PDGF with 1mM genipin-crosslinked CCE constructs could potentially achieve a vascular media equivalent with improved performances.

Several previous studies have determined mechanical properties and degradation of collagen and collagen-chitosan gel materials. Compared to a study done an earlier study, our results showed that

uncrosslinked CCE constructs were mechanically stronger (~50% higher in strength) and degraded more slowly (20% vs. 90% of degradation after 24 hours). In addition to the matrix composition, our results also showed that addition of a low concentrated (1mM) genipin solution significantly increased stiffness, strength and stability. Furthermore, the mechanical strength, stiffness and stability slightly increased with the concentration, but the differences in the mechanical property between genipin with 1mM concentration with those at higher concentrations were not proportional to the fold-increase in the concentration, and no significant difference in the mechanical property and stability was found among the three high crosslinker concentrations (e.g. 5mM, 10mM and 25mM). This could be explained by the changes in functional groups and density by the genipin crosslinking. FTIR data suggested that increase in the genipin solution concentration influenced the crosslinking density only to a small degree, which might be caused by the saturation of the crosslinking sites.

Crosslinking conditions also influenced SMC activities. In agreement with previous studies [109], we found that genipin crosslinking imposed no cytotoxicity on SMCs as cell viability and adhesion were not significantly affected by the genipin concentration. And cell proliferation was also not significantly affected by the genipin concentration except for 25mM genipin. Additionally, we found that directly adding 1mM genipin in cell-containing CCE constructs significantly reduced the cell viability after 24 hr. incubation (~10%) compared to uncrosslinked samples (data not shown here). This finding is different from the study performed by Sundararaghavan et al[91] who reported that directly adding 1mM genipin in cell-containing collagen matrix did not significantly affect fibroblast viability compared to uncrosslinked ones. This might be due to the difference in cells as immortal cell lines were used in that study while primary cells were used here. Our study suggests that cell seeding must be performed after the removal of genipin even though it is one of the most

biocompatible crosslinkers for collagen-based matrix gels. Additionally, we found that crosslinking reduced SMC-matrix interactions and reduced SMC contraction and invasion. Increased crosslinking density further reduced these SMC activities. This was likely caused by the mechanical and biochemical changes crosslinking brought to the gel constructs, altering the microenvironments for SMCs. In particular, genipin crosslinking increased the gel stiffness and might decrease the number of RGD peptide sequences on collagen. The critical role of matrix stiffness in regulating cell behaviors has received great attention recently. Mechanical testing results showed that 1mM genipin significantly increase the stiffness of CCE gel and higher genipin concentration resulted in higher matrix stiffness. A previous study reported that normal epithelial cells and fibroblasts migrated faster on softer substrates than stiff substrates, because softer substrates resulted in more focal adhesions in cells and thus higher forces generated by myosin contraction. As a biomaterial, collagen I has many advantages including its high density of the RGD sequence and other functional sequences for cell attachment and cell differentiation. Genipin-crosslinking among functional peptides inhibits cellular recognition and interaction with the construct by crosslinking the primary amine found on the end of the arginine R-group of the RGD integrin binding sequence. The consumption of NH_2 was also shown by the FTIR characterizations in this study.

To enhance or induce SMC contraction of and invasion in the crosslinking-strengthened constructs, soluble cues such as growth factors were introduced in the ECM gel. We selected factors that were often used or studied in vascular grafting to stimulate SMC activity. Results showed that balancing mechanical and biological properties can be achieved by adding h-FBS and PDGF in 1mM genipin-treated CCE matrix. PDGF is a well-known SMC chemoattractant. The PDGF molecules in the crosslinked gels stimulate SMC migration. It is known that FBS contains an array of soluble factors including PDGF, TGF-β, and adhesion molecules such as fibronectin. The addition of h-FBS likely

stimulated the matrix deposition by SMCs which may provide an intermediate way for the cells to interact with the crosslinked constructs which exhibited a reduced number of RGD sites, thus stimulating contraction. Heparin is often incorporated on the vascular graft to prevent thrombosis. It is also well known as an endothelial growth factor. However, it inhibited SMC growth, differentiation and other activity. Our results suggested that heparin should be localized on the luminal surface of an engineered vascular construct, instead of being uniformly distributed throughout the construct or presented in the media equivalent which should encourage SMC growth, invasion and remodeling during the initial stage of implantation.

Optimization of mechanical properties and SMC environments are important for vascular media equivalents and for vascular graft constructs that facilitate immediate use and in vivo cell seeding. The present study suggests that we may strike a balance between mechanical and biological properties, by selecting a low concentration (1mM) of biocompatible crosslinker (genipin), together with insoluble biomimetic matrix (CCE) and soluble chemoattractants and differentiators (PDGF and h-FBS). The two sets of cues, the soluble medium and the insoluble matrices, should be co-optimized for the best results, since they may affect same signaling pathways through crosstalk as suggested by previous studies. Proper designs of scaffold compositions, its stiffness, and molecular presentation to the cell may significantly improve the biological relevance of constructs to cells since the cell acts and looks far more like its *in vivo* counterpart.

3.5 Conclusion

Results from this study have demonstrated the effects of genipin concentration on the mechanical properties, SMC activity and degradation of genipin-crosslinked CCE constructs. Though the mechanical properties of the CCE constructs improved with the increase in genipin concentration, SMC activity (contraction and invasion) on the CCE constructs greatly reduced. The degradation of the matrix also depended on the concentration of genipin making the crosslinked sample more and more resistant to degradation. The addition of growth factors to the scaffold had a positive effect to scaffold contraction by SMCs. The 1mM crosslinked scaffolds showed a remarkable amount of contraction with the presence of heparin, PDGF, a combination of heparin and PDGF, h-FBS, and a combination of h-FBS and PDGF in that order. With the presence of growth factors, it was also seen that that the invasion depth of SMCs in the low concentration crosslinked scaffold varied with h-FBS, a combination of heparin and PDGF, a combination of h-FBS and PDGF and PDGF in that order. Hence, by balancing the mechanical and biological properties and in the presence of growth factors such as PDGF, low concentration crosslinked CCE scaffolds can act as a suitable medial layer in tissue engineered vascular grafts.

CHAPTER 4

MECHANICAL AND BIOCOMPATIBLE CHARACTERIZATIONS OF A READILY AVAILABLE MULTILAYER VASCULAR GRAFT

Abstract

There is a considerable need for alternatives to autologous vein or artery tissues for vascular graft uses; synthetic graft materials such as polytetrafluoroethylene have not matched the efficacy of native tissues, mainly due to their low compliance and limited capability of regenerating tissues. Considering the graft availability to surgery, the required physical and mechanical properties, and the potential for vascular regeneration, we aimed to design a readily-available, strong and compliant graft consisting of layer-specific matrices that respectively define environments for different vascular cells. This study thus focused on developing and characterizing multilayered biodegradable constructs, in which heterogeneous materials and structures were integrated to offer properties for readily grafting and environments for culture or ingrowth of diverse vascular cells. The multilayer constructs consisted of a thin, dense, nanofibrous layer composed of stiff poly-ε-caprolactone (PCL) materials, and a thick, highly-porous layer of genipin-crosslinked collagen-chitosan (GCC) hydrogel. Because of large differences in physiochemical properties of the layer materials, the material interface was identified as an important determinant to the graft integrity and property. The interface modifications for improving the layer adhesion, including physically increasing porosity of the PCL surface and chemically increasing hydrophilicity or crosslinking were studied. Microscopic examination as well as results of graft physical properties showed increasing porosity of the PCL was

an effective way of providing layer adhesion for successful construct integration, and offering desired graft permeability (528 mL/cm^2/min), required implant burst strength (695mmHg) and suture strength (2.38N), and high compliance (4.5%) for graft implant applications. Results also showed that PCL mainly contributed to the biomechanical properties such as burst strength, compliance and suture strength, while GCC reduced the water permeability. In addition to the complementary function in physical and mechanical properties, the two-layer design also provided layered structure for cell seeding or ingrowth *in vitro* and *in vivo*. Acellular multilayer constructs were readily implantable to replace abdominal aorta in rabbits, resulting in rapid cell ingrowth, flow reperfusion and free of thrombosis. The engineered constructs capable of sustaining physiological conditions and promote appropriate cellular activity could serve as a platform for future developments of regenerative vascular grafts.

4.1 Introduction

There is a considerable need for alternatives to autologous vein and artery tissues for vascular reconstructive uses [17, 70], including coronary bypass, lower limb bypass, hemodialysis access, and arteriovenous shunt. Until now, synthetic materials such as polytetrafluoroethylene (PTFE) have not matched the efficacy of native tissues, particularly in the small-diameter vessel (<6mm) applications [23, 111]. In the past decade, impressive progress in vascular tissue engineering has demonstrated the possibility of using a living biograft as a blood vessel substitute [36, 41, 42, 55, 112-114]. The biograft is often characterized by a multilayer structure mimicking intima, media or adventitia of native vessels and is capable of withstanding physiological stresses. In these *in vitro* engineered vascular biografts, synthetic or natural biomaterials are used as three-dimensional (3D) scaffolds to provide temporary mechanical support for culture of cells which are stimulated to synthesize matrix

components for the formation of vascular structure and property. However, the clinical potential of current approaches is thought to be tempered by time-consuming, labor-intensive preparations, complicated storage requirements and rigorous culture regulation [36, 41, 55]. Development of vascular replacement demands further investigations into engineering technologies that not only provide regenerative growth of blood vessels without immunogenic, thrombogenic or inflammatory responses, but also consider the availability, ideally "off-the-shelf", to vascular surgeons [17, 19]. These require that grafts should not only provide layer-specific microenvironments supporting regenerative activities of diverse vascular cells, but also possess physical and mechanical properties to sustain graft remodeling under hemodynamic conditions *in vivo*.

A long-standing challenge in the development of synthetic vascular grafts is the balance between mechanical strength of a vascular graft to withstand physiological stresses and its compliance to provide appropriate hemodynamic environments to cells. On one hand, robust physical and mechanical properties, including burst strength, water permeability and suture strength, are required for graft implantation. On the other hand, high compliance or low stiffness is desired, since compliance mismatch at the site of anastomosis between a vascular graft and neighboring arteries is a major cause of graft failure, because disturbed blood flow at the junction of mismatched compliance leads to adverse cell responses and/or pro-inflammatory milieu [16, 17, 23]. Compliance mismatch generally results from high stiffness of grafts [16], or the lack of optimal pore sizes [115]. Pore sizes, however, also alter water permeability and cell synthesis [116].

From the tissue regeneration point of view, an ideal scaffold is to provide microenvironments for ingrowth and proliferation of vascular cells, vascular endothelial cells (ECs) and smooth muscle cells (SMCs) [12, 19]. The artery exhibits a multilayer structure with layer-specific matrix

microenvironments for specific cell or tissue functions [20]. Considering the availability to surgery, the required physical and mechanical properties as well as vascular regenerative potential, we will need a strong, compliant scaffold with thromboresistant surface and layer-specific matrices that respectively define environments for ECs and SMCs to guide vascular regeneration *in vivo*. This study thus focuses on developing multilayered biodegradable constructs, in which heterogeneous structures are integrated to offer properties for the "off-the-shelf" implant, as well as high compliance and layer-specific scaffolding materials to provide physiological microenvironments for vascular cells. The multilayer constructs consisting of a thin, dense, nanofibrous layer composed of strong poly-ε-caprolactone (PCL) materials, and a thick, highly-porous layer of genipin-crosslinked collagen-chitosan (GCC) hydrogel, aim to provide properties for immediate grafting and structural guidance for cell growth. We previously have demonstrated the GCC scaffold as a vascular medial equivalent due to its structural, mechanical and biochemical properties as well as its function of supporting SMC growth and contraction [109, 117]. We have also shown that electrospun PCL constructs possess mechanical strength for vascular applications [118]. Additionally, both GCC and PCL are biodegradable, and hence can be readily remodeled by cells. However, the water affinity, structure and physiochemical properties of PCL and GCC are quite opposite. Thus, an important design challenge of using these materials for multilayer vascular grafts is interface engineering. Herein, we have developed several interface strategies to integrate the layers, and studied their influences on structural adhesion, graft integrity, as well as biomechanical and physical properties. Finally, evaluation of the multilayer vascular grafts was performed *in vitro* with vascular cells and *in vivo* as grafts interpositioned in infrarenal abdominal aorta of rabbits.

4.2 Materials and methods

4.2.1 Materials

Poly-ε-caprolactone ($\overline{M_n}$=80,000 g/mol) and polyethylene oxide ($\overline{M_n}$=500,000 g/mol) were purchased from Sigma Aldrich Inc. (St Louis, MO). Dry porcine skin collagen type I was purchased from Elastin Products Co. (Owensville, MO). Acetonitrile (ACN) and 1, 1, 1, 3, 3, 3 – hexafluoro – 2 – propanol solution (HFIP) was obtained from Sigma Aldrich. N, N-Dimethylformamide (DMF, minimum purity 99.9%) and dichloromethane (DCM, minimum purity 99.5%) were purchased from Mallinckrodt Chemicals (Phillipsburg, NJ). The electrospinning apparatus comprised of a Gamma High Voltage Research ES30P-10W power supply (Gamma High Voltage Research Inc., Ormond Beach, FL), a pair of syringe pumps (Pump 11 Plus - Harvard Apparatus, Crisel Instrument, Rome, Italy), a cylindrical aluminum collector with 4.76mm in diameter, a brushless rotating electric motor (BLF230C-A Oriental Motor, Italia S.R.L., Milan, Italy), 5 ml polystyrene syringes to dispense the polymer solutions, stainless-steel 18G blunt-ended needles and flexible PTFE tubing. Oxygen plasma treatment apparatus consisted of a Plasmod Plasma Etcher (March Instruments Inc., Concord, CA), comprising of an etcher, a pump and oxygen-flow system.

4.2.2 Electrospinning fabrication and surface modification of the inner core

PCL was dissolved in a 5:3:2 mixture of DCM, DMF and a heparin-methanol solution to obtain an 8% by weight PCL solution. Heparin, a thromboresistant molecule and EC attractant [119], was dissolved in the methanol to obtain a heparin-methanol solution (8% wt) and the total heparin

concentration in the resulting PCL solution was 0.5% by weight. PEO was dissolved ACN to obtain a PEO solution (4.5% wt). Collagen (COL) was dissolved in HFIP to obtain a COL solution (8.3% wt). Single-polymer nanofibrous materials were fabricated by a single electrospinning apparatus (Figure 4.1A). Rotation speed was set at 400 rpm. To facilitate detachment of scaffold materials from the collector and protect the scaffold lumen surface, the collector was tightly wrapped with a thin aluminum foil with an ultrathin PEO layer covering its surface. PEO fibers electrospun prior to PCL were dissolved in DI water, which released PCL fibers from the foil. PCL fibers were collected with a needle-collector distance of 22cm. The voltage and flow rate for collecting the PCL fiber were set to 27kV and 1mL/hr, respectively. PCL was spun up to a thickness of 120μm with or without the surface modifications.

To enhance the interface interactions and thus the integration between the layers, three surface modification strategies of PCL fibers were introduced: (a) creating high porosity (HP) at the surface, (b) forming double-spun collagen/PCL layer (DC) on the surface, and (c) using oxygen plasma (OP) to activate the surface. PCL(HP) and PCL(DC) fiber scaffolds were fabricated by collecting PCL nanofibers until the point where the thickness of the tube reaches approximately 100μm. After that, PEO or COL was simultaneously spun with PCL, forming interwoven nanofibers on the collector for the next 20μm (Figure 4.1B). Thus, the single-fiber segment and the two-fiber segment were structurally integrated through a continuous spinning process. The production of interwoven fiber networks was based on our previously established double-electrospinning technique [118]. The voltage and collector distance for collecting the PEO or COL fibers were set to 30kV and 18cm, respectively. The flow rates of PCL and PEO or COL were programmed to vary with time, according to Figure 4.1C. The PCL scaffold was cut into small tubes of uniform length of about 30mm. To create PCL(HP) scaffolds, PCL scaffolds with PCL/PEO surface were soaked for an

hour in deionized or ultrapure water to eliminate the PEO component and solvent residuals, thus increasing higher porosity on the surface. PCL(DC) fiber scaffolds were fabricated by first obtaining unmodified PCL samples (120μm), removing them from the aluminum foil, and then placing them in the vacuum chamber of an etcher at 0.2 Torr by applying oxygen plasma for 5 minutes. The oxygen flow rate and the RF power were set to 0.5 cm^3/min and 5.0W, respectively. It was shown that oxygen plasma activated PCL surfaces by introducing hydroxyl and carboxyl groups [120, 121]. As the reactive species were not stable, the treated materials were used immediately.

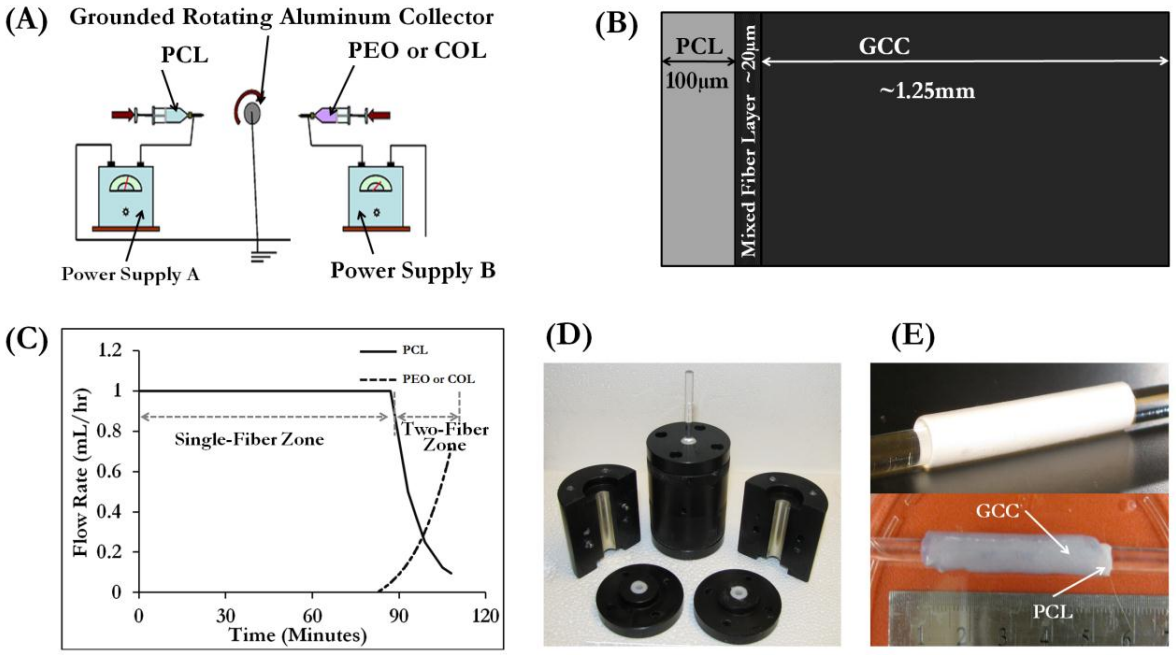

Figure 4.1: Illustration of the graft fabrication process: (A) Illustration of the double electrospinning apparatus used to spin PCL with PEO or COL on a rotating aluminum collector; (B) Schematic illustration of the multilayer vascular graft design; (C) Feed rate for spinning of 120μm PCL tube with a 20μm-thick mixed fiber layer with PEO or COL; (D) Mold used to produce multilayer grafts; (E) Illustration of a one-layer PCL graft (top) and a multilayer graft (bottom).

4.2.3 Preparation of multilayer vascular grafts

Preparation of the gel for the outer shell was followed the protocol we developed previously [117]. Briefly, rat tail collagen (type I) in 0.02N acetic acid (pH 4.0) at 9 mg/ml (BD Biosciences Inc., San Jose, CA) was first transferred to a centrifuge tube. Then, 1X Dulbecco's Phosphate Buffered Saline (DPBS, Invitrogen Corporation, Carlsbad, CA) and 10X Hank's balanced salt solution containing phenol red was added to the solution, followed by the addition of chitosan suspension. Chitosan (Molecular Weight = 100,000-300,000 g/mol, 90% deacetylation, Milan Panic Biomedicals Inc., Solon, OH) was dissolved in 1% acetic acid resulting in a chitosan suspension of 10 mg/ml concentration with a viscosity of 2000-3000 mPa.s. The pH of the pre-gel mixture was adjusted to 7.3 by the careful addition of 1M NaOH. Finally, the mixture was finally topped off with 1X DPBS solution to achieve the desired volume. The final concentrations of the COL and chitosan in the collagen-chitosan constructs were 3mg/ml and 3.5 mg/ml, respectively. The inner core manufactured by the electrospinning process was slid over a dry glass rod. This rod was then placed in the vascular graft mold. The neutralized collagen-chitosan mixture was slowly poured into the graft mold (Figure 4.1D) around the PCL tube. To further remove bubbles which influence mechanical properties by introducing void defects in gel constructs, the pre-gel solution was placed at room temperature for five minutes before it was transferred into the incubator. Finally, the mold was transferred into an incubator to initiate gelation at 37 °C. After 10 hours of gelation, the outer shell was crosslinked by diffusion with 1mM or 2.5mM genipin in 1X DPBS for 10 hours. The crosslinker concentration was determined by our previous study [117], according to its effect on SMC migration. The samples were washed 5 times in 1X DPBS to remove an excess unreacted genipin. The PCL tubes without the outer GCC shell and have thicknesses of 120μm and 240μm were referred to as PCL(120μm) and PCL(240μm), respectively. The multilayer grafts using

PCL(HP) for the inner core were denoted as PCL(HP)-GCC, those using PCL(DC) as PCL(DC)-GCC, and those using PCL(OP) as PCL(OP)-GCC. Figure 4.1E demonstrated a one-layer graft and a multilayer graft after fabrication.

4.2.4 Structural characterizations

Small graft-sections were obtained from all the samples in hydrated and dehydrated conditions. Cut sections (~10mm length) of the graft samples were frozen in liquid nitrogen (~195 °C) following which they were dried in a critical chamber for approximately 48 hours. The outer surfaces of PCL (120μm) without and with surface modifications were imaged. Both dry and hydrated grafts were frozen in liquid nitrogen and dried in a critical-point drying chamber (Labconco, Kansas City, MO). All of these graft samples were embedded in a cryo-optimum-cutting-temperature compound (Andwin Scientific, Schaumburg, IL), and then sectioned in a cryostat. These samples were sectioned transversely in parallel to the cross-section. Resultant 15-μm thick histological sections were placed on glass slides. The slides were then stained with Van Gieson stain or modified Movat's Pentachrome stain, and observed under a light microscope (Zeiss Axiovert S100, Carl Zeiss, Germany) at 20X magnification. The graft samples were also imaged under a field emission scanning electron microscope (Zeiss FESEM Supra40, Carl Zeiss, Germany).

4.2.5 Fourier transform infrared spectroscopy (FTIR) analysis

Transverse cross-sections of unmodified PCL, uncrosslinked collagen scaffold and PCL(DC) were frozen in liquid nitrogen (~195°C), following which they were dried in a critical-point drying

chamber (Labconco, Kansas City, MO) for approximately 48 h. The incorporation of collagen nanofibers in the PCL nanofibrous matrix was studied using an attenuated total reflectance fourier transform infrared (ATR–FTIR) spectrometer, Nicolet 4700 (Thermo Fisher Scientific, Waltham, MA). Comparisons were made between samples. IGOR software (WaveMetrics Inc., Tigard, OR) was used to identify the peaks and to calculate the areas under the peaks.

4.2.6 Physical and biomechanical characterizations of vascular grafts

Water permeability, burst strength, compliance and suture retention strength of the vascular grafts were determined according to the method prescribed in ANSI/AAMI/ISO 7198:1998/2001/(R) 2004 (Cardiovascular Implants: Tubular Vascular Prostheses).

Water Permeability: Tube adapters were inserted on both ends of the multilayer graft. Suture threads were used to secure the graft on the adapters. The graft was, then, cannulated by connecting one end of the graft to a water reservoir and closing the other end using a flow valve. Air, pressurized at 16kPa (120mmHg), was forced on the water column in the reservoir. Due to the pressure, water permeated through the membrane. Once the flow became steady, the permeate fluid was collected in a beaker and the volume of water collected in 1 minute was measured. The permeability of the graft ($mL/cm^2/min^{-1}$) was determined using the equation:

$$\tau = \frac{Q}{A}$$

where, τ was the scaffold's permeability, Q was the fluid volume passing through the scaffold, A was the cross sectional area of the aperture in the sample holder.

Burst Strength: To perform burst strength on hydrated grafts, a thin latex tube was slid into the lumen of the tubular graft and the tube adapters were inserted on both ends. Suture threads were used to secure the graft on to the latex tube near the adapters. The tubular graft was, then, cannulated with CO_2 being pumped in through one end of the graft, using PTFE tubing, while closing the other end using a flow valve. Due to the increase of CO_2 flow in to the latex tube, the latex tube expanded causing the vascular graft outside to expand. The expansion was allowed until graft failure occurred. The pressure at which this failure of the vascular graft occurs is recorded as burst strength or burst pressure of the graft.

Compliance: For compliance tests, the tubular graft was cannulated with the insertion of a latex tube similar to the burst strength test. The graft was then loaded onto a custom-made fixture and connected to a flow network via pressure gauges on both ends of the graft (Figure 4.2). The pressure in the graft was controlled using varying speed of a water pump from 0mmHg to 160 mmHg, with an increment of 10mmHg. At each pressure point, images of the graft dilatation were taken using a Canon EOS 450D camera (Canon Inc., Tokyo, Japan). These images were analyzed using a customized script in Matlab® (MathWorks Inc., Natick, MA) to measure the graft diameter at each pressure point. Then, the compliance of the graft (% mmHg x 10^2) was determined with the following equation,

$$C = \frac{\frac{R_2 - R_1}{R_1}}{P_2 - P_1} \times 10^4$$

where R is the radius of the graft at pressure P.

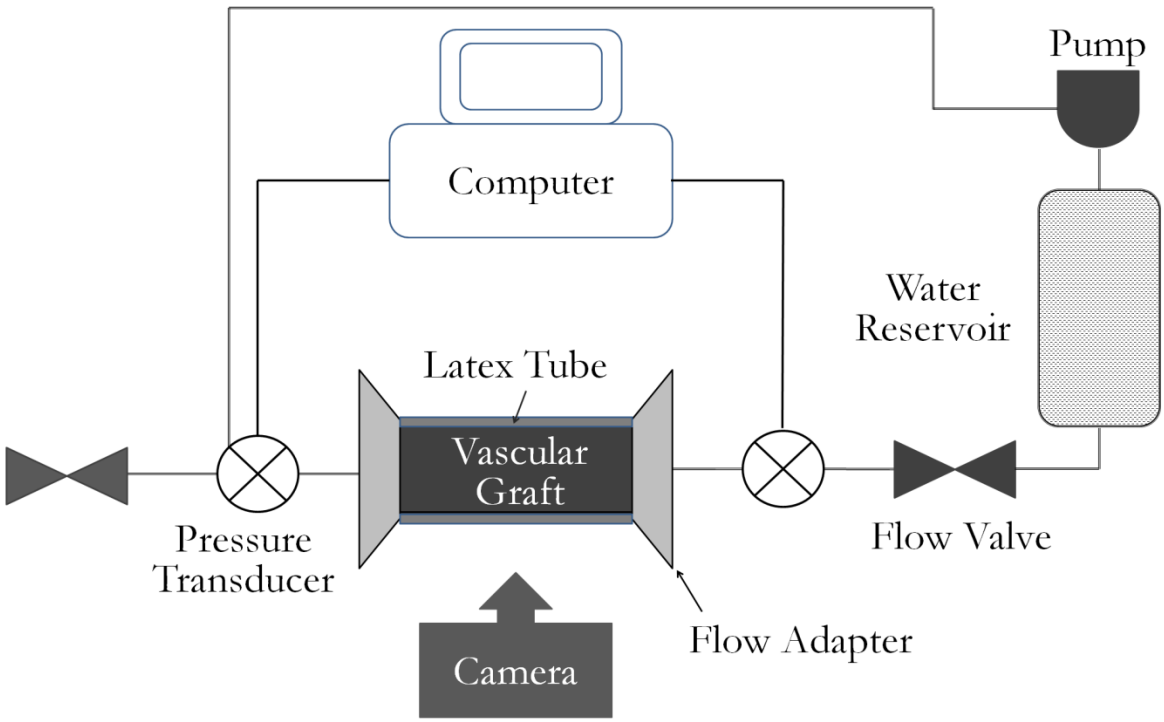

Figure 4.2: Schematic illustration of the system setup for vascular graft compliance test

Suture Retention Strength: To determine the suture retention strength, the vascular graft was cut normal to the long axis into small strips of dimensions (10mm X 5mm). A suture was inserted 2 mm from the end of the stretched strip of the graft through the wall of the graft to form a half loop and the other end of the graft was attached to the lower end of the MTS Insight electromechanical testing system (MTS Systems Corp., Eden Prairie, MN). The other end of the suture was attached to a 2000N load cell (MTS Systems Corp., Eden Prairie, MN). The suture was pulled at the rate of 150 mm/min. The force required to pull the suture through the graft or cause the wall of the graft to rupture were recorded. In this study, the suture retention strengths of PCL(120μm) and PCL(HP)-GCC were compared.

4.2.7 Vascular cell characterization

Vascular grafts were frozen in liquid nitrogen and dried in a critical-point drying chamber (Labconco, Kansas City, MO) prior to seeding of cells into them. PCL(HP)-GCC grafts were used for cell characterization. To seed a 4.76mm multilayer vascular graft with bovine pulmonary artery ECs, the multilayer graft, suture strings and adapters were sterilized in 100% ethanol for 1 hour. All jackets and plugs used in the seeding process were autoclaved for 20 minutes. Seeding ECs onto the surface of the graft lumen was done by adapting protocols developed previously [122, 123]. The vascular grafts were then rehydrated by soaking into sterile 1X DPBS. One end of the graft was then secured with an adapter plug with sutures. For seeding, the EC suspension with a density of 1 x 10^6 cells/ml was obtained in the cell culture medium which contains 10% fetal bovine serum and 1% penicillin-streptomycin in Dulbecco's Modified Eagle Medium (DMEM). After filling the space in the graft lumen with ECs, the other end of the graft was secured with an adapter plug. Custom-made jacket rings were then wrapped around the graft to fit it into a centrifuge tube and adapter spacer rinds were placed around both the adapters. The fully assembled centrifuge tube was then placed in the center of a centrifuge. The tube was aligned perfectly to the center to avoid any wobbling or uneven spinning. Then, the system was allowed to spin at 2000 rpm for 5 minutes. After centrifuge seeding, the graft secured with the adapters was allowed to sit for about an hour before carefully removing the adapters. After seeding ECs in the lumen, bovine pulmonary artery SMCs were seeded onto the outer shell of the grafts. The SMC suspension was prepared in the similar medium and with the same cell density as ECs. The liquid on the outer shell of the grafts was removed by gently and quickly rolling the graft on cotton gauge. The SMC suspension (1mL) was then allowed to be absorbed by the outer shell layer. Finally, the tube containing the graft seeded with ECs and SMCs was incubated for about an hour. The graft was transferred into a centrifuge

tube filled with fresh medium, which was put onto a rotator placed inside an incubator set at 37ºC and 5% CO_2. Graft samples were collected after culture for 1 hour, 3 days and 6 days, respectively. Samples were fixed in 10% formaldehyde. Samples were directly stained with DAPI and observed under a fluorescent microscope at 20X magnification. Samples were also cryo-sectioned and histological sections were stained with hematoxylin and eosin stain and observed under a light microscope at 20X magnification. Additionally, EC morphology on the graft lumen was imaged under a field emission scanning electron microscope (FESEM Supra40 Zeiss, Carl Zeiss – Advanced Imaging Microscopy, Germany). These samples were cut transversely in parallel to the cross section for en face imaging.

4.2.8 Short-term implantation in rabbit models

Four New Zealand white rabbits were premedicated with subcutaneous injections of Medetomidin (210 mcg/kg), Midazolam (0.5 mg/kg) and Morphine (1 mg/kg). An intravenous catheter was placed in a vein in the ear and propofol (5 to 8 mg/kg) was used to induce anesthesia. After intubation, anesthesia was maintained with Isofluran in 100% oxygen. At the time of induction, rabbits receive Enrofloxacin at a dose of 5mg/kg. The rabbits were placed on dorsal recumbency. The abdomen was clipped with a #40 blade and prepared with chlorhexidine for surgery. After draping the abdomen with sterile surgical drape, a midline incision was performed. The colon was retracted medially and the infrarenal aorta exposed. They were ligated with 5-0 polypropylene suture. Heparin was administered at the dose of 200 U/kg intravenously. After dissection of the infrarenal aorta over 2 cm, vascular clamps were applied to isolate the infrarenal aorta. The aorta was transected between the clamps. An acellular PCL(HP)-GCC graft with a 3mm inner diameter was anastomosed in an end to end fashion with two continuous 7-0 polypropylene sutures. After

completion of the anastomosis the clamps were removed and the anastomosis inspected for leakage and patency. The abdominal incision was then closed in a routine fashion. The animals received buprenorphine (0.05mg/kg subcutaneously twice a day for 3 days) and meloxicam (0.3 mg/kg subcutaneously twice a day for 3 days). After one day, the graft and the distal and proximal aortal sections were explanted and fixed in 10% formaldehyde, cryo-sectioned and stained with hematoxylin and eosin. These stained sections were observed under the light microscope at 20X magnification.

4.2.9 Ultrasound sonography

Ultrasound images of the grafts, the upstream and downstream neighboring artery, were taken after 1-Day of implantation to visualize any thrombus formation or narrowing of the graft.

4.2.10 Data analysis and statistics

Data were statistically analyzed using the one-way ANOVA test. Student's t test was then used to compare the means of each individual group. The level of significance was set at $\alpha = 0.05$ for 95% statistical significance. Error bars on all the histogram charts represent the standard error of the mean based on the total number of the samples.

4.3 Results

4.3.1 Structure and interface characterization

The histological sections of the multilayer grafts, as observed under an optical microscope (Figure 4.3), clearly demonstrate the adhesion between the inner core and the outer shell under dehydrated and hydrated conditions. Consistency of adhesion was dependent on the method of surface modification. The multilayer adhesion in PCL(OP)-GCC and PCL(HP)-GCC was more stable than PCL(DC)-GCC. It was also clear that hydration plays an important role to maintain the graft integrity. The surface modifications of the PCL inner core were examined using scanning electron micrographs (Figure 4.4). PCL layer is a porous network of fibers (Figure 4.4A) whose porosity can be increased by electrospinning and removal of PEO (Figure 4.4B). The SEM micrograph of the oxygen-plasma treated PCL fibers (Figure 4.4D) showed that some of the fibers have melted away causing the pores to be filled with the melted PCL. It is difficult to distinguish between electrospun COL and PCL fibers in the SEM images since they are similar in the structure (Figure 4.4C). But we were able to confirm the collagen component by performing FTIR spectroscopy analysis on the PCL(DC)-GCC samples.

4.3.2 FTIR-ATR characterization results showing the incorporation of electrospun collagen fibers in the electrospun PCL matrix

The characteristic peaks derived from the symmetric and asymmetric stretching vibrations of CH_2, C=O, C-O, C-C, CO-C and C-O-C, in the crystalline and amorphous phases, are exhibited in the

FTIR spectra of the PCL and the PCL(DC) fiber matrices. The characteristic peaks derived from the stretching vibrations of N–H_y (y = 1, 2), O–H, C–H_y (y = 1–3), C–O–C, C=O, and the bending vibrations of N–H, C–O–C, C–H, are exhibited in FTIR spectra of the Collagen and the PCL(DC) fiber matrices. The peaks which are common to PCL, COL and PCL(DC) are presented in Table 4.1. Figure 4.5 demonstrates the spectrum of each matrix component and the spectra of the different types of collagen-based matrices, showing the incorporation of component additives. For the spectra of COL (Curve 4.5B) and PCL(DC) (Curve 4.5C), typical peaks are derived from amide I (C=O stretching at 1630 cm^{-1}), amide II (N–H bending at 1550 cm^{-1}) and the mixed stretching and bending vibrations of the C–O–C bond (1150–970 cm^{-1})are clearly present. For the spectra of PCL(Curve 4.5A) and PCL(DC) (Curve 4.5B), the typical peaks are derived from asymmetric CH_2 stretching (2949 cm^{-1}), symmetric CH_2 stretching (2865 cm^{-1}), C=O stretching (1727 cm^{-1}), C–O and C-C stretching in the crystalline phase (1293 cm^{-1}), asymmetric COC stretching (1240 cm^{-1}), OC–O stretching (1190 cm^{-1}), symmetric COC stretching (1170 cm^{-1}) and C–O and C-C stretching in the amorphous phase (1157 cm^{-1}).

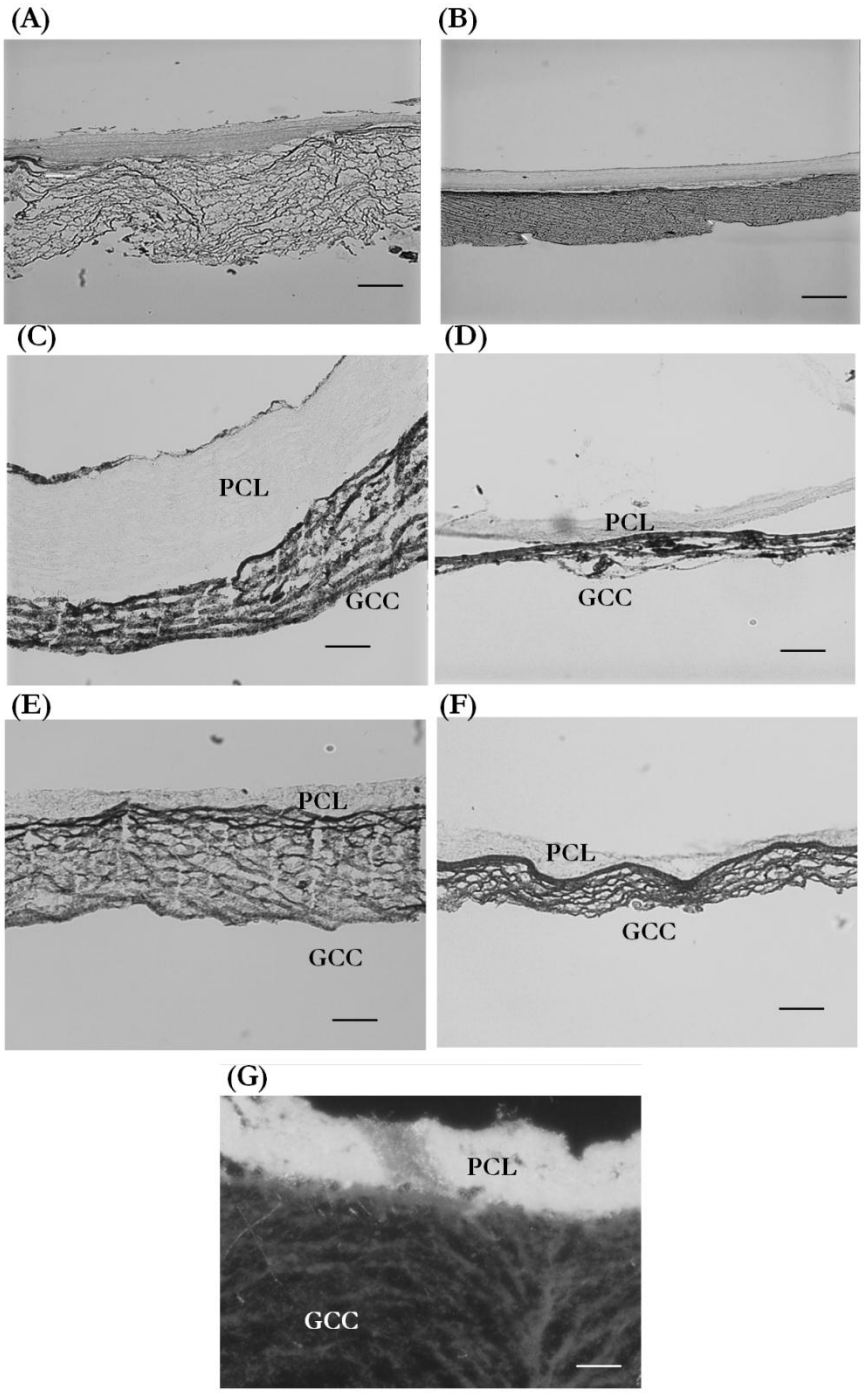

Figure 4.3: Optical microscopy images of the hydrated and dehydrated samples after freeze-drying process. (A) Hydrated PCL(HP)-GCC; (B) Dehydrated PCL(HP)-GCC; (C) Hydrated PCL(DC)-GCC; (D) Dehydrated PCL(DC)-GCC; (E) Hydrated PCL(OP)-GCC; (F) Dehydrated PCL(OP)-GCC. (G) Hydrated PCL(HP)-GCC under dark field. Scale bar: 100μm

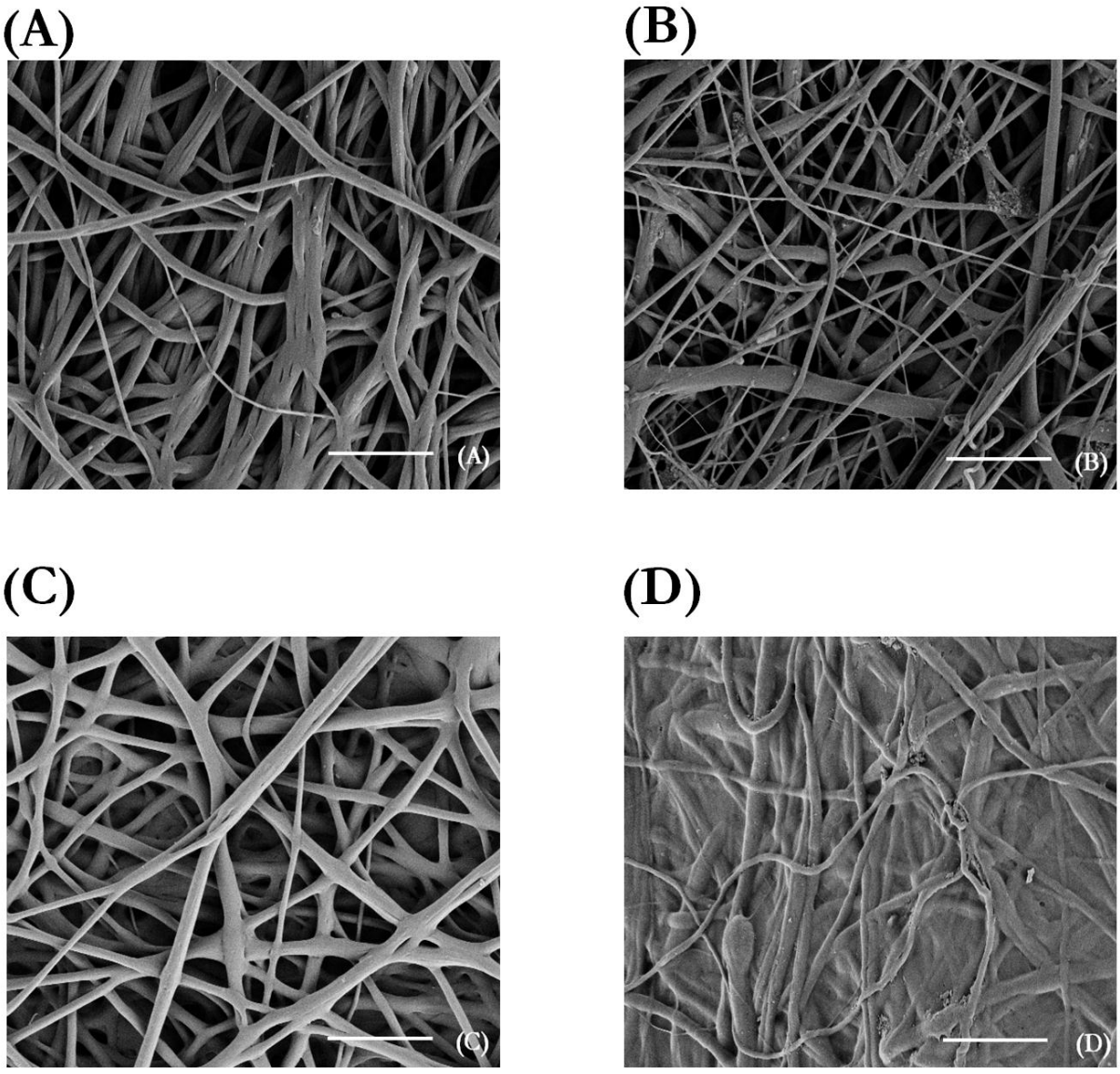

Figure 4.4: SEM images of graft interfaces. (A) PCL without any surface modifications; (B) PCL double electrospun with PEO which was removed by dissolution in DI H_2O; (C) PCL double electrospun with COL; (D) PCL treated with oxygen-plasma. Scale bar: 10μm

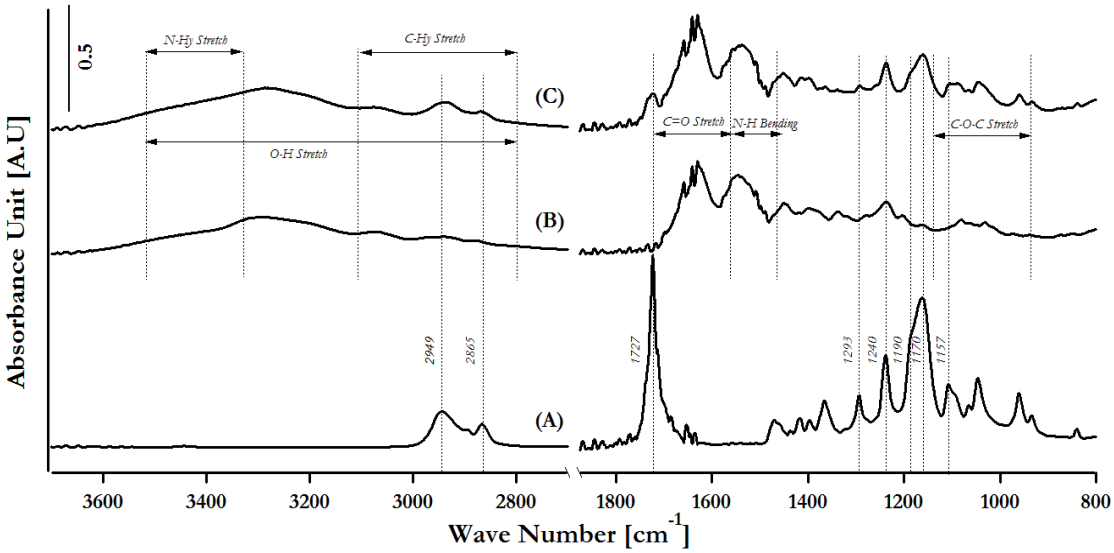

Figure 4.5: Fourier Transform Infrared Spectroscopy on (A): PCL; (B): Collagen and (C): PCL Double Electrospun with Collagen.

Position(cm^{-1})	PCL
2949	Asymmetric CH_2 Stretching
2865	Symmetric CH_2 Stretching
1727	C=O Stretching
1293	C–O and C-C Stretching in the Crystalline Phase
1240	Asymmetric COC Stretching
1190	OC–O Stretching
1170	Symmetric COC Stretching
1157	C–O and C-C Stretching in the Amorphous Phase
Position(cm^{-1})	**Collagen**
3500-2800	O-H Stretching
3500-3450	N-H_y Stretching
3100-2800	C-H_y Stretching
1790-1580	C=O Stretching
1580-1470	N-H bending
1150-940	C-O-C Stretching

Table 4.1: FTIR Curve Analysis: Incorporation of Collagen in PCL Matrix

4.3.3 Physical and biomechanical characterizations of multilayer grafts

Physical and biomechanical properties of vascular grafts play critical roles in maintaining structure and function of the grafts *in vivo* and thus are included in the FDA standards. Herein, we determined several essential graft properties including permeability, burst strength, compliance and suture strength, and studied the effects of graft structure designs on these properties.

Water Permeability: Results from water permeability tests showed that the mean permeability value of single layer 120μm-thick PCL grafts without outer shells was 2380mL/cm^2/min (Figure 4.6A). With the addition of an outer shell using various surface modification strategies on the PCL inner core (120μm), the mean water permeability values were found to be 528mL/cm^2/min, 1112mL/cm^2/min, and 553mL/cm^2/min for the PCL(HP)-GCC, PCL(DC)-GCC and PCL(OP)-GCC grafts, respectively. The water permeability values of PCL(HP)-GCC and PCL(OP)-GCC showed four times reductions when compared to the PCL(120μm) samples. The water permeability value of PCL(DC)-GCC samples was significantly higher than PCL(HP)-GCC and PCL(OP)-GCC, and about two times reductions when compared to the PCL(120μm) samples. In addition, we respectively varied the design parameters of the PCL layer and the GCC layer, the inner core thickness and the crosslinking condition of the outer shell, to examine their influences on water permeability (Figure 4.6B). Results showed that the mean permeability value of the single layer 240μm-thick PCL grafts was 1030mL/cm^2/min. There was a significant decrease in the mean permeability value with the increase of PCL thickness; about two times reduction in permeability with two times increase in the PCL thickness. We also found that the permeability value for the graft with outer shells of a high crosslinking density, 10mM (264mL/cm^2/min), decreased two times, when compared to the multilayer grafts with outer shells of lower crosslinking densities, 1mM

(609mL/cm^2/min) and 2.5mM (528mL/cm^2/min). We previously determined the effects of these crosslinking conditions on the crosslinking density [117]. Our results here, thus, demonstrated that engineering the integration of a multilayer structure, in addition to the individual layer designs such as varying PCL thickness or GCC crosslinking density could significantly influence the water permeability values of the vascular grafts.

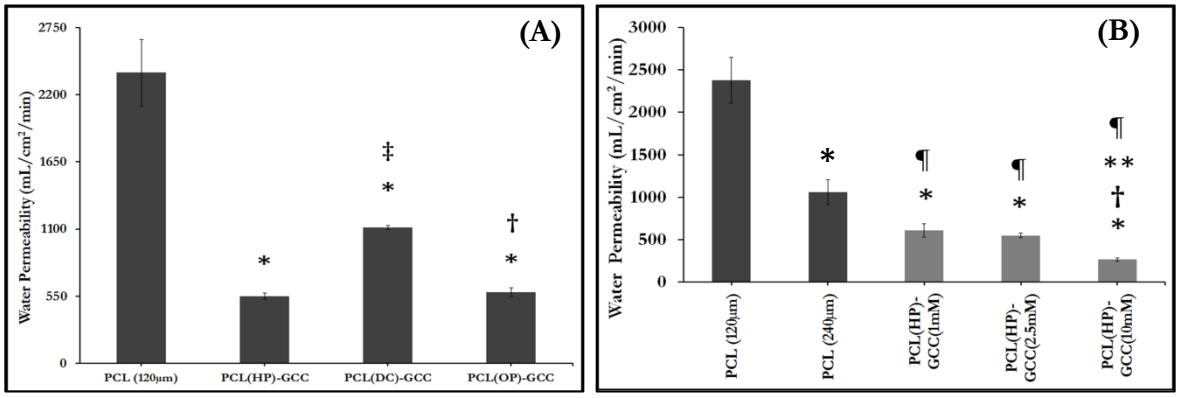

Figure 4.6: Graft water permeability. (A) Single-layer PCL grafts showed higher permeability than multilayer grafts with various interfacing strategies. * - $p<0.05$ w.r.t. PCL (120μm), and ‡ - $p<0.05$ w.r.t. PCL(HP)-GCC. (B) Graft permeability varies with the thickness of PCL inner core (black bars) or the crosslinking condition of outer shell (grey bars). * - $p<0.05$ w.r.t. PCL (120μm), ¶ - $p<0.05$ w.r.t. PCL(240μm), † - $p<0.05$ w.r.t. PCL(HP)-GCC(1mM), and ** - $p<0.05$ w.r.t. PCL(HP)-GCC(2.5mM).

Burst Strength: Results from burst strength tests showed that the mean burst strength values of PCL scaffolds (Figure 4.7A) without an outer shell were 684 and 1172mmHg, for the 120μm- and 240μm- thick samples, respectively. Burst strength was significantly improved by increasing the inner core PCL thickness. The burst strength values of multilayer grafts with different interfaces or

integration strategies, PCL(HP)-GCC, PCL(DC)-GCC and PCL(OP)-GCC, were found to be 695, 638, and 611 mmHg, respectively. No significant differences in burst strength were found among these three multilayer grafts or between any multilayer graft and single layer graft with the same PCL thickness (120μm). Additionally, there was no significant difference in burst strength between the multilayer grafts with differently crosslinked outer shells (Figure 4.7B).

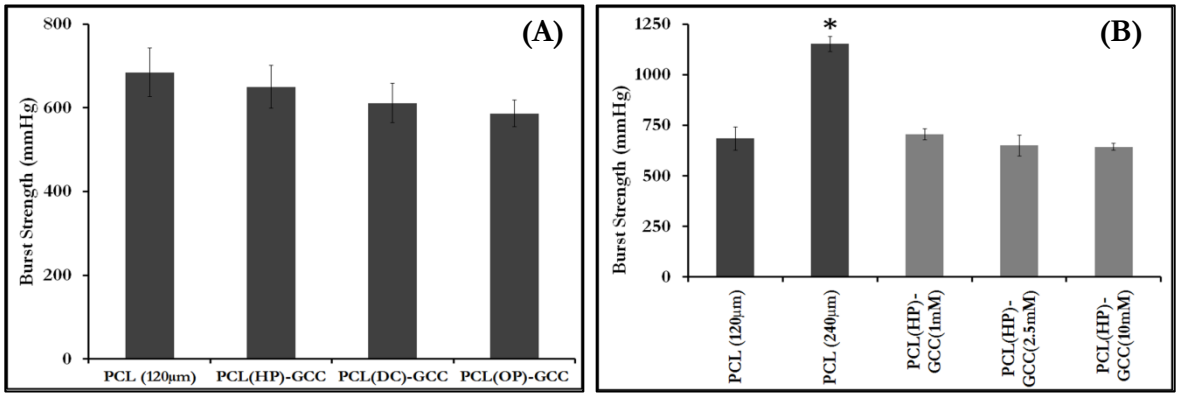

Figure 4.7: Graft burst strength. (A) Burst strength of PCL grafts and multilayer grafts with various interfacing strategies; (B) Burst Strength of grafts with varied thickness of PCL inner core (black bars) or varied crosslinking condition of outer shell (grey bars).

*- $p<0.05$ statistical difference w.r.t. PCL (inner core alone).

Compliance: Results from compliance tests between 80-120mmHg of cannulation pressure showed that PCL (120μm) had an average compliance of 5.3%, while the multilayer grafts, PCL(HP)-GCC, PCL(COL)-GCC, and PCL(OP)-GCC possessed average compliance values of 4.5%, 4.2% and 3.8%, respectively (Figure 4.8). PCL(240μm) exhibited a lower compliance of 2.7%. The compliance of unmodified PCL was significantly higher than that of PCL(240μm), PCL(HP)-GCC, PCL(COL)-GCC and PCL(OP)-GCC, respectively.

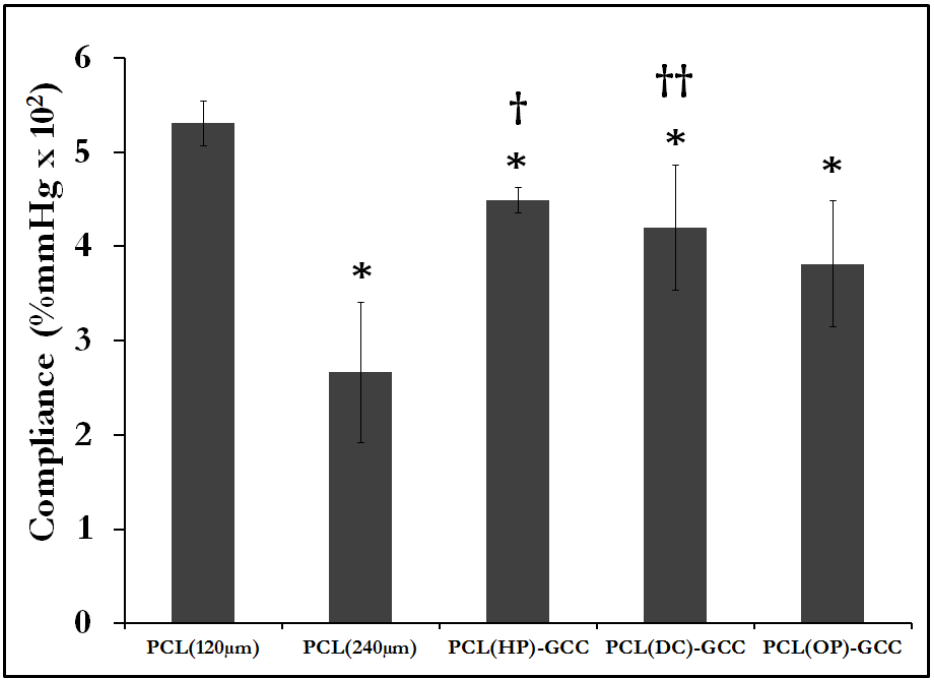

Figure 4.8: Compliance (%mmHg x 102) of PCL grafts and multilayer grafts with various interfacing strategies. *- p<0.05 w.r.t PCL (120μm), †- p<0.05 w.r.t PCL(240μm) and ††- p<0.1 w.r.t PCL(240μm).

Suture Strength: The suture retention strength of PCL(120μm) and PCL(HP)-GCC were found to be 2.05N and 2.38N, respectively, with no significant difference between them. This value was comparable to previously reported values of other PCL-based synthetic graft [113, 124], though it was lower than saphenous vein (~4N), and PTFE graft (4.9-6.7N).

Graft	Average Suture Retention Strength (N)
PCL (120μm)	2.1±0.3
PCL(HP)-GCC	2.4±0.1
Saphenous Vein [124]	4
e-PTFE [124]	4.9-6.7
PCL-COL-ELN [124]	0.9-3.5
PCL-COL [113]	3-5

Table 4.2: Suture Retention Strength

4.3.4 EC and SMC activities on the graft *in vitro*

Results from graft characterization with cells have demonstrated the utility of the multilayer graft for fast cellularization and cell proliferation to form engineered blood vessel *in vitro*. The successful seeding of both ECs and SMCs in the multilayer scaffold was shown by the histological sections stained with hematoxylin and eosin stain (Figure 4.9). The SEM micrographs clearly indicate the formation of a more confluent layer of ECs with the increase in cell density due to proliferation after 3 days (Figure 4.9B), compared to the initial cell density (Figure 4.9A). There was further cell proliferation and higher level of cell confluency after 6 days of cell-seeding (Figure 4.9C). Optical images of histological section of the cell-seeded grafts also demonstrated similar EC proliferation in the lumen (Figure 4.9D-E). In addition, these images also showed the increase in SMC number in the GCC outer core of the graft. The fluorescence imaging using DAPI also demonstrated seeding of ECs and SMCs in the different layers of the grafts (Figure 4.9F).

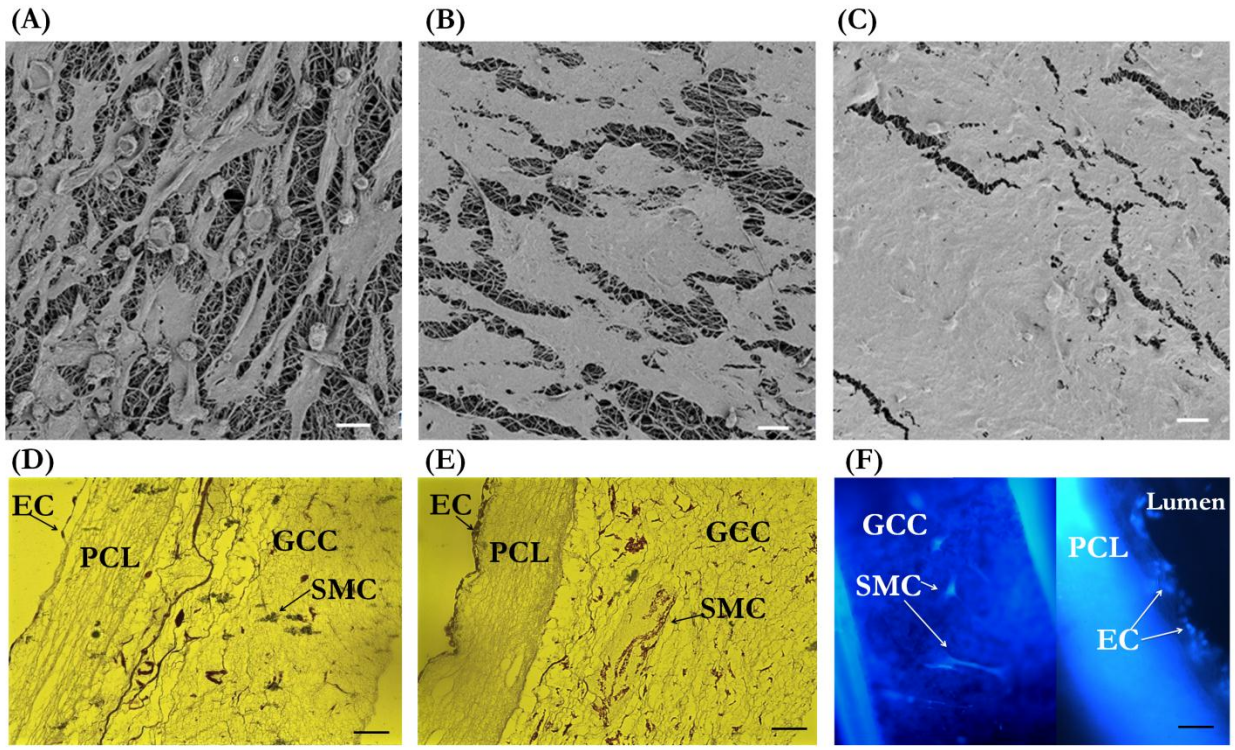

Figure 4.9: Microscopic examination of cell-seeded grafts. SEM images of EC-seeded graft lumen after 1 hour (A), 3 days (B), and 6 days (C) of cell seeding. Optimal microscopy images of the transverse cross-section of cell-seeded graft after 1 hour (D) and 6 days (E) of cell seeding. Fluorescent microscope image of DAPI-stained cells after 3 days of cell seeding (F).

Scale bar for A-C: 20μm and for D-F: 100μm

4.3.5 Short-term implantation evaluation results

Acellular grafts were used in this initial *in vivo* evaluation of vascular grafts. Figure 4.10A shows the implanted 3mm multilayer vascular graft replacing the abdominal aorta of a rabbit with anastomosis covered with gauge to stop bleeding. There were no unfavorable inflammatory or thrombogenic reactions produced by the graft. Explanted vascular grafts revealed a clean lumen with no blood

clots or platelet adhesion (Figure 4.10B). The sectioned and stained explanted graft showed cell invasion at the site of anastomosis (Figure 4.10C). These cells exhibited preference to invade the GCC layer and not the PCL layer. Additionally, these cells were stained negatively with monocyte marker, suggesting that they are not inflammatory cells and could be myofibroblasts or SMCs migrating from the surrounding tissues. Additionally, ultrasonic evaluation of the post-implantation blood flow through the graft revealed reperfusion of the grafts with pulsatile blood flow (Figure 4.10D).

4.4 Discussion

This study reported the development and characterization of robust, compliant, biodegradable multilayer constructs for vascular graft applications. The developed grafts were made from a densely-packed fibrous PCL membrane and a porous GCC gel, respectively to model the matrix environments in the vascular intima and media. Importantly, various interfacial designs were examined here to enhance the integration of the layers with drastically different structures and physiochemical properties to prevent delamination. Effects of the interfacial design on the material structure as well as physical and mechanical properties (i.e. permeability, burst strength, and compliance) under the physiological flow pressure were characterized. Results showed that the PCL(HP)-GCC graft with increased porosity at the interface provided layer adhesion for successful construct integration, desired graft permeability, required implant strength and high compliance (4.5%) for graft implants. Additionally, the multilayer construct supported culture and growth of vascular cells *in vitro*, and are readily implantable to replace artery *in vivo* resulting in cell ingrowth, flow reperfusion and free of thrombosis.

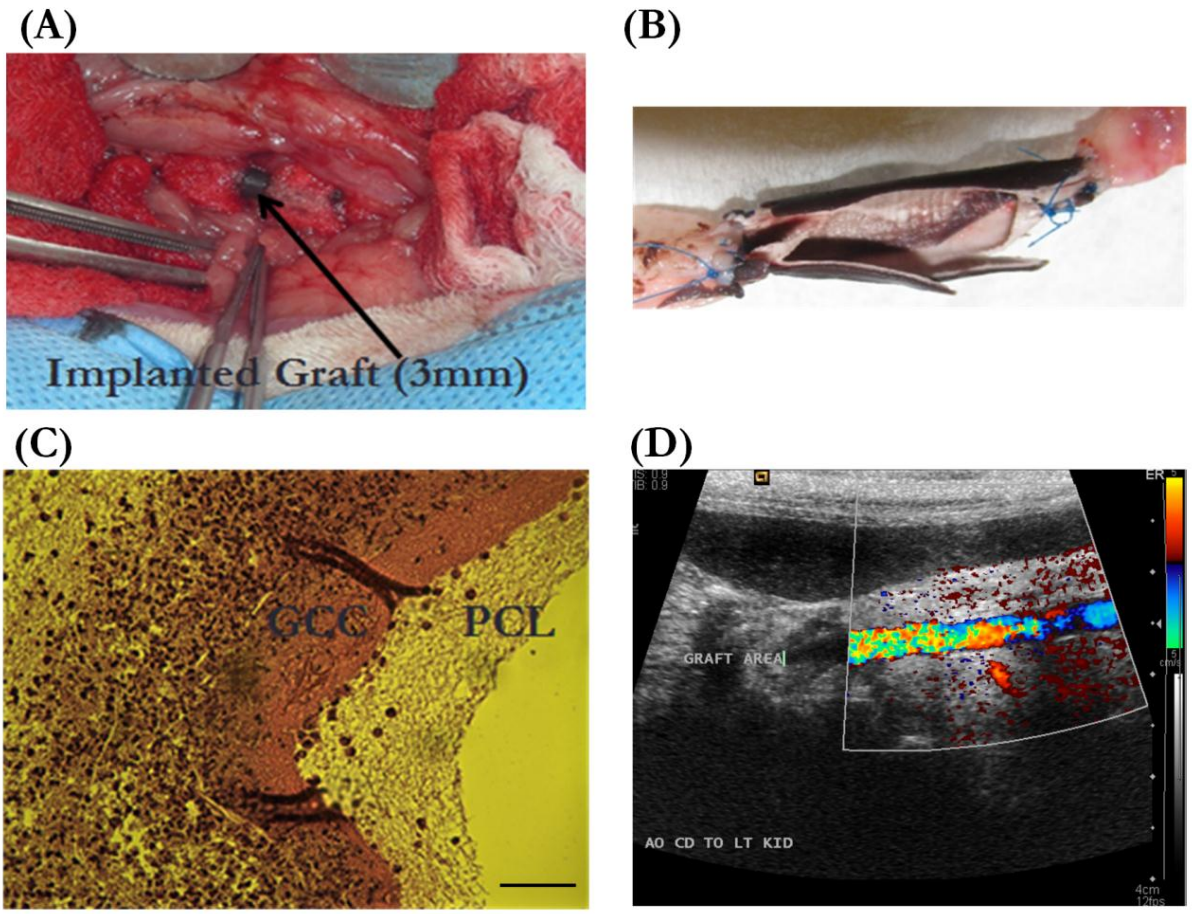

Figure 4.10: Biocompatibility evaluation of vascular grafts *in vivo* with a rabbit model. (A) Multilayer vascular graft Implanted 3mm replacing the abdominal aorta of a rabbit with anastomosis covered with gauge that stop bleeding; (B) Open-lumen of an explanted 3mm multilayer vascular graft with adjoining arteries, showing no thrombosis or occlusion in the lumen of the graft; (C) Optical image of H&E stained, histological section of explanted graft, showing the migration of cells from surrounding tissue mainly into the GCC layer rather than the PCL layer; (D) Ultrasonic image showing blood reperfusion through the graft and the lumen with no stenosis. Scale Bar for C: 100μm.

PCL is highly hydrophobic, stiff and strong, whereas GCC is highly hydrophilic, elastic and mechanically weaker. The combination of the biomaterials with drastically different properties made

the formation of a multilayer graft a challenging process. Without any surface modifications, GCC easily slipped over the PCL surface. Herein, the adhesion between the two layers was designed using a physical or a chemical attachment process. The physical process involved the entanglement of collagen-chitosan gel in the large pores of PCL fibers near the interface between the two materials. During the outer shell formation, the collagen-chitosan pre-gel mixture could more readily enter larger pores. After the gelation, the collagen-chitosan gel with a fiber-sheet structure [109] might interact with PCL fibers with physical entanglement. Within the physiological stresses used for physical and mechanical testing in this study, the multilayer constructs maintained integral structure. The chemical attachment process involved the formation of the covalent chemical bonds between the PCL and GCC layers. This was achieved by two methods. In the first method, PCL was double electrospun with collagen at the interface, and then genipin crosslinker could crosslink the collagen in the double-electrospun PCL-collagen with the collagen and chitosan component in the GCC outer shell [109]. However, this method resulted in excessive shrinkage or expansion of the inner layer during hydration and dehydration process, which could introduce separation and cracking. The second method involved oxygen plasma treatment of an unmodified pure PCL tube [120, 121]. During this process, new reactive oxygen groups were introduced on the surface of the PCL fibers, thereby forming a stable bond between the two layers. The major problem using this process was the appropriate amount of RF power and flow rate in the oxygen plasma process, which was limited to 5.0W and 0.1cm^3/min, respectively. This limit was imposed due to the melting of the inner core at higher RF powers and flow rates, even though higher powers have been used in previous studies [120, 121]. Even under the limited power and flow rate, the SEM image showed melted PCL fibers that filled the pores.

Water permeability is a critical graft function test. Values above 800ml/cm^2/min are generally considered high and preclotting must be applied before implantation, while values below 600ml/cm^2/min are considered low for molecule transport affecting graft healing [125, 126]. By virtue of being a nanofibrous material with connected pores, a thin PCL layer (120μm in this study) allows large quantities of water to permeate under the physiological flow pressure. Yet with the addition of the outer shell, the permeation was reduced considerably when the interface between the two layers showed good adhesion. PCL(DC) and GCC did not form as good adhesion as PCL(HP)-GCC and PCL(OP)-GCC at the interface (Figure 4.3B-C), and thereby permeability of PCL(DC)-GCC significantly higher than that of PCL(HP)-GCC and PCL(OP)-GCC (Figure 4.6A). Due to good adhesion which maintains structural integrity under flow, the GCC layer forms an effective barrier to reduce permeability. The reduction in the permeation can be attributed to the decrease in the water pressure difference across the cross-section of the graft as well as the increase in the thickness of the cross-section. Darcy's law of diffusion states that the permeability of a porous membrane or slab is directly proportional to the pressure gradient across the membrane or slab and inversely proportional to the thickness of the membrane or slab. The equation of the relationship is:

$$q = K_D \frac{\Delta P}{t}$$

where, q is the amount of water permeated through unit area in unit time, K_D is the permeability constant, ΔP is the pressure change, and t is the thickness of the membrane or slab. With the addition of the GCC layer, not only the thickness t increases, but also the pressure gradient across the graft decreases because the hydrophilic GCC matrix has sites for binding of water molecules, thereby reducing the pressure gradient and mass transfer across the graft.

In addition to permeability, compliance and burst strength are both important determinants to graft functioning *in vivo*, but achieving the balance between them as shown by native arteries is a long-standing issue [19]. Herein, our strategies combine two types of materials: PCL, a strong yet stiff material [118] and GCC, a compliant scaffold [117]. The PCL inner core determines both burst strength and compliance of the multilayer graft, while the importance of a GCC layer in reducing permeability has been elaborated above. The multilayer graft can thus possess adequate permeability and burst pressure (five times the higher end of physiological pressure), for immediately implantation. Furthermore, due to a thin PCL inner core, the compliance value of PCL(HP)-GCC (4.5%) is comparable to those of native vessels such as saphenous vein (4.5%) and umbilical vein (4%), and much higher than those of synthetic PTFE and Dacron grafts (2%) [23]. Compared to PCL(HP)-GCC, the compliance value of PCL(OP)-GCC is lower. This can be attributed to the melting of PCL fibers during oxygen plasma treatment. PCL-based grafts used in previous studies were characterized by much higher thicknesses, resulting in higher burst strength and lower compliance [113, 114, 124, 127]. As compliance plays an essential role in cell activity and graft healing, due to its influence on hemodynamics at the site of anastomosis [16], Salacinski et al. have used the graft compliance to predict the graft patency [23]. They demonstrated a nearly linear relationship between the graft compliance and the graft patency after one month of implantation. Using this patency-compliance relationship (Table 4.3), we expect that the one-month patency rate of our grafts will be over 75%. The burst strength of the grafts, though low, is also adequate for *in vivo* functioning. One key reason why the burst strength is lower than previously reported values for PCL fiber grafts [113] is the difference in the PCL layer thickness (almost three times our model). Nevertheless, the *in vivo* evaluation demonstrated the graft robustness for the use as artery implants. Studies in rabbit models showed that there was no unfavorable thrombosis or inflammatory reactions. Also, we found that cells preferentially invaded into the GCC layer and not the PCL layer;

immune cells were not recruited to the lumen (Figure 4.10C). This may be due to the higher porosity and lower elastic modulus of the GCC in comparison to the PCL layer. Therefore, in addition to the complementary function in physical and mechanical properties, the two-layer design also provided layered structure for cell seeding or ingrowth *in vitro* and *in vivo*.

Graft	Compliance	Patency
	% mmHg x 10^2	%
PCL (120μm)	5.2±0.6	
PCL (240μm)	2.7±1.5	
PCL(HP)-GCC	4.5±0.6	
Host artery	5.9 ± 0.5	
Saphenous vein [128]	4.4 ± 0.8	75
Umbilical vein [22, 128]	3.7 ± 0.5	60
Bovine heterograft [128]	2.6 ± 0.3	59
Dacron [128]	1.9 ± 0.3	50
e-PTFE [128]	1.6 ± 0.2	40

Table 4.3: Compliance vs. Patency – A Prediction

4.5 Conclusion

This paper reports design and characterization of multilayer vascular grafts which are synthesized with a combination of electrospun PCL fibers and collagen-based scaffolds. Results have identified the design of the material interface as an important determinant to the graft integrity and stability. Results have also shown PCL as graft inner core mainly contributes to the biomechanical properties such as burst strength, compliance and suture strength, while GCC as graft outer shell reduces the

water permeability. Additionally, the PCL core and the GCC shell respectively provide a surface for EC proliferation and support cell ingrowth or 3-dimensional cell culture. Also, the graft when implanted into animal models does not produce any unfavorable inflammatory or thrombogenic reactions. In the future, molecular environments mimicking those in the native blood vessels will be further designed and incorporated into the structure-mimic vascular grafts demonstrated here, and long-term implantation evaluation will be performed.

CHAPTER 5

OVINE IMPLANT MODEL FOR A NOVEL MULTILAYER VASCULAR GRAFT CONSISTING OF AN ELECTROSPUN INNER CORE AND A COLLAGENOUS OUTER SHELL

Abstract

Vascular grafts are a common response to a number of different diseases. To achieve long-term function for small diameter vascular grafts, tissue engineering has been identified as a possible solution. Mechanical and chemical signaling has large effects on cell proliferation and migration. In this study, we replaced the carotid arteries in a sheep with two multilayer grafts, with an inner core made of an electrospun intimal equivalent (poly-ε-caprolactone) and an outer shell made of a collagenous medial equivalent (genipin-crosslinked collagen-chitosan), for a duration of one month. The endothelial cell chemoattractant, heparin, was embedded in the inner core during the process of electrospinning. During the one-month period, ultrasound sonography images were obtained which were used to calculate the changes in the lumen diameter and the wall thickness during each week. The graft was explanted after one-month implantation. During the explantation, it was observed that the graft had fully integrated with the neighboring artery. Sections of the graft, the suture sites and the neighboring artery were then subjected to cryo-sectioning for histological staining. The ultrasound images revealed minimal changes to the graft diameter as well as significant changes to the graft wall thickness during the four weeks. The increase in thickness of the graft wall *in vivo* is due to the integration of the graft with the neighboring artery as well as the formation of the

neointimal hyperplasia. The formation of the neointimal hyperplasia, was also shown in optical images of the stained histological sections. There was no recruitment of endothelial cells in the intimal possibly due to the recruitment of the smooth muscle cells onto the intimal equivalent. The smooth muscle cells and the extracellular matrix were found to have no orientation in the medial equivalent while they were aligned circumferentially in the neointimal hyperplasia. Additionally, the ultrasound sonography images as well as the histological sections confirm that no unfavorable immunogenic response or thrombosis or stenosis occurred *in vivo* during the implantation. With all the superior physiological properties along with some methods to develop *in vivo* endothelialization, this multilayer graft has the potential to serve as a suitable vascular graft scaffold providing the right biomechanical properties and the micro-environments suitable to promote vascular cell migration and proliferation as well as tissue remodeling.

5.1 Introduction

The use of substitutes to treat diseases such as atherosclerosis, and conditions such as congenital defects, damaged blood vessels and hemodialysis access is a very common approach today [17, 70]. In spite of the number of options, such as synthetic and autologous grafts, available to surgeons, most vascular grafts today are not suitable in applications where diameter of the replaced blood vessel is less than 6mm (small-caliber vessels) [23, 111]. During the last few decades there has been a considerable progress made in tissue engineering such vessel substitutes which are able to favorably mimic structure and function of a native blood vessel [36, 41, 42, 55, 112-114]. The emphasis of such research has been directed toward designing a three dimensional (3-D) nanofibrous matrix which is capable of not only being a regenerative blood vessel available readily (i.e. off-the-shelf) to vascular surgeons but also not cause any unfavorable immunogenic, thrombogenic and/or

inflammatory responses *in vivo* [17, 111, 129]. Though it has been difficult to reproduce a design which perfectly replicates a layered structure of a blood vessel, research has been dedicated in developing micro-environments which encourage vascular cells to promote remodeling as well as in imparting appropriate mechanical and physiological properties which will ensure the tissue engineered blood vessel (TEBV) will be able to withstand such remodeling under hemodynamic conditions *in vivo*. Some of the critical reasons of failure during the use of common used grafts as small-caliber substitutes include compliance mismatch, detrimental cellular activity at the site of anastomosis, and lack of endothelialization in the inner surface of the graft [16, 17, 23]. Most of these factors lead to occlusion and neointimal hyperplasia, thereby making the graft less patent *in vivo*. It is well established that the compliance of a graft at the site of anastomosis greatly contributes to the regenerative activity of the vascular cells. Salacinski et al [23] were able to establish a linear relationship between the compliance of the graft and the *in vivo* patency. Less compliant grafts greatly reduce smooth muscle cell (SMC) and fibroblast (FB) migration at anastamosa, thereby causing poor or no remodeling, which leads to occlusion, and, hence, reduction in the patency [16]. This project focuses on studying the *in vivo* properties of one such TEBV which serves as a potential for a suitable grafting materials. The TEBV consists of an electrospun inner core and collagenous outer shell. We have previously established that the inner has core biomechanical properties, particularly compliance, and the outer shell has similar physiological properties similar to native carotid artery.

An ideal blood vessel surrogate is expected to provide a suitable micro-environment for the proliferation and migration of vascular cells such as smooth muscle cells and fibroblasts which will ensure appropriate remodeling *in vivo*. TEBV models are generally multilayered since native artery has three distinct layers – intima, media and adventitia [20]. The inner layer or the intimal equivalent,

which comes in direct contact with blood, is generally expected to be a thromboresistant surface and also act the surface for the attachment of endothelial cells (ECs). The other layer(s) is (are) expected to provide the necessary scaffolding for the migration for SMCs and FBs which are involved in the remodeling of the TEBV matrix [12, 19]. In one of our previous studies [118], poly (ε-caprolactone) (PCL) has been established as a suitable intimal equivalent, since it is a biodegradable and allows the formation of a confluent layer of ECs *in vivo*. Also, in another study [117], we have been able to establish that a genipin-crosslinked collagen-chitosan scaffold (GCC) acts a suitable medial equivalent since it is not only biodegradable but the collagen fibers also possess RGD sites which provide attachment sites to SMCs thereby allowing their proliferation and migration. With completely different affinity to water, the intimal and the medial equivalents demanded special interface modifications which control the stability of the multilayer graft (Chapter 4). In this study, we have brought forward the physical modification process by increasing the PCL surface pore size.

Previous research has shown that the formation of a confluent layer of ECs is critically to the stability of the graft *in vivo* [16, 20]. Non-native arterial tissue generally lacks any inherent property or molecule which can attract ECs in form such confluent layers *in vivo*. This is generally achieved by embedding heparin in the PCL fibers. At an optimal concentration, heparin can attract ECs in forming a confluent layer [130, 131]. Heparin can be also released over a time from the fibers, thereby, resisting the formation of thrombus [130, 131]. The formation of the ECs layer is critical since recruitment of ECs would stop any SMC from migrating on to the inner surface of the intimal equivalent [132, 133], thereby, circumventing any chances of the formation of neointimal hyperplasia. Heparin molecule, by itself is known to control the proliferation and migration of SMCs on to the inner core. Based on our previous study [117], the outer shell with a low crosslinking density, is suitable for promoting SMC activity and tissue remodeling. Addition of chemotaxants

such as platelet-derived transforming growth factor and high-concentration fetal bovine serum has shown to improve the SMC activity in the medial equivalent [117]. In this study, we have studied the release of heparin from the PCL fibers as well as evaluated the *in vitro* performance of these multilayer grafts with a sheep carotid grafting model.

5.2 Materials and methods

5.2.1 Materials for inner core

Poly-ε-caprolactone ($\overline{M_n}$=80,000 g/mol), polyethylene oxide ($\overline{M_n}$=500,000 g/mol) and Acetonitrile (ACN) were purchased from Sigma Aldrich (St Louis, MO). N, N-Dimethylformamide (DMF, minimum purity 99.9%) and dichloromethane (DCM, minimum purity 99.5%) were purchased from Mallinckrodt Chemicals (Phillipsburg, NJ). The electrospinning apparatus comprised of a Gamma High Voltage Research ES30P-10W power supply (Gamma High Voltage Research Inc., Ormond Beach, FL), a pair of syringe pumps (Pump 11 Plus - Harvard Apparatus, Crisel Instrument, Rome, Italy), a cylindrical aluminum collector with 5.56mm in diameter, a brushless rotating electric motor (BLF230C-A Oriental Motor, Italia S.R.L., Milan, Italy), 5 ml polystyrene syringes to dispense the polymer solutions, stainless-steel 18G blunt-ended needles and flexible PTFE tubing.

5.2.2 Electrospinning of inner core

The protocol for electrospinning of PCL has be described in our previous studies [118]. Briefly, PCL was dissolved in a 5:3:2 mixture of DCM, DMF and a heparin-methanol solution to obtain an 8% by

weight PCL solution. Heparin, a thromboresistant molecule and EC attractant [119], was dissolved in the methanol to obtain an 8% by weight heparin-methanol solution and the total heparin concentration in the resulting PCL solution was 0.5% by weight. PEO was dissolved ACN to obtain a 4.5% by weight PEO solution. The mandrel rotation speed was set at 400 rpm. To facilitate the detachment of the scaffold materials, the collector was tightly wrapped with a thin aluminum foil and an ultrathin layer of PEO was electrospun on its surface to avoid PCL fibers sticking to the collector. PCL fibers were collected with needle-collector distance of 22cm. The voltage and flow rate for collecting the PCL fiber were set to 27kV and 1mL/hr., respectively. PCL was spun up to a thickness of 120μm. The enhancement of the interface interactions and thus, the integration between the layers, was achieved by creating high porosity (HP) at the surface. PCL-PEO scaffolds were fabricated by collecting PCL nanofibers until the point where the thickness of the tube reaches approximately 100μm, and then simultaneously spinning PEO with PCL and forming interwoven nanofibers on the collector for the next 20μm with the protocol described in chapter 4. We have previously established double-electrospinning of two fibers as a means of modifying the surface [118]. The PCL scaffold was cut into small tubes of uniform length of about 30mm. To create PCL(HP) scaffolds, PCL scaffolds with PCL-PEO surface were soaked for an hour in deionized or ultrapure water to eliminate the PEO and the solvent residuals, before they were removed from the aluminum foil.

5.2.3 Preparation of outer shell

Preparation of the gel for the outer shell was followed the protocol we developed previously [109]. Briefly, rat tail collagen (type I) in 0.02N acetic acid (pH 4.0) at 9 mg/ml (BD Biosciences Inc., San Jose, CA) was first transferred to a centrifuge tube. Then, 1X Dulbecco's Phosphate Buffered Saline

(DPBS, Invitrogen Corporation, Carlsbad, CA) and 10X DPBS (Invitrogen Corporation, Carlsbad, CA) was added to the solution, followed by the addition of chitosan suspension. Chitosan (Molecular Weight = 100,000-300,000 g/mol, 90% deacetylation, Milan Panic Biomedicals Inc., Solon, OH) was dissolved in 1% acetic acid resulting in a chitosan suspension of 10 mg/ml concentration with a viscosity of 2000-3000 mPa.s. The pH of the pre-gel mixture was adjusted to 7.3 by the careful addition of 1M NaOH. Finally, the mixture was finally topped off with 1X DPBS solution to achieve the desired volume. The final concentrations of the collagen and chitosan in the collagen-chitosan constructs were 3mg/ml and 3.5 mg/ml, respectively. The inner core manufactured by the electrospinning process was slid over a dry glass rod. This rod was then placed in the vascular graft mold. The neutralized collagen-chitosan mixture was slowly poured into a cylindrical graft mold around the PCL tube on the glass rod. To further remove bubbles which influence mechanical properties by introducing void defects and high variations in gel constructs, the pre-gel solution was placed at room temperature for five minutes before it was transferred into the incubator. Finally, the mold was transferred into an incubator to initiate gel formation at 37 °C. After 10 hours of gelation, the outer shell was crosslinked by diffusion with 2.5mM genipin in 1X DPBS for 10 hours. The crosslinker concentration was determined by our previous study [117] according to its effect on SMC migration. The samples were washed 5 times in 1X DPBS to remove an excess unreacted genipin. The multilayer grafts have been designated as PCL(HP)-GCC for simplicity.

5.2.4 Heparin release test

Heparin impregnated unmodified PCL scaffolds were cut in pieces (25mm x 5 mm x 0.15 mm, approximate weight 60 mg). Each one was soaked in 5 ml of DPBS), at 37°C, under constant mild

shaking on a shaker table. After 12h, and 1, 4, 7, 10, 13, 16, 23 and 30 days 150µl were extracted for heparin content measure and replaced with fresh DPBS. The Biophen heparin Anti-Xa Assay/Detection Kit (HYPHEN BioMed, Mason, OH) was used to detect the amount of heparin released during each time point. Heparin Anti-Xa method is a two-stage chromogenic assay capable of measuring for their Anti-Xa activity of homogeneous heparin in plasma or in purified solutions. A cumulative release curve was built with experimental data. The standard deviation at each time point over 4 samples was also plotted along with the average release values.

5.2.5 Sterilization of grafts

The vascular grafts were frozen in liquid nitrogen (~195˚C), following which they were dried in a critical-point drying chamber (Labconco, Kansas City, MO) for approximately 48 hours. Then, the grafts were immersed in absolute ethanol (100%) for one hour. Then, the grafts were washed with 1X DPBS five times to remove any impurities.

5.2.6 Ovine implantation

Two vascular grafts were implanted in a healthy, female sheep in both the Left and Right Carotid arteries, subcutaneously (Figure 5.1A). The sheep were premedicated with subcutaneous injections of Medetomidin (210 mcg/kg), Midazolam (0.5 mg/kg) and Morphine (1 mg/kg). An intravenous catheter was placed in a vein in the ear and propofol (5 to 8 mg/kg) was used to induce anesthesia. After intubation, anesthesia was maintained with Isofluran in 100% oxygen. At the time of induction, the sheep receive Enrofloxacin at a dose of 5mg/kg. The sheep were placed on dorsal

recumbency. The ventral part of the neck was clipped with a # 40 blade and prepared with Chlorhexidine soap and alcohol. After draping the neck with sterile towels and drapes, a ventral midline incision was performed to expose both carotid arteries. Heparin was administered at the dose of 200 U/kg intravenously. After exposure of both carotid arteries, a graft was implanted in each artery. One artery at a time was isolated and clamped with vascular clamps. The artery was transected between the two clamps. A graft was anastomosed in an end to end fashion with 7-0 propylene suture in a continuous fashion. The graft was de-aired before completion of the anastomosis. Blood flow was re-established and Gelfoam was applied around the sites of anastomosis for hemostasis. The second artery was treated in a similar fashion. Subcutaneous tissue and skin were closed in a routine fashion. The sheep received buprenorphine (0.05mg/kg subcutaneously twice a day for 3 days) and meloxicam (0.3 mg/kg subcutaneously twice a day for 3 days).

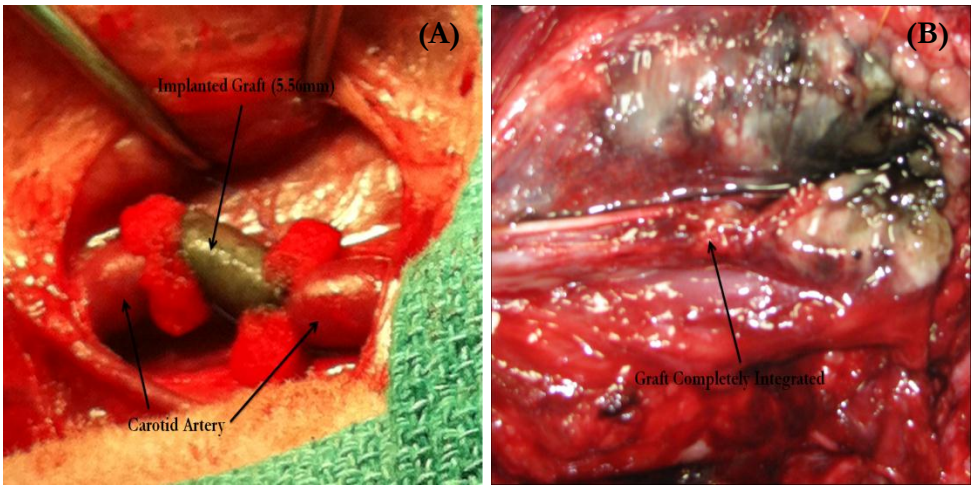

Figure 5.1: (A) Ovine Implantation: Implanted 5.56mm multilayer vascular graft replacing the carotid artery of a sheep with anastomosis covered with gauge to stop bleeding. (B) Explanted graft fully integrated with the neighboring artery

5.2.7 Ultrasound sonography

Ultrasound images of the grafts, the upstream and downstream neighboring artery, were taken after 2-Days, 1-week, 2-Weeks, 3-Weeks and 4-Weeks (1-month) of implantation to visualize any thrombus formation or narrowing of the graft. Lumen diameter and wall thickness was measured using the open-sourced imaging software ImageJ (National Institutes of Health).

5.2.8 Graft explantation

The explantation of the grafts from the sheep was performed four weeks (1-month) after the implantation. Grafts were located by feel, and removed with approximately 20 millimeters of upstream and downstream neighboring artery for comparison.

5.2.9 Histology

Cross sections of the graft, the neighboring artery, and the site of anastomosis were fixed in 10% formaldehyde and cryo-sectioned. Stained specimens were placed on the slide normal to the longitudinal axis. The histological sections where then stained with Movat's pentachrome (MP), and hematoxylin and eosin (HE). These stained sections were observed under the light microscope (Zeiss Axiovert S100, Carl Zeiss – Advanced Imaging Microscopy, Germany) at 20X magnification. Unstained sections were imaged for immunofluorescence (IF) under the light microscope at 20X magnification.

5.2.10 Data analysis and statistics

Data were statistically analyzed using the one-way ANOVA test. Student's t test was then used to compare the means of each individual group. The level of significance was set at $\alpha = 0.05$ for 95% statistical significance. Error bars on all the histogram charts represent the standard error of the mean based on the total number of the samples.

5.3 Results

5.3.1 Heparin release

Figure 5.2 shows the cumulative release percentage of heparin from heparin encapsulated unmodified PCL over time in days. Since it is a cumulative curve, each successive time step is a sum of all the releases in the previous time steps. Within the first 24 hours, 14.88±5.31% had been released and after 30 days a total of 59.16±6.12% heparin was released.

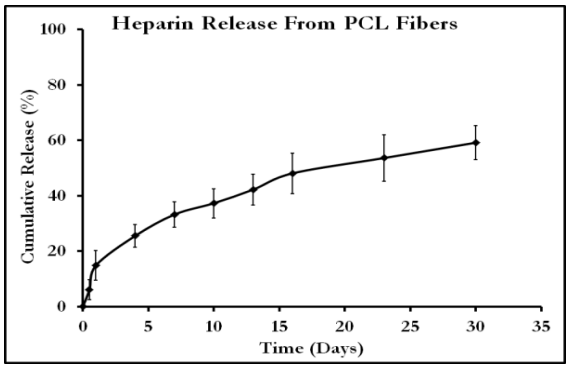

Figure 5.2: Heparin Release from PCL fibers expressed as cumulative release percentage over time in days

5.3.2 No thrombosis, good patency, excellent graft integration & restoration of pulsatile flow

Explantation revealed little complications in the sheep. Grafts had merged with the native artery at anastamosa satisfactorily at anastamosa (Figure 5.1B). Grafts were located through manual examination of the artery. The biodegradable sutures were absorbed into the system without any adverse reactions. The ultrasound images (Figures 5.3A-H) revealed there was no thrombosis or stenosis at any cross-section of the graft, the anastamosa or the neighboring artery during any of weeks (1, 2, 3 or 4). Thus, the graft, the anastamosa as well as the neighboring artery remained patent all through -the study. In all of the 8 images (Figures 5.3A-H), some incongruence at the anastamosa can be seen. Additionally turbulent flow is present, especially in the initial weeks (1-2) of the study. Images from 3rd (Figure 5.3E-F) and 4th weeks (Figure 5.3G-H), clearly, suggests that normal pulsatile flow has been restored in the vessels. The images reveal distinct fluid velocity sections with little flow dispersion. In these images from weeks 3 (Figure 5.3E-F) & 4 (Figure 5.3G-H), some breaks in flow can be observed at the anastamosa toward the neighboring artery.

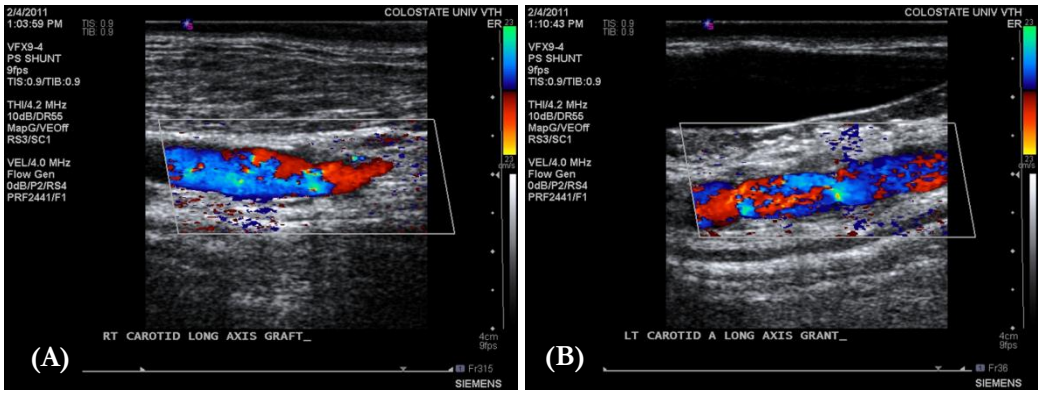

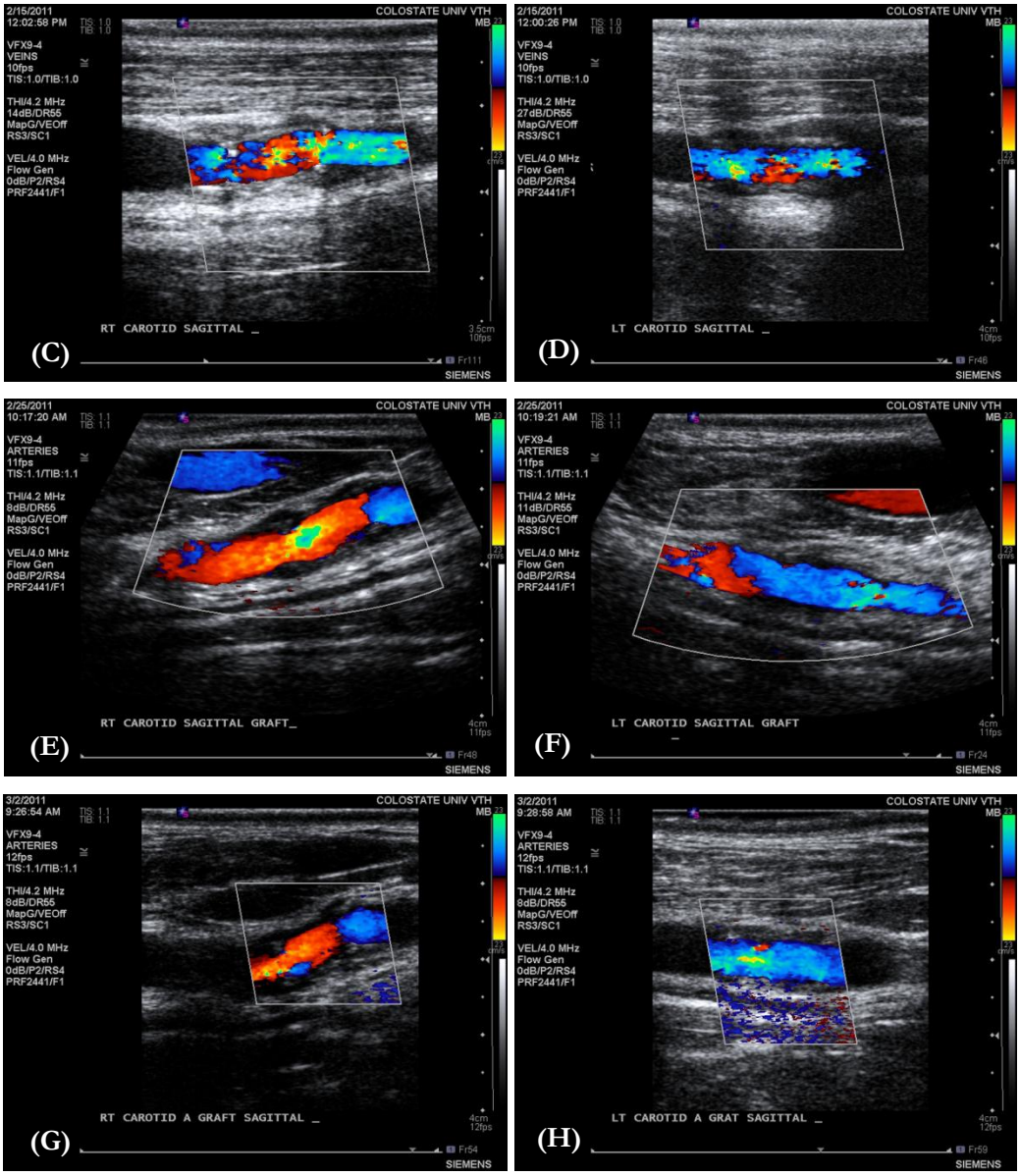

Figure 5.3: Ultrasound Sonography: (A): 1st Week Image of the graft on Right Carotid Artery; (B): 1st Week Image of the graft on Left Carotid Artery; (C): 2nd Week Image of the graft on Right Carotid Artery; (D): 2nd Week Image of the graft on Left Carotid Artery; (E): 3rd Week Image of the graft on Right Carotid Artery; (F): 3rd Week Image of the graft on Left Carotid Artery; (G): 4th Week Image of the graft on Right Carotid Artery; (H): 4th Week Image of the graft on Left Carotid Artery. (Note: Figures (A) & (B) are on the previous page)

5.3.3 No change in vascular graft average lumen diameter

The overall lumen diameter (Figure 5.4A) of the grafts, computed from the ultrasound sonography images, did not show any statistically significant change throughout the four week duration. The lumen diameter of the graft (Figure 5.4B), computed from the ultrasound sonography images, showed no significant increase in diameter when normalized to the diameter of an upstream carotid artery from week 1. Both the cases did not reveal any overall trend.

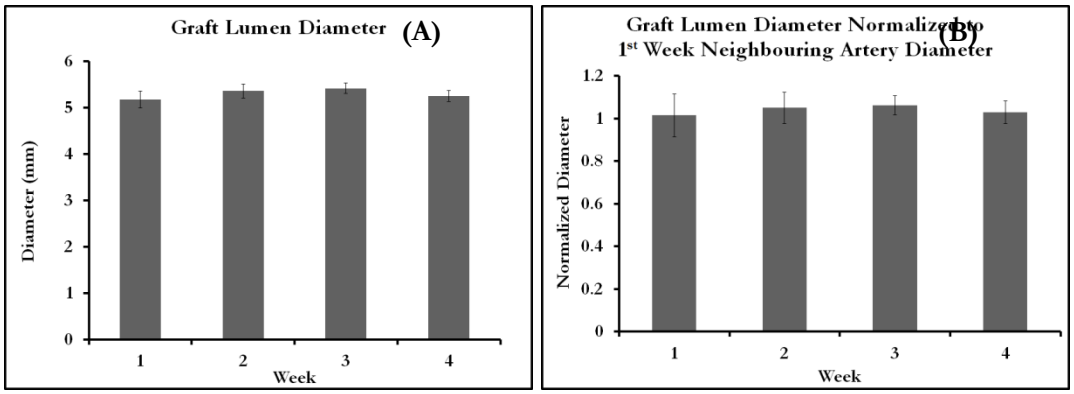

Figure 5.4: (A): Graft Lumen Diameter during each week after implantation; (B): Graft Lumen Diameter Normalized to the 1st Week Neighboring Artery Diameter

5.3.4 Increase in vascular graft average wall thickness

The average graft wall thickness values computed from the ultrasound sonography images are indicated in Figure 5.5A. Figure 5.5B illustrates the changes in the average graft wall thickness normalized to the thickness of the neighboring artery during the 1st week computed from the ultrasound sonography images. Similar results were observed in both cases. There was a significant

change in the graft wall thickness from the 1st week to each of the other three weeks. There was also a significant change in the 3rd and the 4th weeks in comparison to the 2nd week. There were no significant changes in between the 3rd and the 4th weeks.

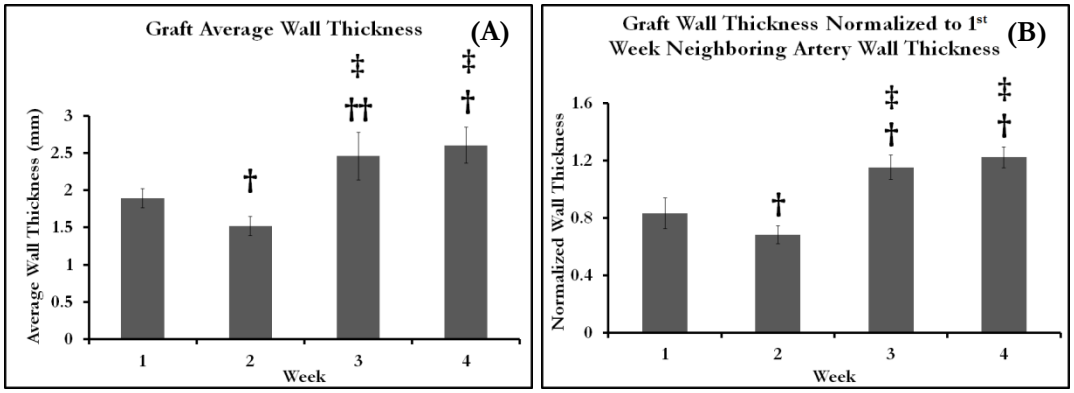

Figure 5.5: (A): Graft Average Wall Thickness. † - $p<0.05$, statistical significance w.r.t. to 1st week graft wall thickness; †† - $p<0.1$, statistical significance w.r.t. to 1st week graft wall thickness; ‡ - $p<0.05$, statistical significance w.r.t. to 2nd week graft wall thickness. (B): Graft Average Wall Thickness Normalized to the 1st Week Neighboring Wall Thickness. † - $p<0.05$, statistical significance w.r.t. to 1st week normalized graft wall thickness; ‡ - $p<0.05$, statistical significance w.r.t. to 2nd week normalized graft wall thickness.

5.3.5 No endothelium regeneration

Immunofluorescence for the SMA, DAPI, and PECAM (CD31) were highlighted to indicate SMCs, nuclei, and endothelial cells respectively. Figure 5.6 shows the HE staining of the neighboring artery (Figure 5.6A) and the graft (Figure 5.6B) and the stain stains the cell cytoplasm red and the nuclei blue. These images reveal no endothelialization at the anastomosa even though there is a confluent

layer of ECs in the neighbouring artery. This is also confirmed by the immunoflorescence imaging (Figure 5.7) and the Movat's Pentachrome staining (Figure 5.8) of the sections. In Figure 5.7, the EC recruting molecule, PECAM (CD31) is also stained green. PECAM (CD31) is clearly present in the neighbouring artery (Figure 5.7A) and the anastamosa (Figure 5.7B) but absent in the graft (Figure 5.7C). Hence, it is clear that there is no endothelium regeneration.

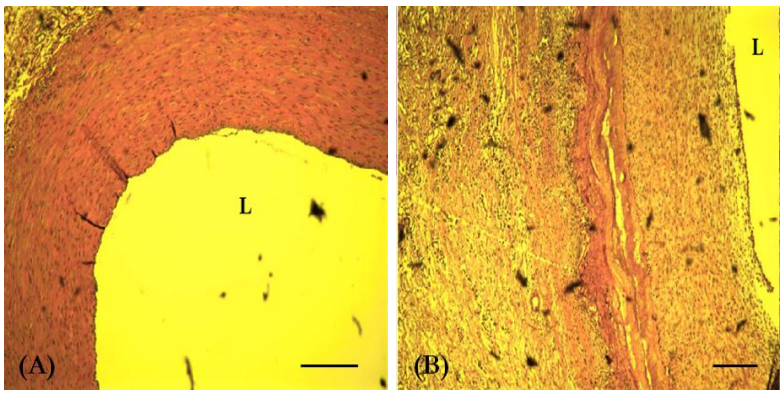

Figure 5.6: Hematoxylin and Eosin (H&E) staining of (A) the sectioned neighboring artery and (B) the sectioned graft. H&E staining displays cell cytoplasm (red) and nuclei (blue). Scale bar: 100μm.

5.3.6 Intimal hyperplasia at anastamosa

Figure 5.7 shows the immunofluorescence of the neighbouring artery (Figure 5.7A), the anastmosa (Figure 5.7B) and the graft (Figure 5.7C). These images reveal the formation of the neointimal hyperplasia which is marked with a yellow line. The size of the neointimal hyperplasia near the anastamosa is approximately 400μm. Though there is fairly large neointimal hyperplasia formed at the anastamosa, its size decreases to zero while moving away from the anastamosa to the center of the graft. This is confirmed by Figure 5.8, which has be obtained by merging the red, the green and the blue intensity images at the center of the graft. The blue dots in Figure 5.8 are the SMCs which

have migrated from the neighboring artery into the graft. Collagen in the outer shell can be observed in red while the PCL in the inner core is observed in green.

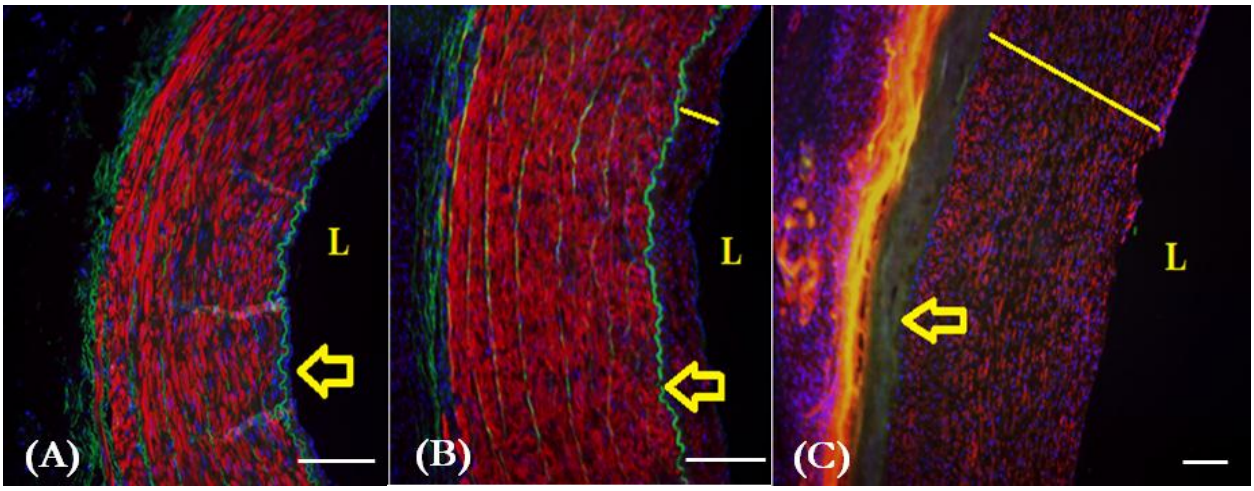

Figure 5.7: Immunofluorescence of (A) the neighboring artery, (B) the Anastamosa and (C) the graft. Pictured are the smooth muscle cells (red), endothelial cells (green), nuclei (blue), and connective tissue (autofluorescent). The basal membrane is marked with the yellow arrow. The lumen is marked "L", and the lumen side neointimal hyperplasia is marked by the yellow line.

Scale Bar for A-B: 100μm & for C: 50μm.

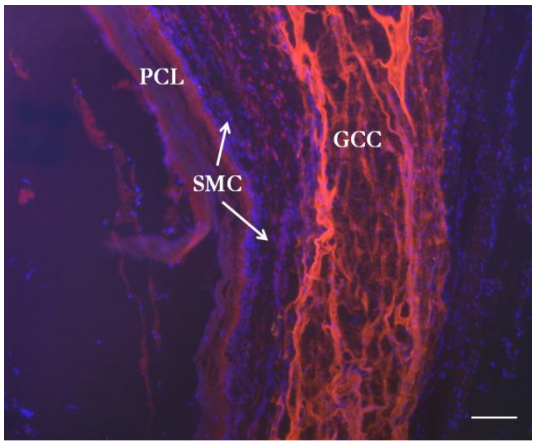

Figure 5.8: Absence of Neointimal Hyperplasia in the Middle of the Graft. Scale Bar: 100μm

5.3.7 Migration of SMCs into graft and production of ECM

In the immunofluorescence images of Figure 5.7, the SMCs, the ECs and their nuclei are stained red, green and blue, respectively. These histological images show SMC migration and proliferation into the graft medial layer. Since there is no endothelium regenerated, the SMCs have, also, migrated on to the PCL surface causing the formation of the neointimal hyperplasia. The SMCs are distinctly aligned on the neointimal hyperplasia, while the media contains a disorganization of randomly aligned fibers and SMCs. Figure 5.9 displays the Movat's Pentachrome staining of the neighboring artery (Figure 5.9A) and the graft (Figure 5.9B). SMCs, elastin, collagen, fibrin and the ground substance are stained red, purplish-black, yellowish-green, deep red and bluish-green, respectively. In addition, little to no ground substance or elastic fibers can be seen in the medial layer. Finally, delamination, seen in all histological images, is a result of the histological sectioning itself.

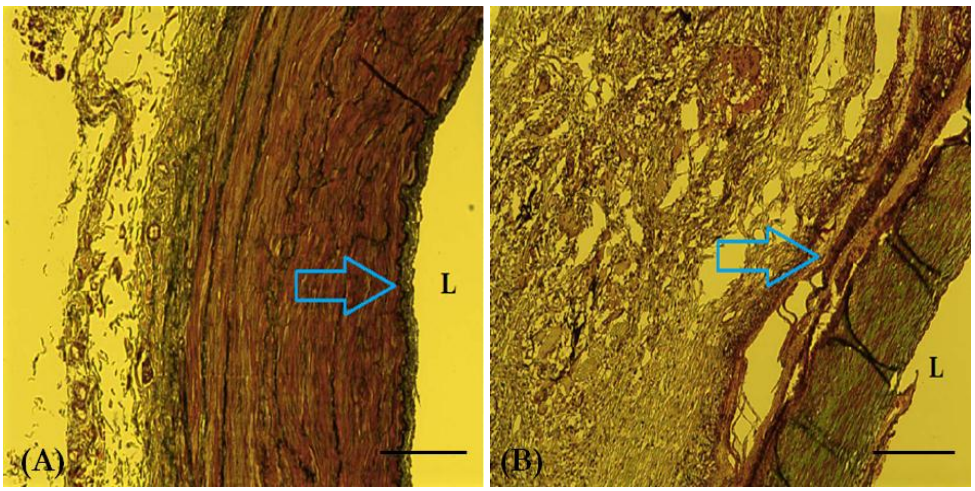

Figure 5.9: Movat's Pentachrome staining of the Neighboring Artery (A) and Graft (B). Pictures are the smooth muscle tissue (red), elastin (purplish black), collagen (yellowish green), and glycosaminoglycans (bluish green). The basal membrane is indicated by the blue arrows. The lumen is marked "L". Scale bar: 100μm

5.4 Discussion

This study was performed to study the *in vivo* properties of a grafting scaffold developed in our previous work (Chapter 4). The graft did not reveal any unfavorable immunogenic responses, thrombosis or stenosis when implanted inside a sheep model. The graft had fully integrated with the neighboring artery at anastamosa. Healing and remodeling at anastamosa was also very satisfactory. Image analysis of the images obtained from ultrasound sonography showed minimal changes in the diameter and significant changes to the wall thickness of the graft over the 1-month implantation due to the formation of the neointimal hyperplasia. Histology of the graft revealed the formation of neointimal hyperplasia and the absence of a confluent layer of ECs.

Salacinski et al [23] established a linear relationship between compliance and patency after one month of implantation. Based on this relationship, in our previous study, we have established that these grafts possess compliance similar to that of the carotid artery and hence will be highly patent at the end of 1st month of implantation. Our prediction was confirmed since the graft did not show any kind of patency, except for the formation of a neointimal hyperplasia (approximately 400microns thick), after one month of implantation. This can be attributed to the migration of the SMCs from the neighboring artery to the medial layer of the graft through the anastamosa followed by their proliferation. Even though SMCs migrated, ECs did not get recruited to form a confluent layer adhering to the PCL surface instead a layer of neointimal hyperplasia had formed. Histological imaging provides little doubt about the neointimal hyperplasia, though no stenosis was observed in the specimens during the implantation through the ultrasound images as well as after the explantation using the histological images. This indicates SMCs migrated on to the intima and prevented endothelialization. Plausible reasons for the SMC intimal migration include decreased

fluid shear at the anastamosa due to incongruence of the graft and vessel intima layers and lack of an optimum concentration of EC recruiters such as heparin and PECAM (CD31). The incongruence in the graft and vessel can also be witnessed in the fluid flow ultrasound imaging. It is to be clearly noted that though endothelialization does not occur, stenosis does not occur either, which is possibly due to the low or no compliance mismatch.

Ultrasound images of the grafts *in vivo* show clearly no signs of stenosis, with no change in lumen diameter over the length of the study. In addition, no trend in lumen decrease, when compared to the neighboring artery, was seen, which indicates functional similarity between the artery and the graft flow areas. Percentage change between the upstream artery and the graft for weeks 2 and 4 are significantly different from the upstream artery, showing a decrease in lumen diameter. Because of the peak seen in week 3, this decrease in diameter could be resulting from difficulty in differentiating the anastomosis from the neighboring artery, as well as differentiating vessel structures in the neighboring artery. Ultrasound additionally showed an increase in graft wall thickness, when compared to initial values (week 1) and when compared to the upstream artery for each image taken. Two reasons which contribute to the increase in the wall thickness are as follow. The increase in the wall thickness indicates the advanced integration of the graft into the neighboring artery, with tissue growth around graft walls. Additionally, when taken in conjunction with the histological images, the increased wall thickness is also due to the formation of the neointimal hyperplasia.

SMCs present in the neointimal hyperplasia are circumferentially aligned, and viable, and could act as a functional media layer, which could be a limitation in long-term studies. Improvements to the construct should necessitate the formation of a confluent layer of ECs attached to the intima to avoid any SMC migration or formation of neointimal hyperplasia. Improved EC migration and

attachment could be influenced by fiber alignment or material property changes to the intimal construct. In addition, circumferential alignment of SMCs should be achieved through fiber alignment in GCC, the outer shell of the multilayer graft. SMC morphology in the medial layer can also be seen to have a random orientation, in contrast to the circumferential alignment seen in the native blood vessels. Hemodynamic loading of the SMC scaffold is required to align them in the direction of highest stress which will also ensure that the ECM production will also be circumferential. Without this alignment, vessels may fail under systolic pressures. PCL, a slow-degrading high-strength polymer, provides a suitable attachment layer for ECs and restricts the migration of medial SMCs into the intima. It was assumed that due to its low decay rate, medial vessel wall stresses will increase, gradually, leading to the alignment of the ECM and SMCs in a long-term *in vivo*. To address the issues which have arisen in this study, a new intimal layer structure could be investigated and effect way of communicating with the ECs *in vivo* should be developed. It has also been established in our previous studies (Chapter 4), that the integrity of the graft would be dependent on the interface between the intimal and the medial equivalents. Any improvement in the attachment of the intimal and the medial equivalents would provide a stronger interface bond between intima and media, as well as provide better cell proliferation/migration and attachment. Endothelialization would be the most important issue to be answered from the study. With improvements in endothelialization, this multilayer layer grafting scaffold, consisting of an electrospun intimal equivalent (PCL) and a collagenous medial equivalent (GCC), has the potential to serve as a suitable replacement to damaged or diseased small-caliber blood vessels by providing the balance between the biomechanical and the physiological requirements to TEBV and well as a micro-environment which will promote favorable responses and remodeling *in vivo*.

5.5 Conclusions

This study demonstrated that the graft did not reveal any unfavorable immunogenic responses, thrombosis or stenosis when implanted inside a sheep model while fully integrating with the neighboring artery. Healing and remodeling at anastamosa after one-month of implantation was also very satisfactory. Analysis of the ultrasound sonography images showed no change in the average lumen diameter of the graft while there were significant changes to the average wall thickness over the 1-month implantation possibly due to the integration of the graft with the neighboring artery as well as the formation of the neointimal hyperplasia. Histology of the graft revealed the formation of neointimal hyperplasia whose thickness decreased from the anastamosa to the center of the graft. Histology also revealed there was no endothelium regenerated in the graft and the structure of the extracellular matrix in the medial layer was quite distinct from that of the neighboring artery.

CHAPTER 6

DISCUSSION AND FUTURE WORK

6.1 Discussion

This Ph. D. dissertation has focused on the design and the development of a multilayer vascular graft consisting of an electrospun inner core (intimal equivalent) and a collagenous outer core (medial equivalent). The dissertation can broadly be divided into three sections: Material Selection, Multilayer Graft and Interface Design, Multilayer Graft *in vitro* Testing and Multilayer Graft *in vivo* Testing.

6.1.1 Material selection

To explore an alternative approach to design a material a suitable vascular grafting scaffold, the material selection process involved the engineering of collagenous scaffolds by the incorporation of mimetic components and crosslinking the construct with different crosslinkers. The effects of component additives, such as chitosan and elastin, were evaluated in terms of their mechanical and biological properties. Results demonstrated that the incorporation of chitosan and/or elastin altered stress-strain curves in the low stress loading region, and significantly improved the stretching ratio and ultimate stress of modified collagenous scaffolds compared to pure collagen scaffolds. Electron microscopy results suggested that the mechanical improvements were plausibly due to microstructural modifications by the sheets of chitosan and elastin fibers embedded in the collagen

scaffold like an interfibrillar network. The effects of crosslinkers, such as formaldehyde, genipin and ethyl-(dimethyl aminopropyl) carbodiimide hydrochloride (EDAC) were also evaluated. Fourier transform infrared spectroscopy results demonstrated that formaldehyde, EDAC and genipin employed different mechanisms to crosslink the collagenous scaffolds, and use of genipin as a scaffold crosslinker improved the elongation and the endothelial cell attachment as compared to formaldehyde and EDAC. In addition, extending gelation time increased the elastic modulus but not the ultimate strength.

Following this, the biocompatible crosslinker, genipin was, then, used to crosslink collagen-chitosan-elastin scaffolds, and the effects of genipin concentration on the mechanical properties, smooth muscle cell activity and degradation of collagen-chitosan-elastin scaffolds were examined. Results revealed that mechanical strength, stiffness and stability of collagen-chitosan-elastin scaffolds increased with the concentration of the genipin crosslinker increasing from 1mM to 25mM, but, also, significantly inhibited smooth muscle cell contraction of and invasion in the collagen-chitosan-elastin scaffolds. No smooth muscle cell contraction or invasion was observed in the scaffolds crosslinked with genipin at a concentration of 5mM or above. These results were shown to be correlated with the chemical characterization results from fourier transform infrared spectroscopy. We, also, incorporated several growth factor conditions in the genipin-crosslinked collagen-chitosan-elastin scaffolds and evaluated their effects on smooth muscle cell activities. These conditions included heparin, platelet-derived transforming growth factor, high-concentration fetal bovine serum and their combinations. Results showed that the addition of high-concentration fetal bovine serum in genipin-crosslinked gels significantly increased smooth muscle cell contraction and invasion, platelet-derived transforming growth factor increased smooth muscle cell invasion while heparin reduced this platelet-derived transforming growth factor effect, and the synergetic effects of high-

concentration fetal bovine serum and platelet-derived transforming growth factor stimulated smooth muscle cell invasion more significantly than a single factor. Thus, this study suggested that the use of combination of high-concentration fetal bovine serum and platelet-derived transforming growth factor with low-concentration (1mM) genipin-crosslinked collagen-chitosan-elastin scaffolds might potentially achieve a vascular media equivalent with superior performances.

6.1.2 Multilayer graft & interface design with *in vitro* testing

From our study suggested that designing a suitable engineering equivalent to blood vessels which allow immediate implantation and encourage tissue regeneration *in vivo* should employ an appropriate combination of crosslinking condition and soluble biomolecule factors, striking a balance between mechanical and biological properties. To keep our multilayer graft design simple, it was decided to carry forward the low-concentration genipin-crosslinked collagen-chitosan scaffold. The concentration of the genipin crosslinker was fixed at 2.5mM since lower crosslinker concentrations did not impart desired shape of the tubular vascular graft. Also, since the low-concentration genipin-crosslinked collagenous scaffold lacked sufficient strength, a thin layer of electrospun scaffold was introduced underneath the collagenous scaffold. In this study, we designed a multilayer grafting scaffold from a combination of electrospun poly-ε-caprolactone, as the intimal equivalent, and a genipin crosslinked collagen-chitosan scaffold as the medial equivalent. The adhesion between the two layers played a critical role in the design of the vascular graft and the improvement of the adhesion was done either, physically, by increasing porosity of the top surface or by improving the hydrophilicity of the intimal equivalent or chemically by crosslinking the two layers. The grafts used for biomechanical testing possessed an inner diameter of 4.76mm, poly-ε-caprolactone layer thickness of 120μm and genipin-crosslinked collagen-chitosan scaffold thickness of 1.25mm (approximately).

These grafts exhibited burst strengths varying between 644mmHg to 1152mmHg and compliance (80-120mmHg range) between 2.6-5.2%. The water permeability of the electrospun poly-ε-caprolactone scaffold reduced from 2380mL/cm^2/min to 551mL/cm^2/min due to the addition of the genipin-crosslinked collagen-chitosan layer over them. The suture strengths of the single poly-ε-caprolactone as well as the multilayer scaffolds were 2N and 2.4N, respectively. Both compliance and burst strength were found to be dependent on the thickness (120μm & 240μm) of the intimal equivalent layer while the genipin concentration (1mM, 2.5mM and 10mM) for crosslinking the genipin-crosslinked collagen-chitosan scaffold had no effect on them. As a preliminary study, the multilayer graft (inner diameter 3mm) was implanted for short duration of 1-day into rabbits replacing the abdominal aorta. These grafts on explantation showed no unfavorable immunogenic or inflammatory responses. Our study suggests that designing a suitable engineering equivalent to blood vessels which would sustain the physiological conditions and promote appropriate cellular activity *in vivo* would involve the balancing of biomechanical and biochemical properties of fibrous scaffolds synthesized by the mimicry of natural blood vessels.

6.1.3 Multilayer graft *in vivo* testing

Since in our preliminary implantation studies, no unfavorable immunogenic responses or thrombosis were seen after a day of implantation, in this study, we replaced the carotid arteries in a sheep with two multilayer grafts, with an inner core made of an electrospun intimal equivalent (Poly-ε-Caprolactone) and an outer shell made of a collagenous medial equivalent (genipin-crosslinked collagen-chitosan), for a duration of one month. The endothelial cell chemoattractant, heparin, was embedded in the inner core during the process of electrospinning. During the one-month period,

ultrasound sonography images were obtained which were used to calculate the changes in the lumen diameter and the wall thickness during each week. The graft was explanted after a month after implantation. During the explantation, it was observed that the graft had fully integrated with the neighboring artery. Sections of the graft, the suture sites and the neighboring artery were then subjected to cryo-sectioning for histological staining.

The ultrasound images revealed minimal changes to the graft diameter as well as significant changes to the graft wall thickness during the four weeks. The increase in thickness of the graft wall *in vivo* is due to the integration of the graft with the neighboring artery as well as the formation of the neointimal hyperplasia. The formation of the neointimal hyperplasia, about 400 microns in thickness, is also confirmed by the stained histological sections. There was no recruitment of endothelial cells in the intimal possibly due to the recruitment of the smooth muscle cells onto the intimal equivalent. The smooth muscle cells and the extracellular matrix were found to have no orientation in the medial equivalent while they were aligned circumferentially in the neointimal hyperplasia. Additionally, the ultrasound sonography images as well as the histological sections confirm that no unfavorable immunogenic response or thrombosis or stenosis occurred *in vivo* during the implantation. With all the superior physiological properties along with some methods to develop *in vivo* endothelialization, this multilayer graft has the potential to serve as a suitable vascular graft scaffold providing the right biomechanical properties and the micro-environments suitable to promote vascular cell migration and proliferation as well as tissue remodeling.

6.2 Suggestions & future work

6.2.1 Interface characterization & adhesion improvement:

Some of the major issue faced during this project was that the interface was very critical in designing the multilayer vascular graft. Since two materials with completely different water affinities were being combined, it was quite difficult to combine them without a proper interface design. Fair degree of success was achieved with the creation of high porosity in the top surface of the inner core which subsequently imparted suitable biomechanical properties and integrity to the graft. By the oxygen-plasma treatment, even though the adhesion was superior, the biomechanical properties were drastically reduced since the treatment rendered the inner core to become very stiff. The chemical crosslinking process yielded less success. To improve the adhesion, it is suggested to first create the high porous at the top surface and then, bind gelatin to the inner core fiber surface using the oxygen-plasma treatment and then crosslink the inner core and the outer shell with low-concentration genipin. This method has been employed by other researchers for cell attachment procedure with a fair degree of success [120, 134].

6.2.2 Stiffness and thickness of inner core

The inner core thickness was set to 120μm based on the work done by our group member, Walter Bonani [118]. Other researchers have used higher thicknesses. Lee et al used a 300 μm [113] while McClure et al used thickness varying from 200μm to 500μm [124]. Due this difference, it can be clearly seen that their burst strength values were much superior to ours while our compliance values

where superior to theirs. In the future, the inner core has to be designed in such a way that the fibers are able impart superior burst strength as well as compliance. This can be achieved by electrospinning poly-ε-caprolactone with collagen and/or elastin and/or chitosan as done by other researchers [113, 124] to the same thickness of 120μm. This will definitely improve the mechanical properties of the inner core as well as improve the attachment with the outer shell via crosslinking. This will also provide a better surface for endothelial cell attachment.

6.2.3 Endothelialization

Endothelialization is very critical for the performance of the graft *in vivo*. Our results have suggested that there was no endothelialization possibly due to the recruitment of the smooth muscle cell on to the inner surface of the intimal equivalent as well as low concentration of the endothelial recruiter. First method to solve this problem of no-endothelialization would be to find the optimum level of heparin and/or other chemoattractants like PECAM (CD31). This can be done by setting up a flow system with circulating endothelial cells. The concentration of the chemotaxant on the inner core fiber surface can be varied and the threshold concentration which instigates the attachment of the endothelial cells on to the inner core can be determined. The other method would be to seed endothelial cells on to the surface of the inner core and then, they are allowed to proliferate to form a smooth confluent layer. Then the cell-seeded multilayer graft can be used to study performance *in vivo*.

6.2.4 Inclusion of elastin in outer shell scaffold

Elastin plays a critical role in the physiological functioning of any vascular vessel [14, 81]. We have been able to show that a collagen scaffold reinforced with chitosan and elastin and crosslinked with genipin performs biologically better than a pure collagen or collagen-chitosan scaffold. The next level of research will involve the incorporation of soluble elastin [80] in the outer shell scaffold. This will not only improve cell activity but will also improve the structural stability of the outer shell.

BIBLIOGRAPHY

[1] American Heart Foundation. Cardiovascular Disease Statistics. 2009.

[2] World Health Organization. Cardiovascular Diseases - Fact Sheet. 2009.

[3] National Institutes of Health - National Institute of Diabetes and Digestive and Kidney Diseases. Vascular Access for Hemodialysis. 2009.

[4] Wikipedia Page. Circulatory System. 2011.

[5] Wikipedia Page. Artery. 2011.

[6] Henry G. Anatomy of the human body: Lea and Febiger; 1918.

[7] Wikipedia Page. Collagen. 2011.

[8] Glycosaminoglycan. Wikipedia Page. 2011.

[9] Esko JD, Kimata K, Lindahl U. Proteoglycans and sulfated glycosaminoglycans. In: Varki A, editor. Essentials of glycobiology: NCBI; 2009.

[10] Wikipedia Page. Elastin. 2011.

[11] Uemura S, Fathman CG, Rothbard JB, Cooke JP. Rapid and efficient vascular transport of arginine polymers inhibits myointimal hyperplasia. Circulation. 2000;102:2629-35.

[12] Teebken OE, Haverich A. Tissue engineering of small diameter vascular grafts. European Journal of Vascular and Endovascular Surgery. 2002;23:475-85.

[13] Mitchell SL, Niklason LE. Requirements for growing tissue-engineered vascular grafts. Cardiovascular Pathology. 2003;12:59-64.

[14] Patel A, Fine B, Sandig M, Mequanint K. Elastin biosynthesis: The missing link in tissue-engineered blood vessels. Journal Cardiovascular Research. 2006;71:40-9.

[15] Campbell GR, Campbell JH. Development of tissue engineered vascular grafts. Current Pharmaceutical Biotechnology. 2007;8:43-50.

[16] Zilla P, Bezuidenhout D, Human P. Prosthetic vascular grafts: wrong models, wrong questions and no healing. Biomaterials. 2007;28:5009-27.

[17] Venkatraman S, Boey F, Lao LL. Implanted cardiovascular polymers: natural, synthetic and bio-inspired. Progress in Polymer Science. 2008;33:853-74.

[18] Zdrahala RJ. Small caliber vascular grafts. Part I: State of the art. Journal of Biomaterial Applications. 1996;10:309-29.

[19] Sarkar S, Schmitz-Rixen T, Hamilton G, Seifalian A. Achieving the ideal properties for vascular bypass grafts using a tissue engineered approach: a review. Medical and Biological Engineering and Computing. 2007;45:327-36.

[20] Ratcliffe A. Tissue engineering of vascular grafts. Matrix Biology. 2000;19:353-7.

[21] Edwards WH, Mulherin Jr JL. The role of graft material in femorotibial bypass grafts. Annals of Surgery. 1980;191:7.

[22] Dardik H, Ibrahim IM, Sussman, B, Jarrah M, Dardik II. Glutaraldehyde-stabilized umbilical vein prosthesis for revascularization of the legs. Three year results by life table analysis. American Journal of Surgery. 1979;138:5.

[23] Salacinski HJ, Goldner S, Giudiceandrea A, Hamilton G, Seifalian AM, Edwards A, et al. The mechanical behavior of vascular grafts: A Review. Journal of Biomaterial Applications. 2001;15:241-78.

[24] Cameron BL, Suchida HT, Connall TP, Nagae T, Furukawa K, Wilson SE. High porosity PTFE improves endothelialization of arterial grafts without increasing early thrombogenicity. Journal of Cardiovascular Surgery. 1993;34:6.

[25] Jeschke MG, Hermanutz V, Wolf SE, Köveker GB. Polyurethane vascular prostheses decreases neointimal formation compared with expanded polytetrafluoroethylene. Journal of Vascular Surgery. 1999;29:168-76.

[26] Pinchuk L. A review of the biostability and carcinogenicity of polyurethanes in medicine and the new generation of 'biostable' polyurethanes. Journal of Biomaterials Science, Polymer Edition. 1994;6:225-67.

[27] Tanzi MC, Fare S, Petrini P. *in vitro* stability of polyether and polycarbonate Urethanes. Journal of Biomaterial Applications. 2000;14:325-48.

[28] [28] Teijeira FJ, Lamoureux G, Tbreault JP, Bauset R, Guidoin R, Marois Y, et al. Hydrophilic polyurethane versus autologous femoral vein as substitutes in the femoral arteries of dogs: quantification of platelets and fibrin deposits. Biomaterials. 1989;10:5.

[29] Zhang Z, Marois Y, Guidoin RG, Bull P, Marois M, How T, et al. Vascugraft® polyurethane arterial prosthesis as femoro-popliteal and femoro-peroneal bypasses in humans: pathological, structural and chemical analyses of four excised grafts. Biomaterials. 1997;18:113-24.

[30] Gupta BS, A. KV. Biomechanics of human common carotid artery and design of novel hybrid textile compliant vascular grafts. Journal of Biomedical Materials Research. 1997;34:341-9.

[31] Gomez-Alonso A, García-Criado FJ, Parreño-Manchado FC, García-Sánchez JE, García-Sánchez E, Parreño-Manchado A, et al. Study of the efficacy of coated VICRYL Plus® antibacterial suture (coated polyglactin 910 suture with triclosan) in two animal models of general surgery. Journal of Infection. 2007;54:82-8.

[32] Greisler HP. Arterial regeneration over absorbable prostheses. Archives of Surgery. 1982;117:1425-31.

[33] Greisler HP, Ellinger J, Schwarcz TH, Golan J, Raymond RM, Kim DU. Arterial regeneration over polydioxanone prostheses in the rabbit. Archives of Surgery. 1987;122:715-21.

[34] Greisler HP, Tattersall CW, Klosak JJ, Cabusao EA, Garfeild JD, Kim DU. Partially bioresorbable vascular grafts in dogs. Surgery. 1991;110:11.

[35] Weinberg C, Bell E. A blood vessel model constructed from collagen and cultured vascular cells. Science. 1986;231:397-400.

[36] L'Heureux N, Paquet S, Labbe R, Germain L, Auger FA. A completely biological tissue-engineered human blood vessel. Journal of the Federation of American Societies for Experimental Biology. 1998;12:47-56.

[37] Dobrin PB. Mechanical behavior of vascular smooth muscle in cylindrical segments of arteries *in vitro*. Annals of Biomedical Engineering. 1984;12:14.

[38] Girerd XJ, Acar C, Mourad J-J, Boutouyrie P, Safar ME, Laurentt S. Incompressibility of the human arterial wall: an *in vitro* ultrasound study. Journal of Hypertension. 1992;10:5.

[39] Chamiot-Clerc P, Copie X, Renaud J-F, Safar M, Girerd X. Comparative reactivity and mechanical properties of human isolated internal mammary and radial arteries. Cardiovascular Research. 1998;37:9.

[40] Tranquillo RT, Girton TS, Bromberek BA, Triebes TG, Mooradian DL. Magnetically orientated tissue-equivalent tubes: application to a circumferentially orientated media-equivalent. Biomaterials. 1996;17:349-57.

[41] Niklason LE, Gao J, Abbott WM, Hirschi KK, Houser S, Marini R, et al. Functional arteries grown *in vitro*. Science. 1999;284:489-93.

[42] Berglund JD, Mohseni MM, Nerem RM, Sambanis A. A biological hybrid model for collagen-based tissue engineered vascular constructs. Biomaterials. 2003;24:1241-54.

[43] Roeder BA, Kokini K, Sturgis JE, Robinson JP, Voytik-Harbin SL. Tensile mechanical properties of three-dimensional type I collagen extracellular matrices with varied microstructure. Journal of Biomechnical Engineering. 2002;124:214-22.

[44] Hirai J, Kanda K, Oka T, Matsuda T. Highly oriented, tubular hybrid vascular tissue for a low pressure circulatory system. American Society for Artificial Internal Organs Journal. 1994;40:M383-M8.

[45] Lyman DJ, Murray-Wijelath J. Vascular graft healing: I. FTIR analysis of an implant model for studying the healing of a vascular graft. Journal of Biomedical Materials Research. 1999;48:172-86.

[46] Werkmeister JA, Edwards GA, White JF, Casagranda F, Hunt JA, Williams DF, et al. *in vivo* evaluation of modified mandrel-grown vascular prostheses. Journal of Biomedical Materials Research. 1999;47:316-23.

[47] Seliktar D, Black R, Vito R, Nerem R. Dynamic mechanical conditioning of collagen-gel blood vessel constructs induces remodeling *in vitro*. Annals of Biomedical Engineering. 2000;28:351-62.

[48] Hoerstrup SP, Zund G, Sodian R, Schnell AM, Grunenfelder J, Turina MI. Tissue engineering of small caliber vascular grafts. European Journal of Cardiothoracic Surgery. 2001;20:164-9.

[49] Grassl ED, Oegema TR, Tranquillo RT. A fibrin-based arterial media equivalent. Journal of Biomedical Materials Research Part A. 2003;66A:550-61.

[50] Ogle BM, Mooradian DL. Manipulation of remodeling pathways to enhance the mechanical properties of a tissue engineered blood vessel. Journal of Biomechanical Engineering. 2002;124:724-33.

[51] Cummings CL, Gawlitta D, Nerem RM, Stegemann JP. Properties of engineered vascular constructs made from collagen, fibrin, and collagen-fibrin mixtures. Biomaterials. 2004;25:3699-706.

[52] Swartz DD, Russell JA, Andreadis ST. Engineering of fibrin-based functional and implantable small-diameter blood vessels. Am J Physiol Heart Circ Physiol. 2005;288:H1451-60.

[53] Jeong SI, Kim SY, Cho SK, Chong MS, Kim KS, Kim H, et al. Tissue-engineered vascular grafts composed of marine collagen and PLGA fibers using pulsatile perfusion bioreactors. Biomaterials. 2007;28:8.

[54] Buttafoco L, Engbers-Buijtenhuijs P, Poot AA, Dijkstra PJ, Vermes I, Feijen J. Physical characterization of vascular grafts cultured in a bioreactor. Biomaterials. 2006;27:2380-9.

[55] L'Heureux N, Dusserre N, Konig G, Victor B, Keire P, Wight TN, et al. Human tissue-engineered blood vessels for adult arterial revascularization. Nature Medicine. 2006;12:361-5.

[56] Chaouat M, Le Visage C, Autissier A, Chaubet F, Letourneur D. The evaluation of a small-diameter polysaccharide-based arterial graft in rats. Biomaterials. 2006;27:5546-53.

[57] Wu H-C, Wang T-W, Kang P-L, Tsuang Y-H, Sun J-S, Lin F-H. Coculture of endothelial and smooth muscle cells on a collagen membrane in the development of a small-diameter vascular graft. Biomaterials. 2007;28:1385-92.

[58] Nagai N, Nakayama Y, Zhou Y-M, Takamizawa K, Mori K, Munekata M. Development of salmon collagen vascular graft: Mechanical and biological properties and preliminary implantation study. Journal of Biomedical Materials Research Part B: Applied Biomaterials. 2008;87B:432-9.

[59] Meyer U, Wiesmann HP. Bone and Cartilage Engineering. In: Schroder G, editor. Bone and Cartilage Engineering2006. p. 127.

[60] Jiang K, Schadler LS, Siegel RW, Zhang X, Zhang H, Terrones M. Protein immobilization on carbon nanotubes via a two-step process of diimide-activated amidation. Journal Of Materials Chemistry. 2004;14:3.

[61] Orban JM, Wilson LB, Kofroth JA, El-Kurdi MS, Maul TM, Vorp DA. Crosslinking of collagen gels by transglutaminase. Journal of Biomedical Materials Research Part A. 2004;68A:756-62.

[62] Gildner CD, Lerner AL, Hocking DC. Fibronectin matrix polymerization increases tensile strength of model tissue. American Journal of Physiology - Heart and Circulatory Physiology. 2004;287:H46-53.

[63] Osborne CS, Barbenel JC, Smith D, Savakis M, Grant MH. Investigation into the tensile properties of collagen/chondroitin-6-sulphate gels: the effect of crosslinking agents and diamines. Medical and Biological Engineering and Computing. 1998;36:129-34.

[64] Chitosan. Wikipedia Page. 2011.

[65] Zhu AP, Ming Z, Jian S. Blood compatibility of chitosan/heparin complex surface modified ePTFE vascular graft. Applied Surface Science. 2005;241:485-92.

[66] Chupa JM, Foster AM, Sumner SR, Madihally SV, Matthew HWT. Vascular cell responses to polysaccharide materials: *in vitro* and *in vivo* evaluations. Biomaterials. 2000;21:2315-22.

[67] Okamoto Y, Minami S, Matsuhashi A, Sashiwa H, Saimoto H, Shigemasa Y, et al. Polymeric N acetyl-D-glucosamine (chitin) induces histionic activation in dogs. Journal of Veterinary Medical Science. 1993;55:4.

[68] Mori T, Okumura M, Matsuura M, Ueno K, Tokura S, Okamoto Y, et al. Effects of chitin and its derivatives on the proliferation and cytokine production of fibroblasts *in vitro*. Biomaterials. 1997;18:947-51.

[69] Tan W, Krishnaraj R, Desai TA. Evaluation of nanostructured composite collagen–chitosan matrices for tissue engineering. Tissue Engineering. 2001;7:203-10.

[70] Lee JM, Wilson GJ. Anisotropic tensile viscoelastic properties of vascular graft materials tested at low strain rates. Biomaterials. 1986;7:423-31.

[71] Chester JF. The causes of synthetic vascular graft failure. Annals of the College of Surgeons of Hong Kong. 2002;6:97-101.

[72] Bhattacharya V, Cleanthis M, Stansby G. Preventing vascular graft failure: endothelial cell seeding and tissue engineering. Vascular Disease Prevention. 2005;2:21-7.

[73] MacDonald RA, Laurenzi BF, Viswanathan G, Ajayan PM, Stegemann JP. Collagen-carbon nanotube composite materials as scaffolds in tissue engineering. Journal of Biomedical Materials Research Part A. 2005;74A:489-96.

[74] Schlapp M, Friess W. Collagen/PLGA microparticle composites for local controlled delivery of gentamicin. Journal of Pharmaceutical Sciences. 2003;92:2145-51.

[75] Cen L, Liu W, Cui L, Zhang W, Cao Y. Collagen tissue engineering: development of novel biomaterials and applications. Pediatric Research. 2008;63:492-6.

[76] Mironov V, Kasyanov V, Markwald RR. Nanotechnology in vascular tissue engineering: from nanoscaffolding towards rapid vessel biofabrication. Trends in Biotechnology. 2008;26:338-44.

[77] Chapuis JF, Agache P. A new technique to study the mechanical properties of collagen lattices. Journal of Biomechanics. 1992;25:115-20.

[78] Daamen WF, van Moerkerk HT, Hafmans T, Buttafoco L, Poot AA, Veerkamp JH, et al. Preparation and evaluation of molecularly-defined collagen-elastin-glycosaminoglycan scaffolds for tissue engineering. Biomaterials. 2003;24:4001-9.

[79] Egan JM. A constitutive model for the mechanical behaviour of soft connective tissues. Journal of Biomechanics. 1987;20:681-92.

[80] Daamen WF, Nillesen STM, Wismans RG, Reinhardt DP, Hafmans T, Veerkamp JH, et al. A biomaterial composed of collagen and solubilized elastin enhances angiogenesis and elastic fiber formation without calcification. Tissue Engineering. 2008;14:349-60.

[81] Leach JB, Wolinsky JB, Stone PJ, Wong JY. Crosslinked alpha-elastin biomaterials: towards a processable elastin mimetic scaffold. Acta Biomaterialia. 2005;1:155-64.

[82] Powell HM, Boyce ST. EDC cross-linking improves skin substitute strength and stability. Biomaterials. 2006;27:5821-7.

[83] Kim S, Cho Y, Kang E, Kwon I, Lee E, Kim J, et al. Three-dimensional porous collagen/chitosan complex sponge for tissue engineering. Fibers and Polymers. 2001;2:64-70.

[84] Gough JE, Scotchford CA, Downes S. Cytotoxicity of glutaraldehyde crosslinked collagen/poly(vinyl alcohol) films is by the mechanism of apoptosis. Journal of Biomedical Materials Research. 2002;61:121-30.

[85] Kiernan JA. Formaldehyde, formalin, paraformaldehyde and glutaraldehyde: what they are and what they do? Microscopy Today. 2000. p. 8-12.

[86] Abe M, Takahashi M, Horiuchi K, Nagano A. The changes in crosslink contents in tissues after formalin fixation. Analytical Biochemistry. 2003;318:118-23.

[87] Singh A, Narvi S, Dutta P, Pandey N. External stimuli response on a novel chitosan hydrogel crosslinked with formaldehyde. Bulletin of Materials Science. 2006;29:233-8.

[88] Chiono V, Pulieri E, Vozzi G, Ciardelli G, Ahluwalia A, Giusti P. Genipin-crosslinked chitosan/gelatin blends for biomedical applications. Journal of Materials Science: Materials in Medicine. 2008;19:889-98.

[89] Cao H, Xu S-Y. EDC/NHS-crosslinked type II collagen-chondroitin sulfate scaffold: characterization and *in vitro* evaluation. Journal of Materials Science: Materials in Medicine. 2008;19:567 - 75.

[90] Thomopoulos S, Fomovsky GM, Chandran PL, Holmes JW. Collagen fiber alignment does not explain mechanical anisotropy in fibroblast populated collagen gels. Journal of Biomechanical Engineering. 2007;129:642-50.

[91] Sundararaghavan HG, Monteiro GA, Lapin NA, Chabal YJ, Miksan JR, Shreiber DI. Genipin-induced changes in collagen gels: correlation of mechanical properties to fluorescence. Journal of Biomedical Materials Research Part A. 2008;87A:308-20.

[92] Ma L, Gao C, Mao Z, Zhou J, Shen J, Hu X, et al. Collagen/chitosan porous scaffolds with improved biostability for skin tissue engineering. Biomaterials. 2003;24:4833-41.

[93] Wu X, Black L, Santacana-Laffitte G, Patrick Jr. CW. Preparation and assessment of glutaraldehyde-crosslinked collagen-chitosan hydrogels for adipose tissue engineering. Journal of Biomedical Materials Research Part A. 2007;81A:59-65.

[94] Horn MM, Martins VCA, de Guzzi Plepis AM. Interaction of anionic collagen with chitosan: Effect on thermal and morphological characteristics. Carbohydrate Polymers. 2009;77:239-43.

[95] Maksym GN, Bates JH. A distributed nonlinear model of lung tissue elasticity. Journal of Applied Physiology. 1997;82:32-41.

[96] Sasaki N, Odajima S. Stress-strain curve and young's modulus of a collagen molecule as determined by the X-ray diffraction technique. Journal of Biomechanics. 1996;29:655-8.

[97] Knapp DM, Barocas VH, Moon AG, Yoo K, Petzold LR, Tranquillo RT. Rheology of reconstituted type I collagen gel in confined compression. Journal of Rheology. 1997;41:971-93.

[98] Sander EA, Barocas VH. Biomimetic collagen tissues: collagenous tissue engineering. In: Fratzl P, editor. Collagen: Structure and Mechanics: Springer; 2008. p. 475-504.

[99] Taravel MN, Domard A. Collagen and its interactions with chitosan, III some biological and mechanical properties. Biomaterials. 1996;17:451-5.

[100] Roach MR, Burton AC. The reason for the shape of the distensibility curves of arteries. Canadian Journal of Biochemisty and Physiology. 1957;35:681-90.

[101] Sauren AA, van Hout MC, van Steenhoven AA, Veldpaus FE, Janssen JD. The mechanical properties of porcine aortic valve tissues. Journal of Biomechics. 1983;16:327-37.

[102] Lammers SR, Kao PH, Qi HJ, Hunter K, Lanning C, Albietz J, et al. Changes in the structure-function relationship of elastin and its impact on the proximal pulmonary arterial mechanics of hypertensive calves. American Journal of Physiology - Heart Circulation Physiology. 2008;295:H1451-9.

[103] van Birgelen APJM, Chou BJ, Renne RA, Grumbein SL, Roycroft JH, Hailey JR, et al. Effects of glutaraldehyde in a 2-year inhalation study in rats and mice. Toxicology Science. 2000;55:195-205.

[104] Kuykendall JR, Bogdanffy MS. Efficiency of DNA-histone crosslinking induced by saturated and unsaturated aldehydes *in vitro*. Mutation Research. 1992;283:131-6.

[105] Kataropoulou M, Henderson C, Grant H. The influence of glycosaminoglycans and crosslinking agents on the phenotype of hepatocytes cultured on collagen gels. Human and Experimental Toxicology. 2003;22:65-71.

[106] Touyama R, Takeda Y, Inoue K, Kawamura I, Yatsuzuka M, Ikumoto T, et al. Studies on the blue pigments produced from genipin and methylamine. I. Structures of the brownish-red pigments, intermediates leading to the blue pigments. Chemical & Pharmaceutical Bulletin. 1994;42:668–73.

[107] Touyama R, Inoue K, Takeda Y, Yatsuzuka M, Ikumoto T, Moritome N, et al. Studies on the blue pigments produced from genipin and methylamine. II. On the formation mechanisms of brownish-red intermediates leading to the blue pigment formation. Chemical & Pharmaceutical Bulletin. 1994;42:1571–8.

[108] Sung H-W, Huang R-N, Huang LLH, Tsai C-C, Chiu C-T. Feasibility study of a natural crosslinking reagent for biological tissue fixation. Journal of Biomedical Materials Research. 1998;42:560-7.

[109] Madhavan K, Belchenko D, Motta A, Tan W. Evaluation of composition and crosslinking effects on collagen-based composite constructs. Acta Biomaterialia. 2010;6:1413-22.

[110] Fung Y-C. Biomechanics - Mechanical Properties of Living Tissues. 2nd ed. New York: Springer-Verlag; 1993.

[111] Esquivel CO, William Blaisdell F. Why small caliber vascular grafts fail: A review of clinical and experimental experience and the significance of the interaction of blood at the interface. Journal of Surgical Research. 1986;41:1-15.

[112] Engbers-Buijtenhuijs P, Buttafoco L, Poot AA, Dijkstra PJ, de Vos RAI, Sterk LMT, et al. Biological characterisation of vascular grafts cultured in a bioreactor. Biomaterials. 2006;27:2390-7.

[113] Lee SJ, Liu J, Oh SH, Soker S, Atala A, Yoo JJ. Development of a composite vascular scaffolding system that withstands physiological vascular conditions. Biomaterials. 2008;29:2891-8.

[114] Tillman BW, Yazdani SK, Lee SJ, Geary RL, Atala A, Yoo JJ. The *in vivo* stability of electrospun polycaprolactone-collagen scaffolds in vascular reconstruction. Biomaterials. 2009;30:6.

[115] Liu SQ, Kodama M. Porous polyurethane vascular prostheses with variable compliances. Journal of Biomedical Materials Research. 1992;26:1489-502.

[116] Lee KW, Stolz DB, Wang Y. Substantial expression of mature elastin in arterial constructs. Proceedings of the National Academy of Sciences of the United States of America. 2011;108:2705-10.

[117] Madhavan K, Belchenko D, Tan W. Roles of genipin crosslinking and biomolecule conditioning in collagen-based biopolymer: Potential for vascular media regeneration. Journal of Biomedical Materials Research Part A. 2011;97A:16-26.

[118] Bonani W, Maniglio D, Motta A, Tan W, Migliaresi C. Biohybrid nanofiber constructs with anisotropic biomechanical properties. Journal of Biomedical Materials Research Part B: Applied Biomaterials. 2011;96B:276-86.

[119] Luong-Van E, Grøndahl L, Chua KN, Leong KW, Nurcombe V, Cool SM. Controlled release of heparin from poly(ε-caprolactone) electrospun fibers. Biomaterials. 2006;27:2042-50.

[120] Ma Z, He W, Yong T, Ramakrishna S. Grafting of gelatin on electrospun poly(caprolactone) nanofibers to improve endothelial cell spreading and proliferation and to control cell orientation. Tissue Engineering. 2005;11:1149-58.

[121] Li X, Xie J, Yuan X, Xia Y. Coating electrospun poly(ε-caprolactone) fibers with gelatin and calcium phosphate and their use as biomimetic scaffolds for bone tissue engineering. Langmuir. 2008;24:14145-50.

[122] Roh JD, Nelson GN, Udelsman BV, Brennan MP, Lockhart B, Fong PM, et al. Centrifugal seeding increases seeding efficiency and cellular distribution of bone marrow stromal cells in porous biodegradable scaffolds. Tissue Engineering. 2007;13:2743-9.

[123] Villalona GA, Udelsman B, Duncan DR, McGillicuddy E, Sawh-Martinez RF, Hibino N, et al. Cell-seeding techniques in vascular tissue engineering. Tissue Engineering Part B: Reviews. 2010;16:341-50.

[124] McClure MJ, Sell SA, Simpson DG, Walpoth BH, Bowlin GL. A three-layered electrospun matrix to mimic native arterial architecture using polycaprolactone, elastin, and collagen: A preliminary study. Acta Biomaterialia. 2010;6:2422-33.

[125] Hall CW, Liotta D, Ghidoni JJ, De Bakey ME, Dressler DP. Velour fabrics applied to medicine. Journal of Biomedical Materials Research. 1967;1.

[126] Wesolowski SA, McMahon JD. Artificial arteries. Association of Perioperative Registered Nurses Journal. 1968;7:35-50.

[127] Ju YM, Choi JS, Atala A, Yoo JJ, Lee SJ. Bilayered scaffold for engineering cellularized blood vessels. Biomaterials. 2010;31:4313-21.

[128] Walden R, L'Italien GJ, Megerman J, Abbott WM. Matched elastic properties and successful arterial grafting. Archives of Surgery. 1980;115:1166-9.

[129] Conte MS. The ideal small arterial substitute: a search for the Holy Grail? The Federation of American Societies of Experimental Biology Journal. 1998;12:43-5.

[130] Salacinski HJ, Hamilton G, Seifalian AM. Surface functionalization and grafting of heparin and/or RGD by an aqueous-based process to a poly(carbonate-urea)urethane cardiovascular graft for cellular engineering applications. Journal of Biomedical Materials Research Part A 2003;66A:688-97.

[131] Lin Q, Ding X, Qiu F, Song X, Fu G, Ji J. In situ endothelialization of intravascular stents coated with an anti-CD34 antibody functionalized heparin–collagen multilayer. Biomaterials. 2010;31:4017-25.

[132] Majack RA, Clowes AW. Inhibition of vascular smooth muscle cell migration by heparin-like glycosaminoglycans. Journal of Cellular Physiology. 1984;118:253-6.

[133] Clowes AW, Clowes MM. Kinetics of cellular proliferation after arterial injury. IV. Heparin inhibits rat smooth muscle mitogenesis and migration. Circulation Research. 1986;58:839-45.

[134] Duan Y, Wang Z, Yan W, Wang S, Zhang S, Jia J. Preparation of collagen-coated electrospun nanofibers by remote plasma treatment and their biological properties. Journal of Biomaterials Science, Polymer Edition. 2007;18:1153-64.

APPENDIX A: METHOD FOR FINDING TRANSITION POINT USING MATLAB

8.1 Matlab code for determination of transition point

```
clc
close all
clear all

%% COLLAGEN
%% Data Import & Storing in Corresponding Matrices
[Time_COL, Extension_COL, Load_COL, Strain_COL, Stress_COL] = importFile('/XXXXX/');
%%/XXXXX/ is the Name of the Directory

%% Smooth Curve using a filter
Sm_COL.Stress = smooth(Strain_COL,Stress_COL,0.25,'rloess');

% Shifting Curve to origin along y-axis
if Sm_COL.Stress(1) < 0
   Smooth_Stress_COL = Sm_COL.Stress(:)+abs(Sm_COL.Stress(1));
elseif Sm_COL.Stress(1) > 0
   Smooth_Stress_COL = Sm_COL.Stress(:)-abs(Sm_COL.Stress(1));
end

%% Curve Fitting

syms x

% Fit Type
```

```
f_COL = fittype('poly5');

% Fit Curve
[cfun_COL,gof_COL,output_COL] = fit(Strain_COL,Smooth_Stress_COL,f_COL);

% Recalculate Fitted Stress Matrix
FitStress_COL = cfun_COL(Strain_COL);

% ReShifting Curve to origin along y-axis
if FitStress_COL(1) < 0
   FitStress_COL = FitStress_COL(:)+abs(FitStress_COL(1));
elseif FitStress_COL(1) > 0
   FitStress_COL = FitStress_COL(:)-abs(FitStress_COL(1));
end

% Peak Stress
peakStress_COL = max(FitStress_COL);

% Strain at Break
n_COL = size(FitStress_COL,1);
strainAtbreak_COL = Strain_COL(n_COL);

%% Calculating Radius of Curvature

% Initialize Radius of Curvature Vector
rho_COL = zeros(n_COL,1);

% Calculate 1st and 2nd Derivatives
[dy_dx_COL, d2y_dx2_COL] = differentiate(cfun_COL,Strain_COL);

% Calculate Curvature
for i = 1:n_COL
```

```
   k_COL(i,1) = abs(d2y_dx2_COL(i))/(1+(dy_dx_COL(i)^2))^(3/2);
end

z_COL = find(k_COL>=0.01*max(k_COL));

m_COL = size(z_COL,1);

% Find point of transition
TransitionStrain_COL = Strain_COL(z_COL(1));
TransitionStress_COL = FitStress_COL(z_COL(1));

% Linear Modulus
LinearModulus_COL = 100*(FitStress_COL(z_COL(m_COL,1))-
FitStress_COL(z_COL(1,1)))/(Strain_COL(z_COL(m_COL,1))-Strain_COL(z_COL(1,1)));

%% COLLAGEN-CHITOSAN
%% Data Import & Storing in Corresponding Matrices
[Time_COL_CHI, Extension_COL_CHI, Load_COL_CHI, Strain_COL_CHI, Stress_COL_CHI]
= importFile('/XXXXX/');
%%/XXXXX/ is the Name of the Directory



%% Smooth Curve using a filter
Sm_COL_CHI.Stress = smooth(Strain_COL_CHI,Stress_COL_CHI,0.25,'rloess');

% Shifting Curve to origin along y-axis
if Sm_COL_CHI.Stress(1) < 0
   Smooth_Stress_COL_CHI = Sm_COL_CHI.Stress(:)+abs(Sm_COL_CHI.Stress(1));
elseif Sm_COL_CHI.Stress(1) > 0
   Smooth_Stress_COL_CHI = Sm_COL_CHI.Stress(:)-abs(Sm_COL_CHI.Stress(1));
end
```

```
%% Curve Fitting

syms x

% Fit Type
f_COL_CHI = fittype('poly5');

% Fit Curve
[cfun_COL_CHI,gof_COL_CHI,output_COL_CHI]                                    =
fit(Strain_COL_CHI,Smooth_Stress_COL_CHI,f_COL_CHI);

% Recalculate Fitted Stress Matrix
FitStress_COL_CHI = cfun_COL_CHI(Strain_COL_CHI);

% ReShifting Curve to origin along y-axis
if FitStress_COL_CHI(1) < 0
   FitStress_COL_CHI = FitStress_COL_CHI(:)+abs(FitStress_COL_CHI(1));
elseif FitStress_COL_CHI(1) > 0
   FitStress_COL_CHI = FitStress_COL_CHI(:)-abs(FitStress_COL_CHI(1));
end

% Peak Stress
peakStress_COL_CHI = max(FitStress_COL_CHI);

% Strain at Break
n_COL_CHI = size(FitStress_COL_CHI,1);
strainAtbreak_COL_CHI = Strain_COL_CHI(n_COL_CHI);

%% Calculating Radius of Curvature

% Initialize Radius of Curvature Vector
rho_COL_CHI = zeros(n_COL_CHI,1);
```

```
% Calculate 1st and 2nd Derivatives
[dy_dx_COL_CHI, d2y_dx2_COL_CHI] = differentiate(cfun_COL_CHI,Strain_COL_CHI);

% Calculate Curvature
for i = 1:n_COL_CHI
   k_COL_CHI(i,1) = abs(d2y_dx2_COL_CHI(i))/(1+(dy_dx_COL_CHI(i)^2))^(3/2);
end

z_COL_CHI = find(k_COL_CHI>=0.01*max(k_COL_CHI));

m_COL_CHI = size(z_COL_CHI,1);

% Find point of transition
TransitionStrain_COL_CHI = Strain_COL_CHI(z_COL_CHI(1));
TransitionStress_COL_CHI = FitStress_COL_CHI(z_COL_CHI(1));

% Linear Modulus
LinearModulus_COL_CHI = 100*(FitStress_COL_CHI(z_COL_CHI(m_COL_CHI,1))-
FitStress_COL_CHI(z_COL_CHI(1,1)))/(Strain_COL_CHI(z_COL_CHI(m_COL_CHI,1))-
Strain_COL_CHI(z_COL_CHI(1,1)));

%% COLLAGEN-CHITOSAN-ELASTIN
%% Data Import & Storing in Corresponding Matrices
[Time_COL_CHI_ELN, Extension_COL_CHI_ELN, Load_COL_CHI_ELN,
Strain_COL_CHI_ELN, Stress_COL_CHI_ELN] = importFile('/XXXXX/');
%%/XXXXX/ is the Name of the Directory

%% Smooth Curve using a filter
Sm_COL_CHI_ELN.Stress =
smooth(Strain_COL_CHI_ELN,Stress_COL_CHI_ELN,0.25,'rloess');
```

```
% Shifting Curve to origin along y-axis
if Sm_COL_CHI_ELN.Stress(1) < 0
   Smooth_Stress_COL_CHI_ELN =
Sm_COL_CHI_ELN.Stress(:)+abs(Sm_COL_CHI_ELN.Stress(1));
elseif Sm__COL_CHI_ELN.Stress(1) > 0
   Smooth_Stress_COL_CHI_ELN = Sm_COL_CHI_ELN.Stress(:)-
abs(Sm_COL_CHI_ELN.Stress(1));
end

%% Curve Fitting

syms x

% Fit Type
f_COL_CHI_ELN = fittype('poly5');

% Fit Curve
[cfun_COL_CHI_ELN,gof_COL_CHI_ELN,output_COL_CHI_ELN] =
fit(Strain_COL_CHI_ELN,Smooth_Stress_COL_CHI_ELN,f_COL_CHI_ELN);

% Recalculate Fitted Stress Matrix
FitStress_COL_CHI_ELN = cfun_COL_CHI_ELN(Strain_COL_CHI_ELN);

% ReShifting Curve to origin along y-axis
if FitStress_COL_CHI_ELN(1) < 0
   FitStress_COL_CHI_ELN = FitStress_COL_CHI_ELN(:)+abs(FitStress_COL_CHI_ELN(1));
elseif FitStress_COL_CHI_ELN(1) > 0
   FitStress_COL_CHI_ELN = FitStress_COL_CHI_ELN(:)-abs(FitStress_COL_CHI_ELN(1));
end

% Peak Stress
peakStress_COL_CHI_ELN = max(FitStress_COL_CHI_ELN);
```

```
% Strain at Break
n_COL_CHI_ELN = size(FitStress_COL_CHI_ELN,1);
strainAtbreak_COL_CHI_ELN = Strain_COL_CHI_ELN(n_COL_CHI_ELN);

%% Calculating Radius of Curvature

% Initialize Radius of Curvature Vector
rho_COL_CHI_ELN = zeros(n_COL_CHI_ELN,1);

% Calculate 1st and 2nd Derivatives
[dy_dx_COL_CHI_ELN, d2y_dx2_COL_CHI_ELN] =
differentiate(cfun_COL_CHI_ELN,Strain_COL_CHI_ELN);

% Calculate Curvature
for i = 1:n_COL_CHI_ELN
   k_COL_CHI_ELN(i,1) =
abs(d2y_dx2_COL_CHI_ELN(i))/(1+(dy_dx_COL_CHI_ELN(i)^2))^(3/2);
end

z_COL_CHI_ELN = find(k_COL_CHI_ELN>=0.01*max(k_COL_CHI_ELN));

m_COL_CHI_ELN = size(z_COL_CHI_ELN,1);

% Find point of transition
TransitionStrain_COL_CHI_ELN = Strain_COL_CHI_ELN(z_COL_CHI_ELN(1));
TransitionStress_COL_CHI_ELN = FitStress_COL_CHI_ELN(z_COL_CHI_ELN(1));

% Linear Modulus
LinearModulus_COL_CHI_ELN =
100*(FitStress_COL_CHI_ELN(z_COL_CHI_ELN(m_COL_CHI_ELN,1))-
```

```
FitStress_COL_CHI_ELN(z_COL_CHI_ELN(1,1)))/(Strain_COL_CHI_ELN(z_COL_CHI_EL
N(m_COL_CHI_ELN,1))-Strain_COL_CHI_ELN(z_COL_CHI_ELN(1,1)));

%% Calculate the Pressure Values
%Inner Diameter
a=4.76/1000; %m

%Outer Diamter
b=8/1000; %m

%Converting Stress in kPa to Pressure in mmHg
Pressure_COL=7.502*FitStress_COL;
Pressure_COL_CHI=7.502*FitStress_COL_CHI;
Pressure_COL_CHI_ELN=7.502*FitStress_COL_CHI_ELN;

%% Plot Stress vs Strain Curve for all Scaffolds
%%
figure(1)
hold on;
plot(Strain_COL,FitStress_COL,'k','LineWidth',2);
plot(Strain_COL_CHI,FitStress_COL_CHI,'r','LineWidth',2);
plot(Strain_COL_CHI_ELN,FitStress_COL_CHI_ELN,'b','LineWidth',2);
title('Stress-Strain Curves for COL-Based
Scaffolds','fontname','Garamond','fontsize',12,'fontweight','b')
xlabel('Strain (%)','fontname','Garamond','fontsize',12,'fontweight','b')
ylabel('Stress (kPa)','fontname','Garamond','fontsize',12,'fontweight','b')
hold off
%%

%% Plot Radius of Curvature-Strain Curve for each of Scaffolds
%%
figure(2)
```

```
hold on
plot(Strain_COL,max(FitStress_COL)*k_COL/max(k_COL),'b','LineWidth',1);
plot(Strain_COL_CHI,max(FitStress_COL_CHI)*k_COL_CHI/max(k_COL_CHI),'g','LineWidth',
1);
plot(Strain_COL_CHI_ELN,max(FitStress_COL_CHI_ELN)*k_COL_CHI_ELN/max(k_COL_C
HI_ELN),'r','LineWidth',1);
title('Curvature vs Strain for COL-Based
Scaffolds','fontname','Garamond','fontsize',12,'fontweight','b')
xlabel('Strain (%)','fontname','Garamond','fontsize',12,'fontweight','b')
ylabel('Curvature','fontname','Garamond','fontsize',12,'fontweight','b')
hold off;
%%

%% Plot Radius of Curvature-Strain & Stress-Strain Curve for COL Scaffolds
%%
figure(3)
hold on
plot(Strain_COL,FitStress_COL,'b','LineWidth',2);
plot(Strain_COL,max(FitStress_COL)*k_COL/max(k_COL),'k','LineWidth',1);
title('Curvature-Strain & Stress-Strain Curves for COL
Scaffolds','fontname','Garamond','fontsize',12,'fontweight','b')
hold off
%%

%% Plot Radius of Curvature-Strain & Stress-Strain Curve for COL-CHI Scaffolds
%%
figure(4)
hold on
plot(Strain_COL_CHI,FitStress_COL_CHI,'b','LineWidth',2);
plot(Strain_COL_CHI,max(FitStress_COL_CHI)*k_COL_CHI/max(k_COL_CHI),'k','LineWidth',
1);
```

```
title('Curvature-Strain & Stress-Strain Curves for COL-CHI Scaffolds','fontname','Garamond','fontsize',12,'fontweight','b');
hold off
%%

%% Plot Radius of Curvature-Strain & Stress-Strain Curve for COL-CHI-ELN Scaffolds
%%
figure(5)
hold on
plot(Strain_COL_CHI_ELN,FitStress_COL_CHI_ELN,'b','LineWidth',2);
plot(Strain_COL_CHI_ELN,max(FitStress_COL_CHI_ELN)*k_COL_CHI_ELN/max(k_COL_CHI_ELN),'k','LineWidth',1);
title('Curvature-Strain & Stress-Strain Curves for COL-CHI-ELN Scaffolds','fontname','Garamond','fontsize',12,'fontweight','b')
hold off
xlabel('Strain (%)','fontname','Garamond','fontsize',12,'fontweight','b')
ylabel('Stress (kPa)','fontname','Garamond','fontsize',12,'fontweight','b')
%%

%% Plotting Stress-Strain & Pressure-Diameter Curves of COL Scaffolds
%%
figure(6)
[AX,H1,H2]=plotyy(Strain_COL,FitStress_COL,Strain_COL,Pressure_COL,'plot');
h = legend('Stress (kPa)','Pressure (mmHg)',2);
set(h,'Interpreter','none')
set(get(AX(1),'Ylabel'),'String','Stress (kPa)','fontname','Garamond','fontsize',12,'fontweight','b')
ylimits1 = get(AX(1),'YLim');
yinc1 = (ylimits1(2)-ylimits1(1))/10;
set(AX(1),'YTick',ylimits1(1):yinc1:ylimits1(2))
set(AX(1),'XColor','k','YColor','k','fontname','Garamond','fontsize',12,'fontweight','b')
set(get(AX(2),'Ylabel'),'String','Internal Pressure (mmHg)','fontname','Garamond','fontsize',12,'fontweight','b')
```

```
ylimits2 = get(AX(2),'YLim');
yinc2 = (ylimits2(2)-ylimits2(1))/10;
set(AX(2),'YTick',ylimits2(1):yinc2:ylimits2(2))
set(AX(2),'XColor','k','YColor','k','fontname','Garamond','fontsize',12,'fontweight','b')
xlabel('Change in Diameter (%)','fontname','Garamond','fontsize',12,'fontweight','b')
title('Stress-Strain & Pressure-Diameter Curves for COL Scaffolds','fontname','Garamond','fontsize',14,'fontweight','b')
%%

%% Plotting Stress-Strain & Pressure-Diameter Curves of COL-CHI Scaffolds
%%
figure(7)
[AX,H1,H2]=plotyy(Strain_COL_CHI,FitStress_COL_CHI,Strain_COL_CHI,Pressure_COL_CHI,'plot');
h = legend('Stress (kPa)','Pressure (mmHg)',2);
set(h,'Interpreter','none')
set(get(AX(1),'Ylabel'),'String','Stress (kPa)','fontname','Garamond','fontsize',12,'fontweight','b')
ylimits1 = get(AX(1),'YLim');
yinc1 = (ylimits1(2)-ylimits1(1))/10;
set(AX(1),'YTick',ylimits1(1):yinc1:ylimits1(2))
set(AX(1),'XColor','k','YColor','k','fontname','Garamond','fontsize',12,'fontweight','b')
set(get(AX(2),'Ylabel'),'String','Internal Pressure (mmHg)','fontname','Garamond','fontsize',12,'fontweight','b')
ylimits2 = get(AX(2),'YLim');
yinc2 = (ylimits2(2)-ylimits2(1))/10;
set(AX(2),'YTick',ylimits2(1):yinc2:ylimits2(2))
set(AX(2),'XColor','k','YColor','k','fontname','Garamond','fontsize',12,'fontweight','b')
xlabel('Change in Diameter (%)','fontname','Garamond','fontsize',12,'fontweight','b')
title('Stress-Strain & Pressure-Diameter Curves for COL-CHI Scaffolds','fontname','Garamond','fontsize',14,'fontweight','b')
%%
```

```
%% Plotting Stress-Strain & Pressure-Diameter Curves of COL-CHI-ELN Scaffolds
%%
figure(8)
[AX,H1,H2]=plotyy(Strain_COL_CHI_ELN,FitStress_COL_CHI_ELN,Strain_COL_CHI_ELN,P
ressure_COL_CHI_ELN,'plot');
h = legend('Stress (kPa)','Pressure (mmHg)',2);
set(h,'Interpreter','none')
set(get(AX(1),'Ylabel'),'String','Stress (kPa)','fontname','Garamond','fontsize',12,'fontweight','b')
ylimits1 = get(AX(1),'YLim');
yinc1 = (ylimits1(2)-ylimits1(1))/10;
set(AX(1),'YTick',ylimits1(1):yinc1:ylimits1(2))
set(AX(1),'XColor','k','YColor','k','fontname','Garamond','fontsize',12,'fontweight','b')
set(get(AX(2),'Ylabel'),'String','Internal                    Pressure
(mmHg)','fontname','Garamond','fontsize',12,'fontweight','b')
ylimits2 = get(AX(2),'YLim');
yinc2 = (ylimits2(2)-ylimits2(1))/10;
set(AX(2),'YTick',ylimits2(1):yinc2:ylimits2(2))
set(AX(2),'XColor','k','YColor','k','fontname','Garamond','fontsize',12,'fontweight','b')
xlabel('Change in Diameter (%)','fontname','Garamond','fontsize',12,'fontweight','b')
title('Stress-Strain & Pressure-Diameter Curves for COL-CHI-ELN
Scaffolds','fontname','Garamond','fontsize',14,'fontweight','b')
%%
```

8.2 Discussion

The stress-strain curve plotted to determine peak stress, strain at break and linear elastic modulus is first smoothed with the smooth function available in Matlab (R2009b, Mathworks Inc, Natick, MA). This curve was then fit with a 5^{th} order polynomial using the fit function in Matlab. With this fit

data, the curvature of the stress-strain (σ-ε) curve was plotted against the strain. The curvature was calculated using the general curvature formula,

$$k = \frac{\left|\frac{d^2y}{dx^2}\right|}{\left(1 + \left(\frac{dy}{dx}\right)^2\right)^{\frac{3}{2}}}$$

where *k* is the curvature, *y* is the abscissa (stress - σ) and *x* is the ordinate (strain - ε). On the curvature-strain curve, the strain value at the largest local maximum was taken to be the transition point.

(P.S.: The term largest local maximum mathematically may not physically mean anything. Since there was another smaller local maximum been produced because of the fit function, I have used these terms to define the transition point. The method to avoid this artifact is to piecewisely fit curves for the three regions.)

Using the transition point and peak stress, the toe, the linear and the failure regions were determined. The toe region was characterized as the region on the stress-strain curve up to the transition point. The linear elastic modulus was slope of the straight line fit in the region between transition point and peak stress. Data collected were statistically analyzed using the one-way ANOVA test. Student's *t* test was then used to compare the means of each individual group. The level of significance was set at $\alpha = 0.05$ for 95% statistical significance. Error bars on all the

histogram charts represent the standard error of the mean (SEM) based on the total number of the samples.

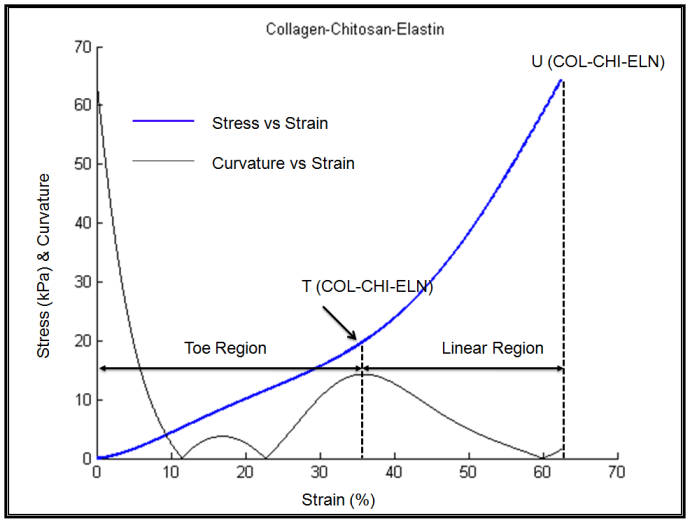

Figure 8.1: Determination of Transition Point in COL-CHI-ELN

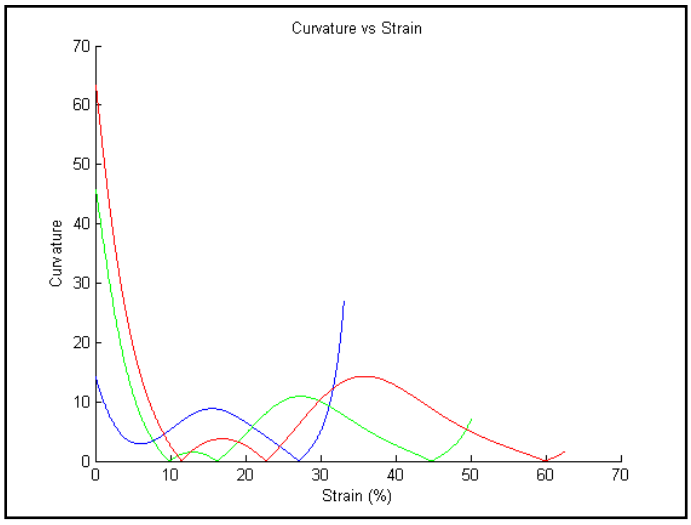

Figure 8.2: Transition Points in COL (Blue), COL-CHI (Green) & COL-CHI-ELN (Red)

APPENDIX B: SYNTHESIS OF 4.76MM LATEX TUBE

1. A 4.76mm diameter aluminum rod was cleaned with isopropyl alcohol and air dried.
2. Next, the aluminum rod was dipped into a coagulant, calcium nitrate solution for approximately 150 seconds.
3. The rod was then air dried for 30 minutes.
4. Once, the rod was dry, the rod was dipped into the latex polymer solution for 150 seconds.
5. The rod was then air dried for 30 minutes once again.
6. Again, once the latex had dried out completely, the rod was immersed in a water bath preheated to 50°C for 6 hours.
7. It was ensured that the water was being constantly stirred to ensure uniform distribution of heat and to dissolve the salts exuded from the surface of latex.
8. After the lapse of 6 hours, the rod was removed from the water bath and left in an oven preheated to 105°C for 3 hours.
9. The rod was then wiped with a clean cloth to remove any water on the surface.
10. The latex was removed after applying some corn starch on the surface to avoid sticking of the latex to itself.
11. The thickness of the latex tube obtained from this process was measured to be 0.05mm.
12. To increase the thickness by increments of 0.05mm, repeat steps 2-6 before immersing in water bath.

APPENDIX C: MATLAB CODE FOR FINDING DIAMETER CHANGE FROM MULTILAYER GRAFT CANNULATION EXPERIMENT (COMPLIANCE TEST)

10.1 Code for cropping images

```
clear all
close all
clc
%% Get the Directory with All the Tiff Image Files
sdirectory = '/XXXXX/'); %% /XXXXX/ is the Name of the  Directory
jpegfiles = dir([sdirectory '\*.jpg']);
%% Get the Total Number of Tiff Image Files in the Directory
n = length(jpegfiles);
for k = 1:n
    %% Get the Directory Image File Name
    filename1 = [sdirectory '\' jpegfiles(k).name];
    %% Read File
    I1 = imread(filename1);
   %% Crop Image File to the position [XXX,XXX,XXX,XXX]
    I2 = imcrop(I1, [XXX,XXX,XXX,XXX]);
    %% Read File Path, Name & Extension
    [pathstr, name, ext] = fileparts(filename1);
    file = [sdirectory '\' name];
    filename2 = sprintf('%s.tif',file);
    %% Save File
    imwrite(I2,filename2,'tif');
end
```

10.2 Code for diameter determination

```
clear all
close all
clc
%% Get the Directory with All the Tiff Image Files
sdirectory = /XXXXX/'); %% /XXXXX/ is the Name of the  Directory
%% Process the Tiff files to calculate the diameter
tifffiles = dir([sdirectory '\*.tif']);
scale = XX.XX; % pixel/mm
n = length(tifffiles);
diameter = zeros(n,1);
file = [sdirectory '\' 'PCL(HP)_GCC_08.txt'];
fid = fopen(file,'w');
v = 0;
%% Actual Diameter Determination
for k = 1:n
   tic
   filename = [sdirectory '\' tifffiles(k).name];
   I1 = imread(filename);
   E = entropyfilt(I1);
   Eim = mat2gray(E);
   I2 = im2bw(Eim,0.5);
   [r2, c2] = size(I2);
   for i = 1:r2
      I2(i,1) = 1;
      I2(i,c2) = 1;
   end
   I3 = imfill(I2, 'holes');
   cc = bwconncomp(I3,4);
   graft_data = regionprops(cc,'all');
   graft_area = max(graft_data(1,:).FilledArea)/(scale^2);
```

```
    I4 = graft_data(1,:).FilledImage;
    [r4, c4] = size(I4);
    graft_length = c4/scale;
    diameter(k,1) = graft_area/graft_length;
    fprintf(fid, '%s \t %f \r\n',tifffiles(k).name, diameter(k,1));
    u = toc;
    fprintf('File %d Analyzed: Elapsed Time = %6.4gseconds\n',k,u);
    v = u + v;
end
fclose(fid);
fprintf('Total Analysis Time for %d Files = %6.4g\n',k,v);
```